




This is to certify that the
dissertation entitled
Synthesis of Biomimetic Model Compounds for
Studies of Proton Coupled Electron Transfer
presented by
Yongqi Deng

has been accepted towards fulfillment
of the requirements for

Ph. D. degree in Chemistry


Major professor

Date 20 August 1997



PLACE IN RETURN BOX
to remove this checkout from your record.
TO AVOID FINES return on or before date due.

DATE DUE	DATE DUE	DATE DUE
<hr/>	<hr/>	<hr/>
<hr/>	<hr/>	<hr/>
<hr/>	<hr/>	<hr/>
<hr/>	<hr/>	<hr/>
<hr/>	<hr/>	<hr/>

**SYNTHESIS OF BIOMIMETIC MODEL COMPOUNDS FOR
STUDIES OF PROTON COUPLED ELECTRON TRANSFER**

By

Yongqi Deng

A DISSERTATION

Submitted to
Michigan State University
in partial fulfillment of the requirements
for the degree of

DOCTOR OF PHILOSOPHY

Department of Chemistry

1997

ABSTRACT

SYNTHESIS OF BIOMIMETIC MODEL COMPOUNDS FOR STUDIES OF PROTON COUPLED ELECTRON TRANSFER

Yongqi Deng

Proton coupled electron transfer (PCET) is a basic energy conversion process in biology. To elucidate the mechanism of PCET reactions, we have studied photoinduced electron transfer between donor/acceptor pairs juxtaposed by a proton interface formed by an amidinium-carboxylate salt bridge. This proton interface, unlike a carboxylic acid dimer, is asymmetric and allows us to control the direction of proton transfer. Porphyrin amidinium and porphyrin phenyl amidinium have been synthesized via their nitrile precursors using $\text{ClAl}(\text{NH}_2)\text{CH}_3$. The corresponding porphyrin carboxylate and porphyrin phenylcarboxylate complexes have been synthesized from aldehyde and ester precursors, respectively. The solubility of these molecules in organic solvents has been improved by introducing trimethoxyphenyl groups. Their capabilities to form amidinium-carboxylate salt bridges have been characterized by X-ray crystallography, NMR and UV-vis spectroscopies. These studies reveal that the amidinium-carboxylate salt bridge is very stable and even persists in polar solvent such as DMSO. When the amidinium group is directly attached to the porphyrin ring, deprotonation of the amidinium causes a spectral shift, indicating a strongly coupled system. However, in porphyrin phenyl amidinium, the coupling is interrupted by the introduction of a phenyl group.

In an effort to further investigate the proton coupling effect on ET rates, purpurin and chlorin molecules attached with amidinium or carboxylate groups have also been synthesized. They exhibit characteristics similar to their porphyrin analogues in the formation of the amidinium-carboxylate salt bridge. A double bond connecting chromophore and amidinium (carboxylate) groups in purpurin provides a strong coupling to the interface, as indicated by UV-vis studies. In chlorin amidinium and carboxylate complexes, this double bond is replaced by a single bond to create a decoupled system. Unlike the porphyrin system, the length and structure of the salt bridge connector for purpurin and chlorin complexes are the same, thus allowing for a better comparison between these two systems.

Preliminary ET studies reveal that the ET is perturbed by the proton interface when it is electronically coupled to the donor/acceptor chromophore. This is rationalized by an increase in the reorganization energy when the proton is transferred.

Finally, we have designed and synthesized a novel porphyrin-quinone complex. This complex, in which the porphyrin is substituted with pyridinium groups, is water-soluble and allows for the study of PCET in aqueous solutions. Proton coupling is observed to slow the back ET reaction by over four orders of magnitude.

ACKNOWLEDGEMENTS

I would like to express my special gratitude to my advisors Professor C. K. Chang and Professor D. G. Nocera for their guidance, advice and encouragement through the course of this work.

I wish to thank the past and present members of Professor Chang and Professor Nocera group — Mr. Craig Shiner, Mr. Chen-Yu Yeh, Dr. Ying Liang, Mr. Baomin Guo, Dr. J. P. Kirby, Dr. James Roberts, Mr. Dan. Engebretson, Dr. Al. Barney, Dr. Sara Helvoigt, Mr. Dimitris Papoutsakis, Dr. Eric Saari, Dr. Wanda Hartmann and Dr. Ann Macintosh for their help and friendship. I also wish to thank Mr. Mike Waldo for his help on American culture and friendship.

Thanks are also extended to Professor Shih-Ming Peng at the Department of Chemistry, National Taiwan University, who carry out the X-ray structure determination of porphyrin amidinium-carboxylate complex.

My deepest appreciation is due to my wife Li Zhen for her love and support. We are looking forward a new life together with our lovely daughter Sherry Deng.

TABLE OF CONTENTS

TABLE OF CONTENTS	v
LIST OF FIGURES	viii
LIST OF TABLES	x
LIST OF APPENDIX FIGURES	xi
ABBREVIATIONS.....	xii

CHAPTER I

INTRODUCTION.....	1
I. SIGNIFICANCE AND BACKGROUND.....	1
A. PCET in photosystem II.....	2
B. PCET in cytochrome <i>c</i> oxidase.....	4
II. STRATEGIES FOR PCET DESIGN	7
A. Overall design.....	7
B. Donor-Acceptors.....	8
C. Porphyrin model compounds for ET studies.....	10
D. Proton interfaces	14
III. RESULTS AND PRESENTATION.....	18

CHAPTER II

SYNTHESIS OF PORPHYRINS MODIFIED WITH AMIDINIUM AND CARBOXYLIC ACID GROUPS	19
---	-----------

I. INTRODUCTION	19
II. SYNTHESIS	22
A. Porphyrin phenyl amidinium and carboxylic acid—decoupled systems.	22
B. Porphyrin amidinium and carboxylic acid—coupling system.....	31
III. PROPERTIES.....	40
A. Coupling effects	40
B. IR studies.....	43
IV. EXPERIMENTAL.....	45

CHAPTER III

CHARACTERIZATION OF AMIDINIUM-CARBOXYLATE SALT BRIDGE ... 74

I. CRYSTAL STRUCTURE.....	74
II. DETERMINATION OF ASSOCIATION CONSTANTS.....	84
A. Proton NMR.....	84
B. UV-vis	87
III. PCET STUDIES	96
IV. CONCLUSIONS.....	98
V. EXPERIMENTAL	101
A. Crystallography.....	101
B. Binding studies.....	101

CHAPTER IV

PURPURIN AND CHLORIN — SYNTHESIS AND ELECTRON TRANSFER.. 103

I. INTRODUCTION	103
II. RESULTS AND DISCUSSION	105
A. Synthesis	105
B. Coupling vs. Decoupling.....	109
C. Binding Studies	111
D. PCET Studies.....	114

III. EXPERIMENTAL	126
 CHAPTER V	
SYNTHESIS OF WATER SOLUBLE PORPHYRIN-QUINONE.....	136
I. INTRODUCTION	136
II. RESULTS AND DISCUSSION	138
A. Synthesis	138
B. Preliminary ET studies.....	142
III. EXPERIMENTAL.....	145
 REFERENCES.....	149
 APPENDIX	
SELECTED PROTON NMR SPECTRA.....	158

LIST OF FIGURES

Figure 1. PCET in Photosystem II (PSII)	3
Figure 2. Electron transfer pathways and rates in cytochrom c oxidase	5
Figure 3. PCET design	9
Figure 4. Secondary electrostatic interactions in amidinium-carboxylate salt bridge	15
Figure 5. Absorption spectral changes of 75 upon addition of DBU in CH ₂ Cl ₂ (The amount of DBU increase with arrows)	41
Figure 6. Absorption spectral of 53 in the absent (—) and the presence of 3.00 eq. DBU (·····) in CH ₂ Cl ₂	42
Figure 7. IR spectra of 75 . (a) protonation form; (b) deprotonation form	44
Figure 8. Top and side views of the ORTEP diagrams of the crystal structure of the salt-bridged supramolecular assembly formed by association of 75 with benzoate (structure 1)	76
Figure 9. Top and side views of the ORTEP diagrams of the crystal structure of the salt-bridged supramolecular assembly formed by association of 75 with benzoate (structure 2)	77
Figure 10. Selected ¹ H NMR spectra of 75 (2.06 mM) with 1 eq. of benzoic acid in the absence of and in the presence of 1.78, 3.56, 5.35, 7.13, 8.92, 10.70, and 12.48 mM (bottom to top) of tetrabutylammonium benzoate in DMSO-d ₆ at room temperature. The spectral range captures the amidinium protons internal (NH _{in}) and external (NH _{ex}) to the salt bridge interface and the three <i>meso</i> protons of the porphyrin ring.	88
Figure 11. Plot of the chemical shift of internal protons of the amidinium versus the concentration of tetrabutylammonium benzoate	89
Figure 12. Job plot of the supramolecular complex formed by 75 and benzoate. The	

total concentration was kept at 3.5 mM and the systems were monitored by ^1H NMR (using the internal proton of amidinium) in DMSO at room temperature.	90
Figure 13. Selected UV-vis spectra of 75 (5.50 μM) in the presence of 0.0, 1.36, 2.71, 4.07, 5.42, 6.78 and 9.48 μM (increase with arrows) of tetrabutylammonium benzoate in dichloromethane.	92
Figure 14. Plot of the absorption change of 75 at 398 nm versus the concentration of tetrabutylammonium benzoate.....	93
Figure 15. Summary of ET rates in coupling system.....	99
Figure 16. Summary of ET rates in decoupling systems	100
Figure 17. Absorption spectra of purpurin 92 (0.81 μM) in the presence of 0.00, 0.20, 0.40, 0.60, 0.80, 1.00, 1.40, 1.80, 2.40 eq. of DBU in CH_2Cl_2 . The arrows represent the increasing of DBU.....	112
Figure 18. Absorption spectra of chlorin 96 (0.93 μM) in the absent (—) and present of 3.00 (.....) eq. of DBU in CH_2Cl_2	113
Figure 19. Selected ^1H NMR spectra of 96 (3.86 mM) with 1 eq. of benzoic acid in the absence of and in the presence of 1.00, 1.69, 2.38, 3.08, 5.16, 7.23, and 10.00 mM (bottom to top) of tetrabutylammonium benzoate in DMSO-d_6 at room temperature. The spectral range captures the amidinium protons internal (NH_{in}) and external (NH_{ex}) to the salt bridge interface and the three <i>meso</i> protons of the purpurin as well as olefinic proton of the cyclopentenyl ring.	115
Figure 20. Plot of the chemical shift of internal protons of the amidinium versus the concentration of tetrabutylammonium benzoate.....	116
Figure 21. Selected UV-vis spectra of 92 (2.74 μM) in the presence of 0.0, 0.63, 1.26, 1.88, 2.51, 3.14, 4.40, 5.65 and 7.54 μM (increase with arrows) of tetrabutylammonium benzoate in dichloromethane.....	117
Figure 22. Plot of the absorption change of 92 at 420 nm versus the concentration of tetrabutylammonium benzoate.....	118
Figure 23. Summary of ET rates in purpurin and chlorin systems	122
Figure 24. pH-dependence of forward ET (O) and back ET rates (●).....	144

LIST OF TABLES

Table 1. Crystal Data and Conditions for Crystallographic Data Collection and Structure Refinement.....	78
Table 2. Selected Bond Distances and Bond Angles and Their Estimated Standard Deviations for Porphyrin Amidinium Benzoate	79
Table 3. Atomic Parameters x,y,z and Beq.	80
Table 4. Association Constants (K_a) and Energies (ΔG^0) of Amidinium-Carboxylate Salt Bridge in DMSO Determined by NMR Titration	91
Table 5. Association Constants (K_a) and Energies (ΔG^0) of Complexes Formed by 75 and Various Carboxylates.....	95
Table 6. Association Constants (K_a) of Amidinium-Carboxylate Salt bridge for Purpurin and Chlorin Systems	119
Table 7. Distances, Driving Forces and ET Rate Constants for Purpurin and Chlorin Systems	123

LIST OF APPENDIX FIGURES

Figure A-1. 300 MHz ^1H -NMR spectrum of 48 in CDCl_3	158
Figure A-2. 300 MHz ^1H -NMR spectrum of 51 in CDCl_3	159
Figure A-3. 300 MHz ^1H -NMR spectrum of 53 in CDCl_3	160
Figure A-4. 300 MHz ^1H -NMR spectrum of 66 in CDCl_3	161
Figure A-5. 300 MHz ^1H -NMR spectrum of 67 in CDCl_3	162
Figure A-6. 300 MHz ^1H -NMR spectrum of 68 in CDCl_3	163
Figure A-7. 300 MHz ^1H -NMR spectrum of 69 in CDCl_3	164
Figure A-8. 300 MHz ^1H -NMR spectrum of 70 in CDCl_3	165
Figure A-9. 300 MHz ^1H -NMR spectrum of 71 in CDCl_3	166
Figure A-10. 300 MHz ^1H -NMR spectrum of 73 in CDCl_3	167
Figure A-11. 300 MHz ^1H -NMR spectrum of 75 in CDCl_3	168
Figure A-12. 300 MHz ^1H -NMR spectrum of 83 in CDCl_3	169
Figure A-13. 300 MHz ^1H -NMR spectrum of 85 in CDCl_3	170
Figure A-14. 300 MHz ^1H -NMR spectrum of 89 in CDCl_3	171
Figure A-15. 300 MHz ^1H -NMR spectrum of 90 in CDCl_3	172
Figure A-16. 300 MHz ^1H -NMR spectrum of 92 in CDCl_3	173
Figure A-17. 300 MHz ^1H -NMR spectrum of 96 in CDCl_3	174
Figure A-18. 300 MHz ^1H -NMR spectrum of 105 in DMSO	175
Figure A-19. 300 MHz ^1H -NMR spectrum of 106 in D_2O	176
Figure A-20. 300 MHz ^1H -NMR spectrum of 108 in D_2O	177

ABBREVIATIONS

DBU	1,8-Diazabicyclo[5,4,0]undec-7-ene
DMF	N,N-Dimethyl Formamide
DMSO	Dimethyl Sulfoxide
DNB	3,5-Dinitrobenzoate
DNBA	3,5-Dinitrobenzamidinium
FAB-MS	Fast Atom Bombardment Mass Spectroscopy
FT-IR	Fourier Transformed Infra Red
OEP	2,3,7,8,12,13,17,18-Octaethylporphyrin
PDC	Pyridinium Dichromate
TABA	Tetrabutylammonium Benzoate
THF	Tetrahydrofuran
TFA	Trifluoroacetic Acid
TLC	Thin Layer Chromatography
TTP	5,10,15,20-Tetraphenylporphyrin

Chapter I

Introduction

I. Significance and Background

Proton coupled electron transfer (PCET) is a basic energy conversion process in biology. The importance of PCET was realized during the 1960s when many biochemists were unsuccessfully searching for a high energy phosphorylated intermediate in the synthesis of adenosine triphosphate (ATP), which is the universal energy storage form in living cells. In 1961, Peter Mithchell¹ suggested such intermediate did not exist. Instead, he proposed a chemiosmotic theory for oxidative and photosynthetic phosphorylation. According to his concept, the key intermediate is an electrochemical gradient across the inner mitochondrial or thylakoid membrane. This gradient was proposed to be formed by coupling the translocation of protons across the membrane to electron transfer reactions between electron transport complexes of those membranes. The electrochemical potential formed in this process was then utilized for the synthesis of ATP.

The chemiosmotic theory was initially received with little enthusiasm. However,

during the 1970s, as evidence accumulated in favor of this hypothesis, the situation gradually changed. By the middle of 1970s, the principle of Mitchell's theory was accepted by most investigators in that field and he was awarded the Nobel Prize for Chemistry in 1978. However, the mechanistic details of how an electron couples to the proton still remains undefined.² The major objective of this dissertation is to elucidate how electrons and protons are coupled by designing and synthesizing new supramolecules which feature integrated electron and proton transfer networks.

A. PCET in Photosystem II

Photosystem II (PSII) is a transmembrane protein that effects a transverse flux of electrons and protons. It consists of at least ten protein subunits.³ However, all the electron-flow events in PS II take place via prosthetic groups bound to only two polypeptides, namely L and M branches, which form the actual reaction center of PS II. These two protein subunits are highly hydrophobic integral proteins of about 32 Kda in the thylakoid membrane. They contain the pigments, redox systems, and other components involved in the light driven redox reaction across the membrane: P680, two monomeric chlorophylls *a*, two pheophyrins, two plastoquinones, and an iron bound via four histidines (Figure 1). The primary light event⁴ takes place at the chlorophyll dimer (P680) that is bound via two histidines (His 198) to two homologous proteins. When the reaction center P680 is excited, charge separation occurs in 10 ps and the electron is passed from the excited primary electron donor P^{*}680 onto a primary electron acceptor, a pheophytin. The pheophytin in turn reduces the first plastoquinone (Q_A) to a semiquinone in about 1 ns. The semiquinone reduces the second plastoquinone (Q_B),

Figure 1. PCET in Photosystem II (PSII)

which is bonded loosely to the b_L protein subunit. The oxidized P680 is reduced to its initial state by the manganese complex of the oxygen evolve system (OES) after charge separation.

After a second similar excitation cycle, Q_B accepts a second electron, concomitant with proton transfer from the external protein matrix to form a hydroquinone. The plastoquinone leaves the quinone-binding pocket and diffuses to the lumen side, where it is later oxidized to a quinone by Cyt b_6 .⁵ The protons in the OEC are released into the inner lumen space of the thylakoid membrane, resulting in a net effect of proton transport opposite to the direction of electron flow across the membrane. In this way, the proton gradient is established between the inner and outer spaces of the thylakoid membrane and results in a proton chemical potential that drives the proton dependent adenine triphosphate (ATP) synthesis.

B. PCET in cytochrome c oxidase

In biological systems, the ET pathway is carefully controlled to reach maximum energy efficiency. The recent breakthrough in determination of the three dimensional structure and electron transfer rates in cytochrome *c* oxidase reveals that the PCET reaction plays a central role in controlling the route of intermolecular electron transfer in the reaction center of this enzyme. As described in Figure 2, when an electron is injected into Cu_A of the fully oxidized enzyme, it initially equilibrates with heme a at a rate constant of 10^4 s^{-1} .⁶ The reduction of heme a_3 occurs at much slower rate of $1\text{-}100 \text{ s}^{-1}$, depending on the experimental conditions.⁷ Consequently, the electron-transfer rates from Cu_A to heme a and a_3 , respectively, differ by 2-4 orders of magnitude. This result is perplexing inasmuch as recent high-resolution three-dimensional structures of

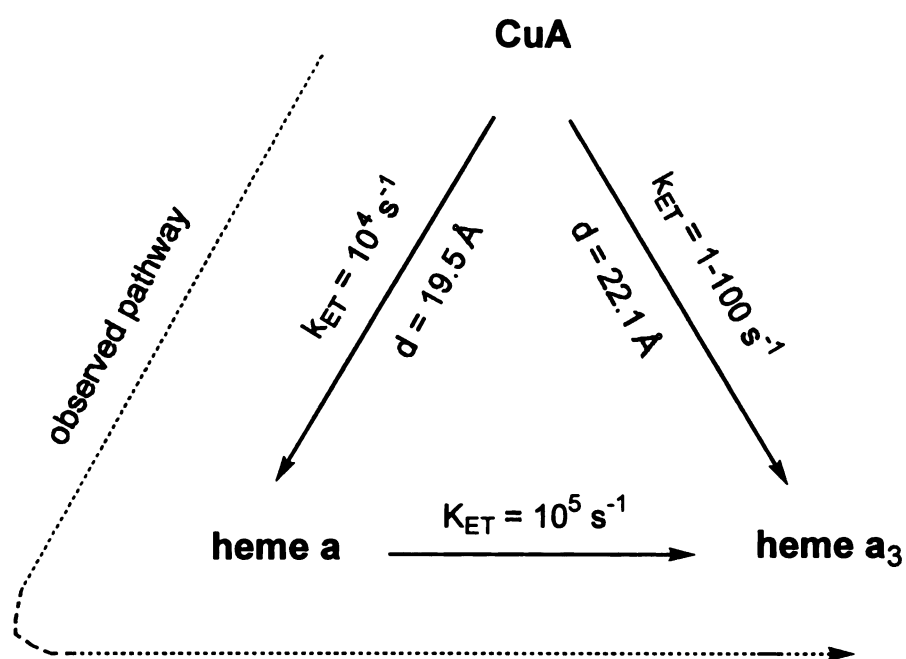


Figure 2. Electron transfer pathways and rates in cytochrome c oxidase

cytochrome *c* oxidases from *Paracoccus denitrificans*⁸ and bovine heart⁹ reveal that the distances from Cu_A to hemes *a* and *a*₃ are similar (19.5 and 22.1 Å, respectively). The relatively small difference in distances cannot alone account for the large difference in the electron transfer rate between Cu_A and the two hemes, and suggests a more complicated operative mechanism.

Indeed, electron transfer from heme *a* to heme *a*₃ displays complex pH dependence¹⁰ and the experimental results suggest that this electron transfer is kinetically coupled to the proton released from a site in the vicinity of heme *a*₃. This group interacts more strongly with heme *a*₃ than with heme *a* and is buried inside the protein, in contact with the bulk protons of a proton-conducting pathway.¹¹ The maximum proton release/uptake at heme *a*₃ was found to be ~0.7 H⁺/e⁻. These results are consistent with the three dimensional *P. denitrificans* structure which shows that a larger number of protonable groups are found around heme *a*₃ than near heme *a*. On the basis of these results, Brzenski¹² has suggested that electron transfer from Cu_A to heme *a* is accompanied by a smaller proton-charge compensation than that associated with electron transfer to heme *a*₃, thereby accounting for the rate difference between the two pathways.

A similar situation has been found on the acceptor side of the photosynthetic reaction center (e. g. from *Rhodobacter sphaeroide*), where the direct electron transfer rate from the electron donor (P) to Q_B is much slower than that from P to Q_A, even though both distances and driving forces are similar.¹³ This difference in rate has been found to be due to a difference in the reorganization energies, with the Q_A reorganization energy being smaller than that associated with Q_B. In this case, Q_B interacts more strongly with protonable groups, resulting in a net proton uptake (0.4-1.0 H⁺/Q_B⁻) upon electron transfer

from Q_A to Q_B in the reaction center.¹⁴

In support of this contention, reorganization energies associated with the electron transfer processes have been estimated from temperature dependent studies.¹² It has been found that when proton uptake is involved, the reorganization energy increases significantly. The reorganization energy λ for the electron transfer from Cu_A to heme a is 0.3 eV and that for the direct electron transfer from Cu_A to heme a_3 is 0.8 eV. The larger reorganization energy associated with heme a_3 over heme a explains why the direct electron transfer from Cu_A to heme a_3 is much slower than the transfer from Cu_A to heme a .

II. Strategies for PCET design

A. Overall design

The above examples demonstrate how proteins control the intramolecular ET pathway through their special three-dimensional structures by utilizing the PCET reaction. To unravel the PCET mechanism, several problems needed to be explored such as: Is the proton and electron transfer concerted? Do they transfer stepwise and which transfer is first? What structural/electronic properties establish consecutive versus concerted PCET? How will the proton transfer rate depend on the electron transfer rate? What structural/electronic features of the proton interface are important in governing the coupling between the electron and the proton? Owing to the complexity of biological systems, the important factors that affect the PCET reaction are difficult to isolate. Therefore, we have chosen to study biomimetic model compounds, which have the advantage that specific properties of the complex can be tuned by proper design and

synthesis. Synthetic analogs may lead to greater understanding, which is difficult or even impossible to elucidate by using biological systems.

The basic strategy for designing our model complexes is to combine photoelectron transfer through a fixed distance with that of photoinduced proton transfer. This strategy lends itself to two design types (Figure 3). One such design is to channel the electron transfer through a proton interface, in which the proton transfer is internal to the electron transfer pathway. In this type of design, an electron donor and acceptor pair is juxtaposed by a proton transfer interface to feature a donor-proton interface-acceptor arrangement. Another design is to locate the proton interface at the terminus of the electron transfer pathway, either on electron donor or acceptor. In this design, the proton transfer is external to electron transfer (PT external to ET). This arrangement of the electron donor, acceptor and proton interface is analogous to that in the photosynthetic reaction center and cytochrome *c* oxidase.

B. Donor-Acceptors

Although electron transfer has been actively pursued for decades, the study of the role of protons on the electron transfer events has only recently gained interest.¹⁵ We have decided to adapt the well-understood fixed-distance electron donor/acceptor strategy to our design of PCET model compounds. Porphyrin and chlorin compounds are particularly attractive ET D/A systems and have been considered as the primary electron donor-acceptor in our study. Upon photo-irradiation, excited states of porphyrin and chlorin are accessed and they become good electron donors. Their redox properties can be tuned by changing the metal (the oxidation potential increase in the order $\text{Mg}^{2+} < \text{Zn}^{2+} < \text{H}_2^{2+} < \text{H}_4^{4+} < \text{Sn}^{4+}$),¹⁶ providing various driving forces for electron transfer. Systems

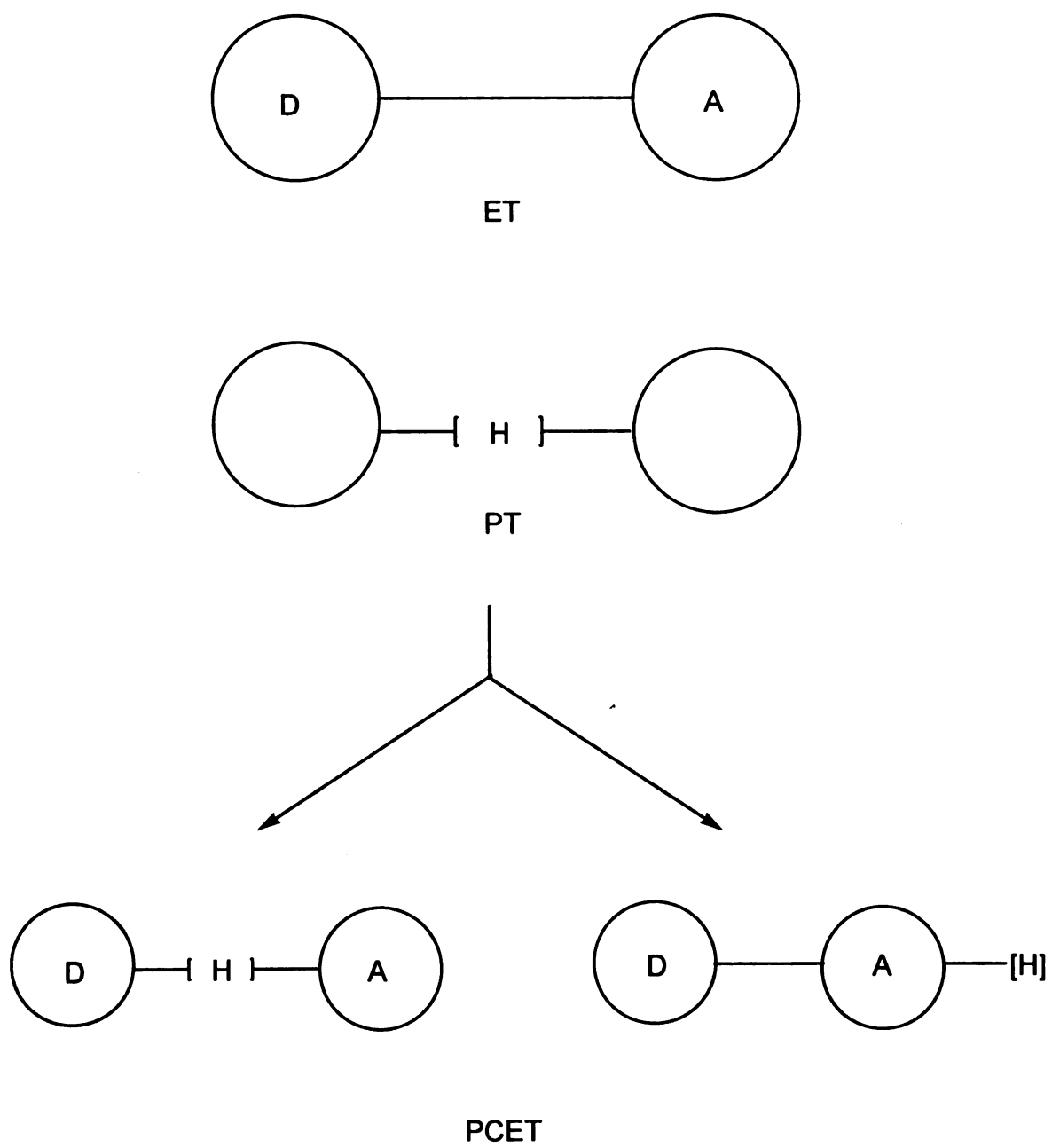


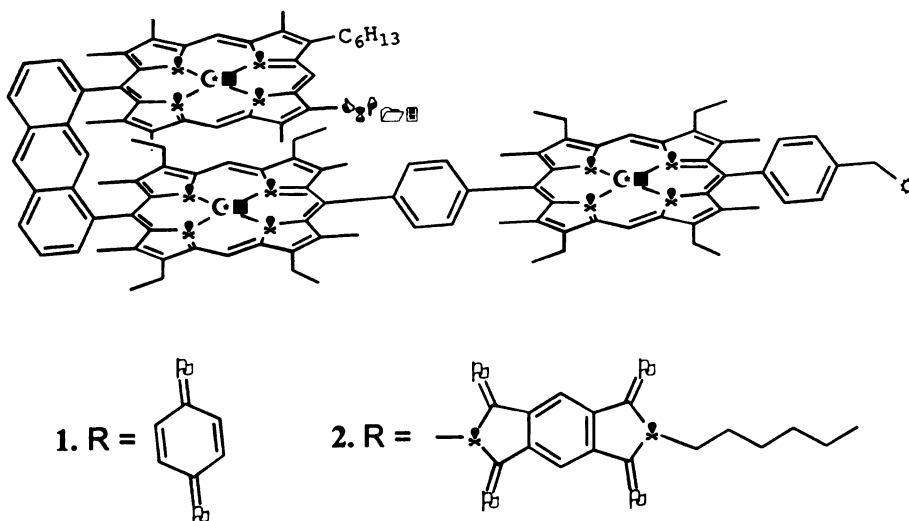
Figure 3. PCET design

based on porphyrin and chlorin molecules have been well studied.¹⁷ The synthesis, electron transfer rates, transient absorption spectra, driving forces and electronic couplings of various systems have been well documented. This large amount of information is of great use in the exploration of new PCET chemistry based on these systems.

C. Porphyrin model compounds for ET studies

Porphyrin complexes have been widely used in building model compounds that resemble the natural pigments of enzyme reaction centers. Osuka et al.¹⁸ have developed a model for the photosynthetic reaction center. Complex **1** consists of three porphyrins with an individual benzoquinone attached to the terminal porphyrin. Two porphyrins are stacked to act like the special pair dimer in photosynthetic systems. The authors showed by picosecond transient optical spectroscopy¹⁹ that rapid electron transfer occurs between the porphyrin and quinone that are adjacent to one another. This electron transfer may be followed by a second dark electron transfer from the dimeric porphyrin to the central porphyrin, although the evidence for this reaction is not particularly strong. The assignment of transient absorption spectra to the various oxidized and reduced species in this series is complicated by broad, indistinct spectra and by similarities between spectra of the excited states and the ionic states.

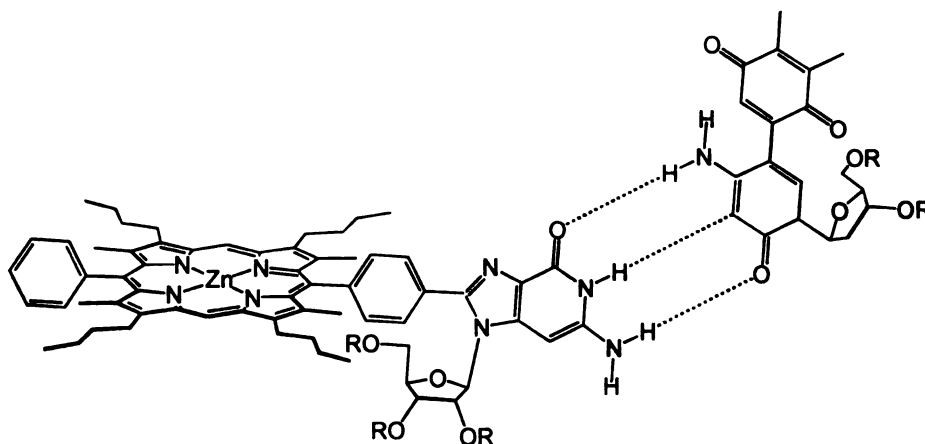
To resolve the problem, Osuka et al.²⁰ have prepared the same type of porphyrins, but the benzoquinone acceptor has been replaced with pyromellitimide (**2**). The pyromellitimide radical anion possesses a distinct, narrow optical transition at 715 nm that is diagnostic of charge separation. For the simple porphyrin-pyromellitimide donor-acceptor pair in THF, the forward electron transfer occurs with a rate constant of



$1.7 \times 10^{10} \text{ s}^{-1}$, while the ion pair recombines with a rate constant of $9.3 \times 10^9 \text{ s}^{-1}$. The free energy of this reaction is about 0.5 eV. The authors observed two-step electron transfer in this complex. Strong interactions between the two sandwiched porphyrins results in lowering of the S_1 energy by 0.19 eV and the correspondingly oxidation potential by 0.17 eV. The pyromellitimide radical anion absorption decays biexponentially with lifetimes of 70 ps and 2.5 us.

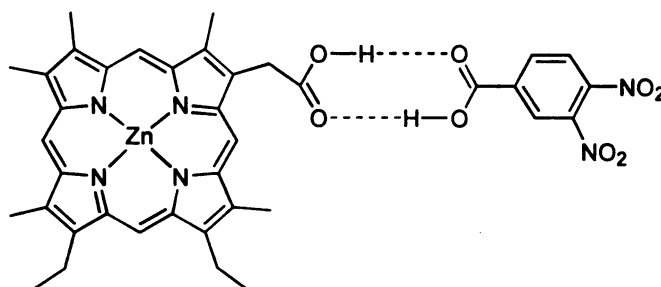
Sessler et al.²¹ have examined an interesting porphyrin-quinone in which the porphyrin is associated with the quinone by means of a Watson-Crick base pairing cytosine-guanine hydrogen bonded linkage. The formation of the hydrogen bond was characterized by ¹H NMR ($K_{\text{assoc}} = 13,000 \text{ M}^{-1}$ in dichloromethane). ET kinetics between a Zn-porphyrin and benzoquinone was determined by using a fluorescence quenching technique. Association of the quinone causes moderate quenching ($\tau = 710 \text{ ps}$) of the 1.8 ns Zn-porphyrin excited state lifetime. From the quenching rate constant, the unimolecular ET rate constant was determined to be $8.6 \times 10^9 \text{ s}^{-1}$. This approach is appealing because it permits photoinduced electron transfer to be probed in a system in

which the electronic coupling between the donor and acceptor is transmitted across weak hydrogen bonds.



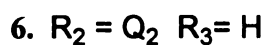
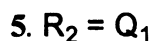
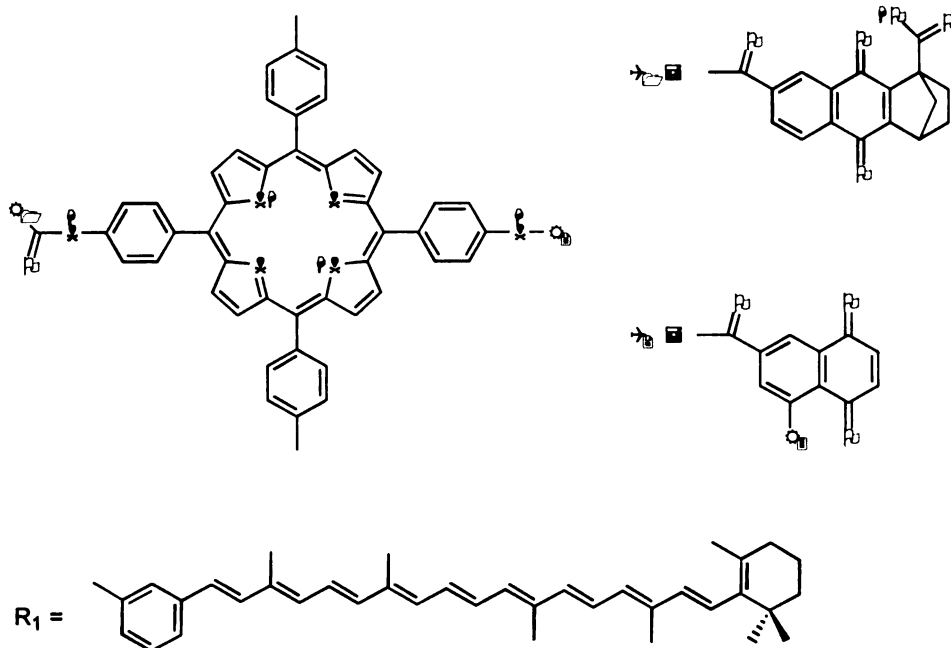
3

To investigate the passive role of protons in modulating of electron transfer, Turro et al.²² have built a model complex in which a Zn-porphyrin and 3,4-dinitrobenzene are linked via a hydrogen bond interface of a carboxylic acid dimer (3). Electron transfer processes were examined by picosecond transient optical spectroscopy. It was found that rate constants for both charge separation and charge recombination of this donor acceptor system were $5.0 \times 10^{10} \text{ s}^{-1}$ and $1.0 \times 10^{10} \text{ s}^{-1}$, respectively. The rates are comparable to those of covalently linked Zn-porphyrin/acceptor systems with similar separations and driving forces.²³ This study showed that hydrogen bond interface is competitive to covalent bond linkages. Moreover, the deuterium isotope effect of $k_{\text{H}}/k_{\text{D}} = 1.7$ and $k_{\text{H}}/k_{\text{D}} = 1.6$ for charge separation and charge recombination respectively, revealed that electron transfer was coupled to proton motion.



4

Gust et al.²⁴ have extensively explored carotenoid-porphyrin-quinone triads to achieve long-lived charge separation in these supramolecular systems. Excitation of the carotenoid-porphyrin-quinone triad yields the porphyrin's first excited singlet state, which decays by electron transfer to give a $C-P^{+}-Q^{-}$ charge-separated state. Competing with the rapid charge recombination is the electron transfer from the carotenoid that produces a long-lived $C^{+}-P-Q^{-}$ species. Various efforts²⁵ have been made to tune the electronic and thermodynamic factors so that forward electron transfer is favored over charge recombination. Recently,²⁶ a PCET reaction has been applied to achieve long-lived charge separation. The naphthoquinone moiety of **5** is fused to a norbornene system bearing a carboxylic acid at a bridgehead so that an intramolecular hydrogen bond from the carboxyl group to the nearby quinone carbonyl can form. Electron transfer from the photoexcited porphyrin results in a marked pKa increase at the quinone, leading to a proton shift from the acid to the quinone, which generates a new state with a reduced recombination rate. The effect of the proton is significant. The quantum yield of the final charge-separated state of **5** is 2 fold higher relative to the reference triads **6** and **7** and the life-time of final charge-separated state for **5** is much longer than those for **6** and **7** (233 ns vs. 62 and 60 ns, respectively).

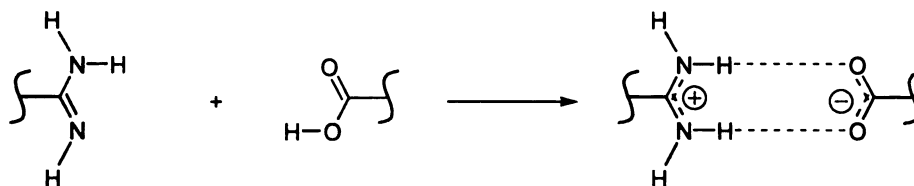


C. Proton interfaces

1. Amidinium-carboxylate salt bridge:

To establish the directionality of proton transfer, it is advantageous to use asymmetric proton interfaces.²⁷ One such proton interface is formed by the association of an amidine to a carboxylic acid (Scheme 1). It can be viewed as a model of the aspartane-arginine salt bridge, which is an important feature found in many structures including RNA stem loops,²⁸ zinc finger/DNA complexes²⁹, and the active site of dihydrofolate reductase.³⁰ However, unlike the guanidinium-carboxylate interaction of

Arg-Asp, amidinium shows only one specific binding mode for carboxylate, which simplifies PCET studies.



Scheme 1

Due to the primary charge interaction and two favorable secondary electrostatic interactions (Figure 4), this proton interface is predicted to be very stable according Jorgenson's hydrogen bond theory.³¹ Indeed, the binding is so strong that it can occur even in polar solvent such as DMSO.²⁷ The association constant measured for the salt bridge formed from bicyclic guanidinium-carboxylate is over 10^5 in chloroform.³² This stability ensures the persistence of proton interface in PCET reactions.

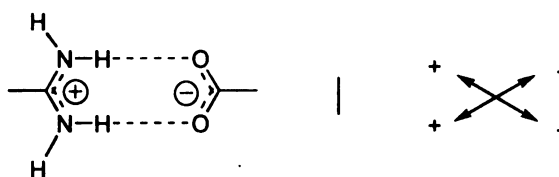
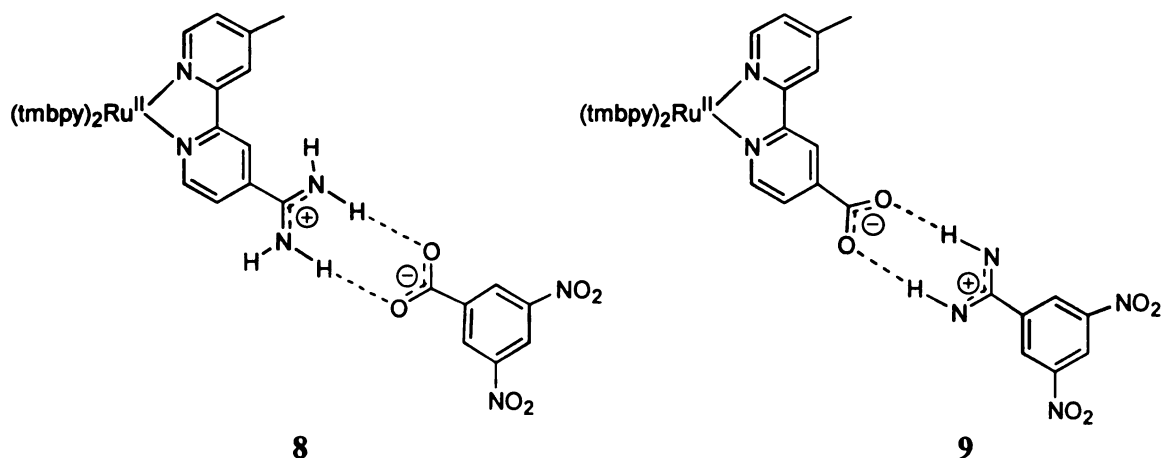


Figure 4. Secondary electrostatic interactions in amidinium-carboxylate salt bridge

Electron transfer through the amidinium-carboxylate asymmetric interface has been initially investigated for **8** and **9**.^{27b} The donor in **8** and **9** is electronically excited

$\text{Ru(II)(tmbpy)}_3^{2+}$ (tmbpy = tetramethylbipyridine) and the acceptor is a dinitroaromatic. Thus, a comparison of **8** and **9** allows the investigation of the directionality of electron transfer through the asymmetric interface.



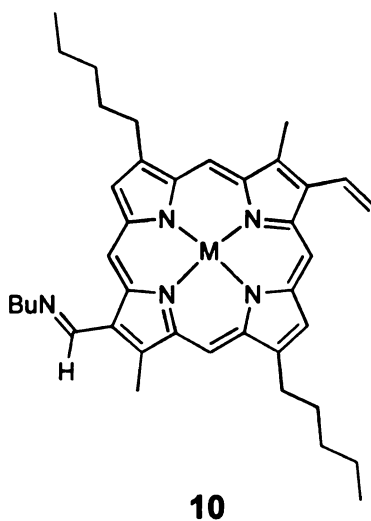
In both cases, lifetime quenching measurements show a biexponential decay in which one lifetime component is concentration dependent and the other is concentration independent. The concentration-dependent rate constant is assigned to bimolecular ET processes and the concentration-independent rate constant is attributed to ET for the associated pairs shown by **8** and **9**. The ET rate through the proton interface for **8** ($8.4 \times 10^6 \text{ s}^{-1}$) is found to be slower than that for **9** ($3.10 \times 10^8 \text{ s}^{-1}$). It is believed in **8**, the ET event drives the proton movement thus greater reorganization energy is associated with the proton interface. This is not the case in **9**, where the proton is already residing on the acceptor and is likely to remain upon the arrival of the electron.

2. Schiff base:

Schiff bases are attractive proton interfaces external to the ET pathway. For

instance, protonation/deprotonation reactions of the retinal Schiff base species *in situ* in *rhodopsin*³³ and in *bacteriorhodopsin*³⁴ have been intimately associated with the proton-pumping reactions of these proteins. In addition, these reactions may be relevant to those that occur for heme *a* in its involvement in proton pumping in the mitochondrial protein and cytochrome oxidase.³⁵

In proteins, the physical and chemical properties of the porphyrin system can be modulated by interactions between its peripheral substituents and nearby amino acid side chains. The Schiff bases show versatility owing to the fact that both formations of the linkage and its subsequent protonation may be subject to functional control. Schiff base porphyrin **10** have previously been prepared and characterized by optical and Raman spectroscopies.³⁶ Upon protonation, the deep red Schiff base turns deep green and the 404 nm Soret band splits to give rise to 377 and 432 nm bands. In addition, the Q-band shows a dramatic shift from 577 to 620 nm. The C=N stretching frequency exhibits a strong resonance enhancement and it shows the typical red shift with the protonation of the Schiff base. These properties provide a unique way to detect proton motion in a PCET study.



III. Results and Presentation

Porphyrin, purpurin and chlorin modified with amidinium or carboxylate groups have been synthesized. These compounds are used for the study of PCET with the proton transfer interface internal to the ET pathway. The formation of donor/acceptor pairs via an amidinium-carboxylate salt bridge has been fully characterized by X-ray crystallography, ^1H NMR and UV-vis spectroscopies. Utilizing UV-vis spectroscopy, we have been able to establish the electronic interaction between the proton interface and chromophore. As discussed in Chapter III, Chapter IV and Chapter V, preliminary electron transfer results reveal that in coupled systems, the proton coupling has a significant effect on the ET rate.

In this dissertation, Chapter II describes the synthesis of porphyrins equipped with amidinium or carboxylate functional groups. Strategies to improve the solubility of these types of molecules and to couple and decouple the proton interface from the porphyrin ring are also presented. Chapter III describes the characterization of the amidinium-carboxylate salt bridge and the study of association constants of this salt bridge. In Chapter IV, an improved coupled/decoupled system based on purpurin/chlorin structures has been synthesized. ET results indicate that the proton is coupled to electron transfer within the amidinium-carboxylate interface. Chapter V describes the synthesis of water soluble porphyrin-quinone complex. In this supramolecule, the porphyrin contains hydrophilic functional groups that enable ET to be performed in aqueous solution. ET studies reveal that protonation occurs upon ET from porphyrin to quinone.

Chapter II

Synthesis of Porphyrins Modified with Amidinium and Carboxylic Acid Groups

I. Introduction

Previous studies of ET through symmetric carboxylic acid dimer interfaces have shown that the proton can mediate ET rates.²² However, theoretical studies³⁷ indicate that the proton displacement on one side of the carboxylic acid dimer interface is compensated by displacement of a proton from the other side. Changes in polarity, charge, and energetics resulting from proton motion within the interface are not easily distinguished in the ET rate. This is not the case in amidinium-carboxylate interfaces. In this asymmetric proton interface, the directionality of electron transfer as perturbed by proton motion can be assessed. Furthermore, the asymmetric interfaces provide specificity in binding. The acceptor can only bind to the donor, which is not the case for symmetric interface in which there are also acceptor-acceptor and donor-donor bindings.

As we stated in Chapter I, the salt bridge can form by association of an amidine to a carboxylic acid. However, the amidine is a strong base (e.g. pKa of acetamidine is

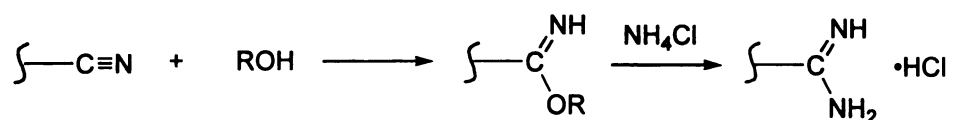
found to be 12.40 in water³⁸) and can be easily protonated to form amidinium under most experimental conditions. Consequently, it is more convenient to make this salt bridge from amidinium and carboxylate. Hence, to obtain the electron donor/acceptor pair juxtaposed by this salt bridge, we need to synthesize donors and acceptors modified with amidinium or carboxylate groups. When the donor amidinium mixes with the acceptor carboxylate, an amidinium-carboxylate salt bridge is formed in such a way that the protons are on the donor side. To switch this proton interface, we can mix the donor carboxylate with acceptor amidinium to form a salt bridge in which the protons are on the acceptor side. In the first case, the proton can move from a donor to an acceptor upon electron transfer, whereas in the second case, the proton is already on the acceptor side and is expected to remain there upon arrival of the electron. This construct therefore allows us to study the effects of proton motion on the electron transfer rate.

The goal of the work described in this Chapter is to synthesize porphyrins modified with either amidinium or carboxylate. In order to investigate whether the electronic interaction between the electron and proton interface is important to PCET reactions, two types of structures have been designed. In one such structure, the amidinium or carboxylate group is directly attached to the porphyrin moieties. This places the proton interface in π -conjugation with the porphyrin. Through this conjugation, changes at the proton interface can affect the electronic structure of the porphyrin and the electron transfer can affect the proton interface. Thus, the porphyrin and proton interface are coupled in this design. In another design, a *meso*-phenyl group is inserted between the porphyrin ring and amidinium or carboxylate group. X-ray structure analyses has shown that the *meso* substituted phenyl group is usually

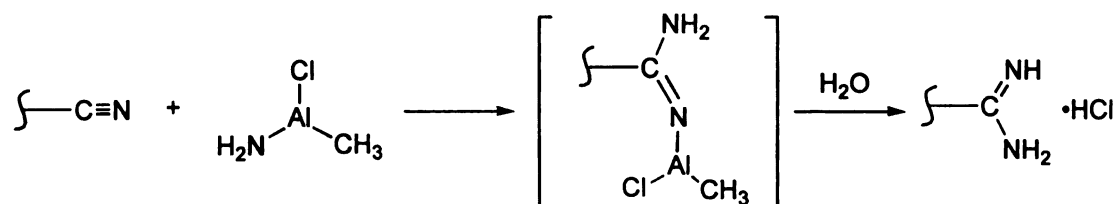
perpendicular to the porphyrin ring, especially when adjacent β positions are substituted owing to steric congestion.³⁹ This orientation minimizes the conjugation between the phenyl and porphyrin moieties and thus, the electronic coupling between the proton interface and porphyrin.

A convenient method to make amidiniums is from nitriles. There are two common methods to convert a nitrile to an amidinium (Scheme 2). The Pinner synthesis⁴⁰ is a two-step reaction, transforming nitriles into imido esters, which are generally isolated, and then condensed with ammonia or an amine in a separate step. Alternatively, Garigipati's⁴¹ utilizes an amide transfer reagent⁴² to convert a nitrile to an amidinium in one step with high yield. Recently, this synthesis was applied successfully in our lab to make Ru(bpy)²⁷ and porphyrin acryl amidinium.⁴³ The disadvantage of this method is that the functional groups such as carbonyl and nitro groups can also react with the amide transfer reagent. Hence in these cases, the Pinner synthesis is applied.

Pinner Synthesis:



Garigipati Synthesis:



Scheme 2

In the case that nitrile can not be directly accessed, it has to be transformed from other derivatives such as aldehyde, ester or amide. Olah's synthesis⁴⁴ provides a convenient method to convert aldehyde to nitrile in one step using hydroxylamine hydrochloride in formic acid. The synthesis from ester and amide is not suitable for porphyrins because the reaction condition involves alcohol as solvent, in which most porphyrins are usually insoluble. Since carboxylic acids can also be synthesized from the oxidation of aldehydes, the synthesis of our target molecules conveniently begins with the synthesis of porphyrin aldehydes.

II. Synthesis

A. Porphyrin phenyl amidinium and carboxylic acid—decoupled systems

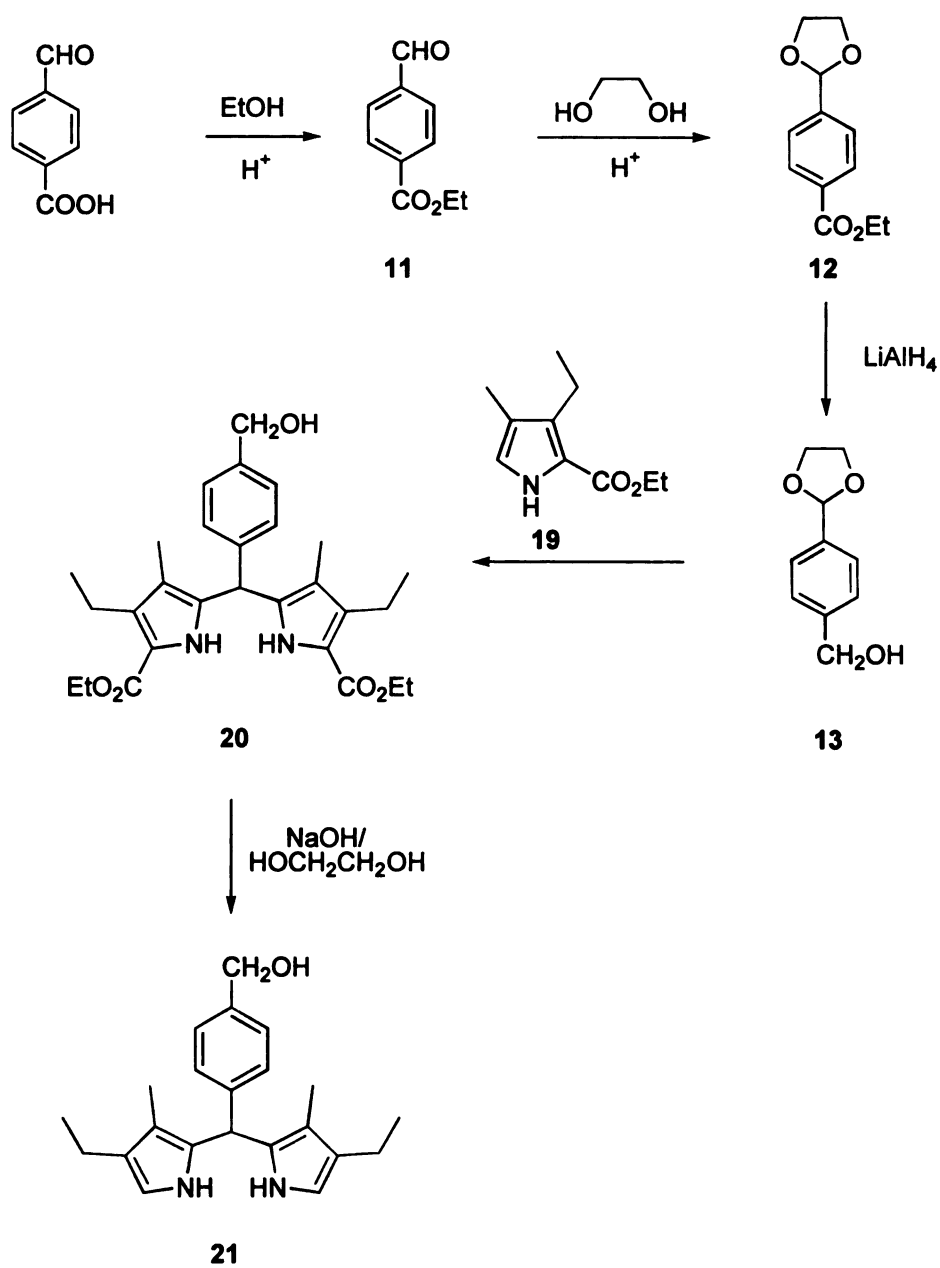
1. First generation:

The strategy for synthesizing porphyrin phenyl aldehyde **27** is based on Sessler's synthesis of porphyrin-porphyrin-quinone triad.⁴⁵ In this approach, two aldehyde groups on the phenyl ring are introduced sequentially. The first aldehyde is for synthesizing dipyrromethane, which may be condensed to give a porphyrin. The second aldehyde group, which is planned to introduce after the porphyrin, will lead the formation of the amidinium group. As described in Scheme 3, 4-carboxy-benzaldehyde was converted to its ethyl ester **11** by reacting with ethanol under acid catalysis. The aldehyde group of **11** was protected by converting to acetal **12**, which was then reduced with lithium aluminum hydride to give the alcohol **13**, as a precursor of the second aldehyde group. Under acid-catalyzed reaction, acetal **13** was converted to aldehyde **14** *in situ* and reacted with ethyl 3-ethyl-4-methylpyrrole-2-carboxylate **19**, which was synthesized by following the

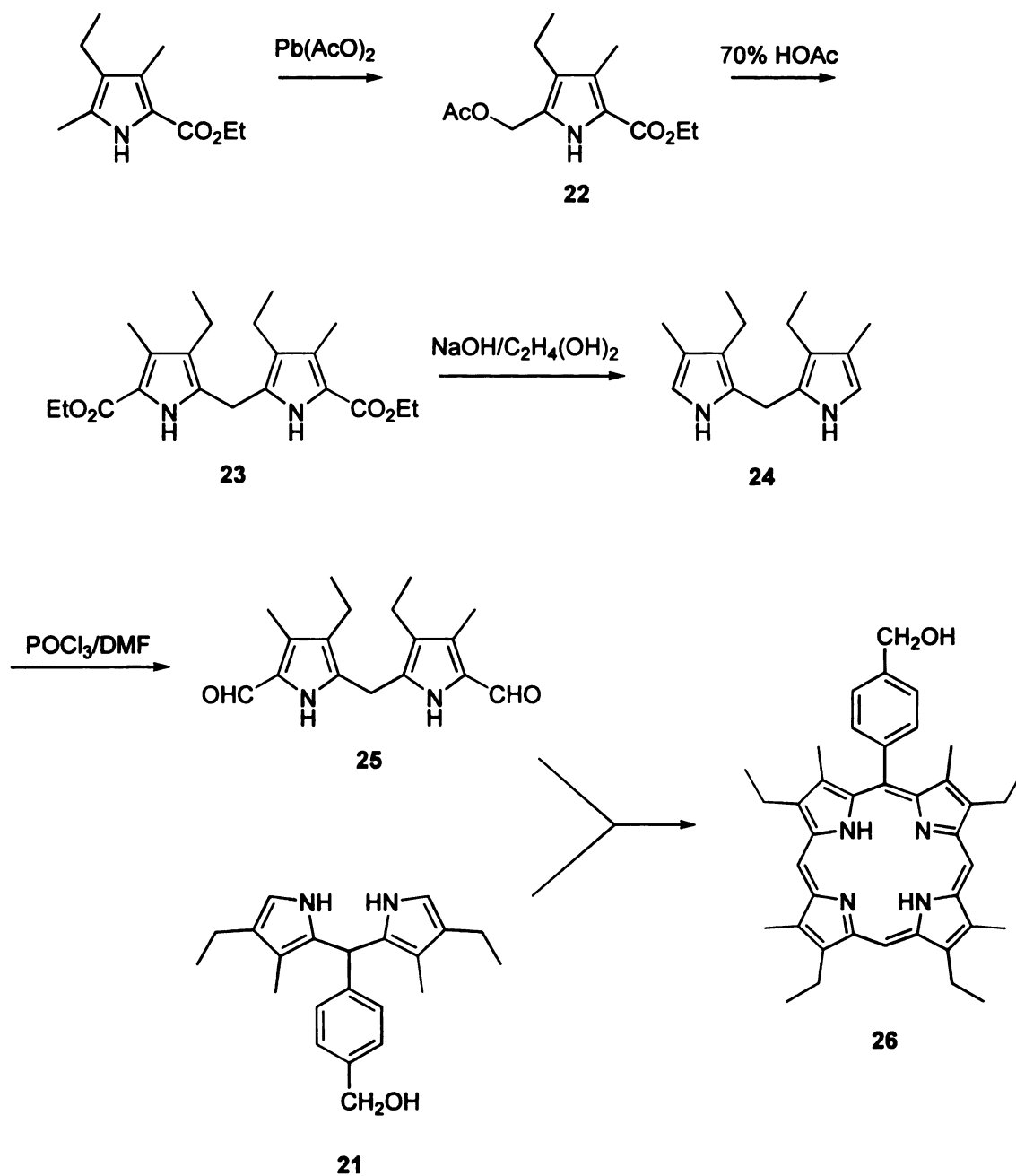
procedure of Barton-Zard⁴⁶, to give dipyrromethane **20** in 75% yield. The resulted **20** was then saponified and decarboxylated using a method reported by Chang⁴⁷ to give α -free dipyrromethane **21** in 95% yield.

In Scheme 4, ethyl 4-ethyl-3,5-dimethylpyrrole-2-carboxylate was quantitatively transformed by oxidation with lead tetraacetate to the 5-acetoxymethyl analogue **22**, which was self-condensed in hot 70% aqueous acetic acid to form the diethoxycarbonyl dipyrromethane **23**. The ethyl ester group of the dipyrromethane **23** was saponified and decarboxylated using the previous procedure to give compound **24** in quantitative yield. Diformyl-dipyrromethane **25** was obtained by treating **24** with the Vilsmeier reagent, which was generated *in situ* by the addition of POCl₃ to DMF. This gave the other half moiety needed for making porphyrin **26**. Reaction of **25** with dipyrromethane **21** underwent a MacDonald condensation to give porphyrin **26** in 47% yield.

The further transformation of porphyrin **26** is described in Scheme 5. Oxidation of porphyrin **26** with PDC in CH₂Cl₂ gave the corresponding porphyrin phenyl aldehyde **27** in 75% yield. Employing the procedure of Olah, **27** was converted to nitrile **28** in one step with hydroxylamine hydrochloride in refluxing formic acid with 88% yield. IR spectrum of this porphyrin showed a moderate absorption at 2235 cm⁻¹, which is the characteristic absorption of CN group. The route from nitrile to amidine is based on the original approach of Garigipati.⁴¹ Porphyrin **28** was first converted to its nickel complex **29** to protect the porphyrin ring from aluminum insertion. Treatment of nickel porphyrin phenyl nitrile **29** with chloromethylaluminum amide⁴² in toluene at 80 °C gave **30** in 85% yield. After isolation, the amidine group was found in the protonated amidinium form.



Scheme 3



Scheme 4

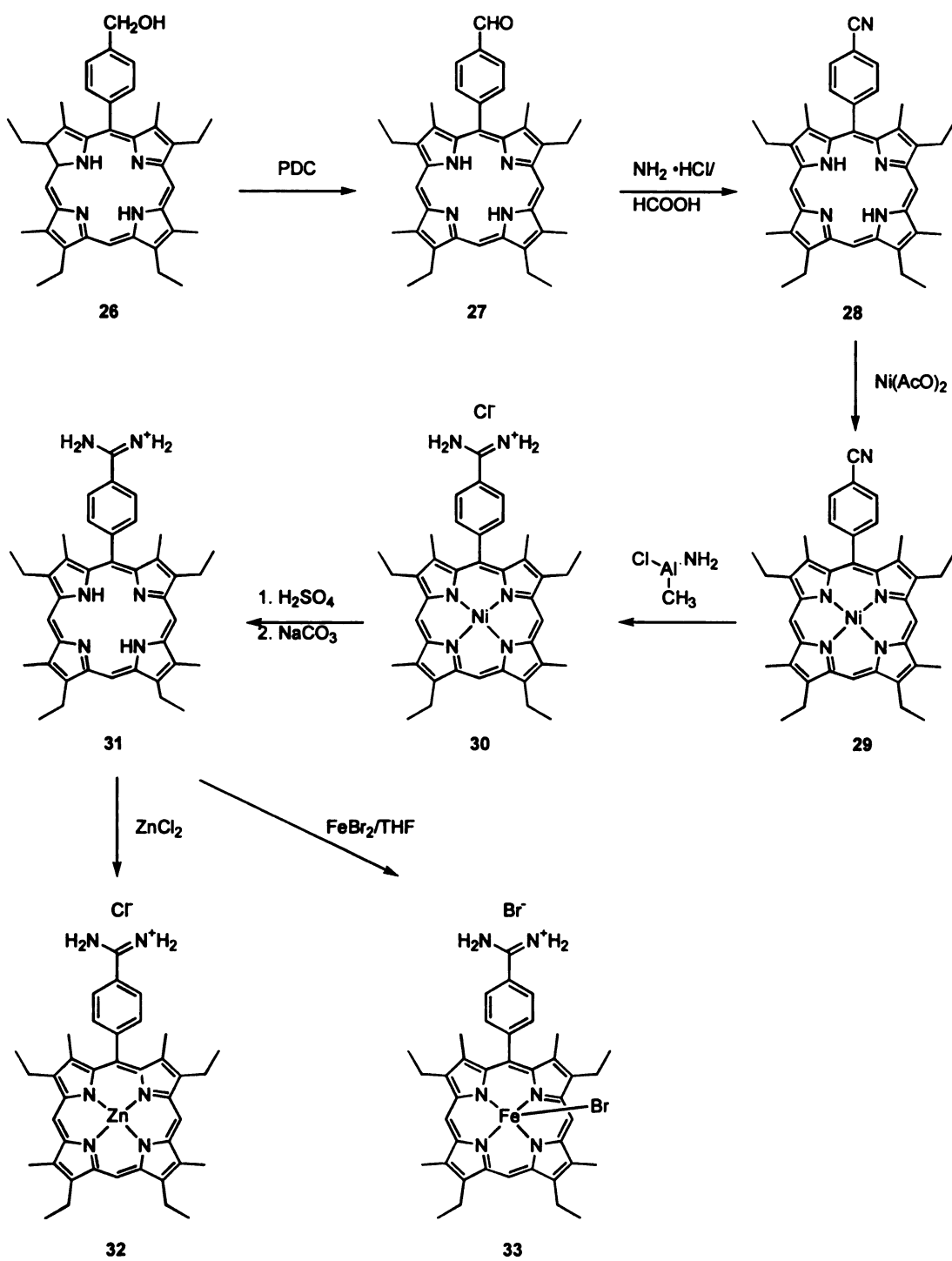
This is supported by proton NMR, in which NH protons appear as two broad peaks at 9.26 and 9.68 ppm; integration indicates that they are in 1:1 ratio and each peak contains two protons. Nickel porphyrin **30** was then demetallated with concentrated sulfuric acid to give free base **31** in quantitative yield. Zinc insertion was accomplished by reacting **31** with ZnCl_2 in DMF and iron porphyrin **33** was made by the standard method⁴⁸.

The synthesis of porphyrin phenyl acid **37** was achieved in an analogous manner (Scheme 6). Acid-catalyzed condensation of pyrrole **19** with 4-carboxybenzaldehyde gave dipyrromethane **34** in 69% yield. The ester group of **34** was then saponified and decarboxylated to give **35** in 90% yield. This di- α free dipyrromethane was condensed with diformyl-dipyrromethane **26** to give porphyrin phenyl acid **36** in 48% yield. Free base porphyrin **37** was obtained by treating **36** with dilute HCl solution followed by neutralization with sodium bicarbonate aqueous solution. The corresponding iron(III) porphyrin **38** and nickel porphyrin **39** were then synthesized from **37**.

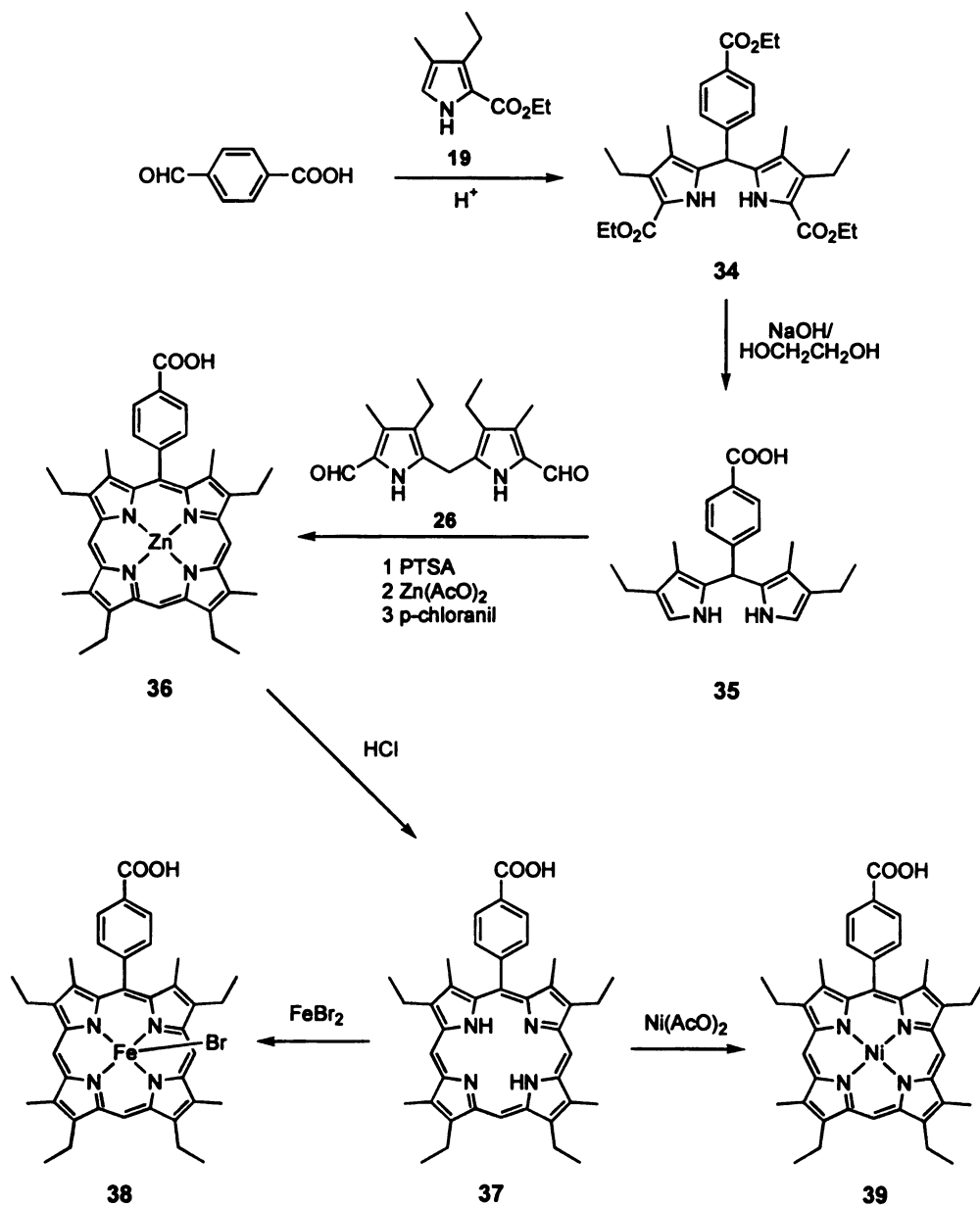
2. Second generation — with improved solubility:

For the formation of hydrogen bonds, a low polar solvent such as acetonitrile, dichloromethane or chloroform should be chosen. These have low dielectric constants and the hydrogen bond is expected to be stable. Unfortunately, the solubility of porphyrins made above in these solvents is very low. For ET study, especially by transient absorption detection, relatively concentrated samples are required. We found it was necessary to modify the peripheral substituents of porphyrins in order to improve their solubility.

Various functional groups have been used to improve porphyrin solubility in



Scheme 5

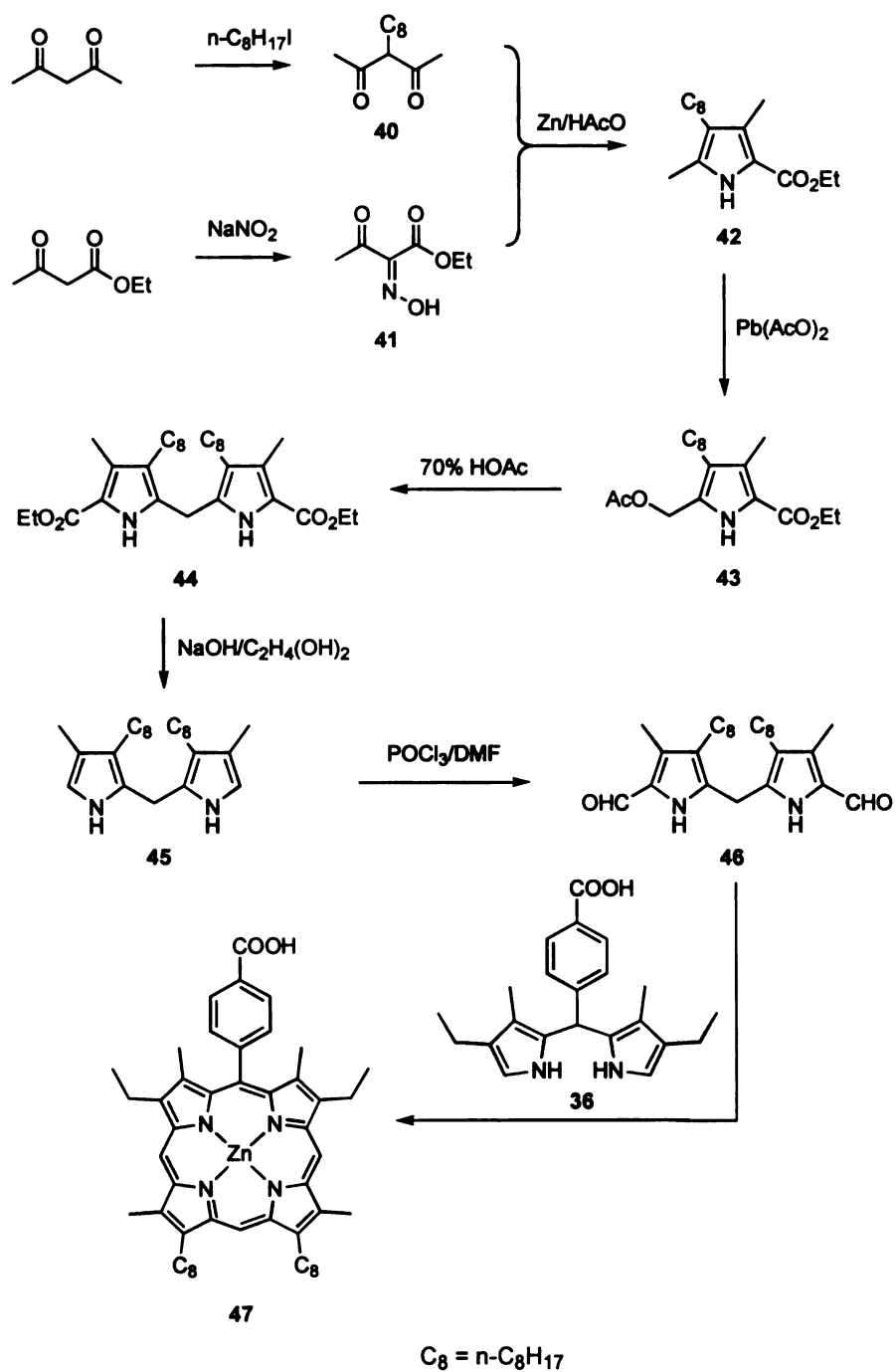


Scheme 6

organic solvents,⁴⁹ one of which is long chain alkyls. We initially tested this approach on porphyrin phenyl acid because it can be synthesized in a reasonable number of steps. To introduce long chain alkyls to a porphyrin molecule, we needed to initially synthesize a pyrrole substituted with such chain alkyls. As described in [Scheme 7](#), 1-iodo-octane reacted with 1,4-pentadione to form 3-acetylundecane-2-one **40**. Compound **40** was then condensed with α -oximinoacetoacetate under Knorr's pyrrole conditions to give **42**. Pyrrole **42** underwent oxidation and self-condensation to form dipyrromethane **44**. After saponification and decarboxylation, **45** was obtained and then treated with the Vilsmeier reagent to give diformyl-dipyrromethane **46**. The 2+2 McDonald condensation of **46** and **36**, using conditions described for making **38**, gave octylporphyrin phenyl acid **47** in 25% yield. Unfortunately, the use of long chain alkyls showed no significant improvement on the solubility of **47** compared to porphyrin **38**.

Another approach for increasing porphyrin solubility involved the incorporation of bulky substituents. In some cases, the poor solubility of porphyrins is caused by intermolecular aggregation,⁵⁰ which may be circumvented by the steric hindrance of bulky groups. In 1995, Therien⁵¹ synthesized 5-carboxyphenyl-10,15,20-tris(3',4',5'-trimethoxyphenyl)-porphyrin to study the electron transfer through the carboxylic acid dimer interface. This porphyrin exhibited good solubility in CH₂Cl₂. Considering the poor solubility we experienced for porphyrin phenyl acid, it was thought that porphyrin modified with trimethoxyphenyl groups may have enhanced solubility. Therefore, we decided to incorporate such groups in our porphyrin structure.

We tested this idea with porphyrin **48**, which contained one trimethoxyphenyl group because it was easily accessible through a one step reaction. As shown in



Scheme 7

Scheme 8, under conditions originally proposed by Chang,⁴⁷ and later optimized by Lindsey,⁵² a 1:1:1 mixture of 3,4,5-trimethoxybenzaldehyde, dipyrromethane **25**, and 4-carboxylic benzaldehyde condensed in the presence of TFA to give a mixture containing three porphyrins. This mixture was separated by careful chromatography on silica gel. Porphyrin **48**, the desired porphyrin, was obtained in 26% yield. It was then converted to its corresponding iron and zinc complexes. All forms of porphyrin phenyl acid showed good solubility in dichloromethane.

Encouraged by this success, the same strategy was employed to make porphyrin phenyl amidinium **54**. As described in **Scheme 9**, the cross condensation of a 1:1:1 mixture of 3,4,5-trimethoxybenzaldehyde, dipyrromethane **25** and 4-cyanobenzaldehyde also gave a mixture of porphyrins, from which **51** was separated and obtained in 36% yield. After nickel insertion, porphyrin phenyl nitrile **52** was converted to its corresponding amidinium **53** using the amide transfer reagent, $\text{ClAl}(\text{NH}_2)\text{CH}_3$. The nickel porphyrin **53** was subsequently transformed into its zinc and iron complexes via free base **54**. Again, the trimethoxyphenyl group showed a dramatic enhancement in the solubility and all forms of porphyrin phenyl amidinium compounds showed satisfactory solubility.

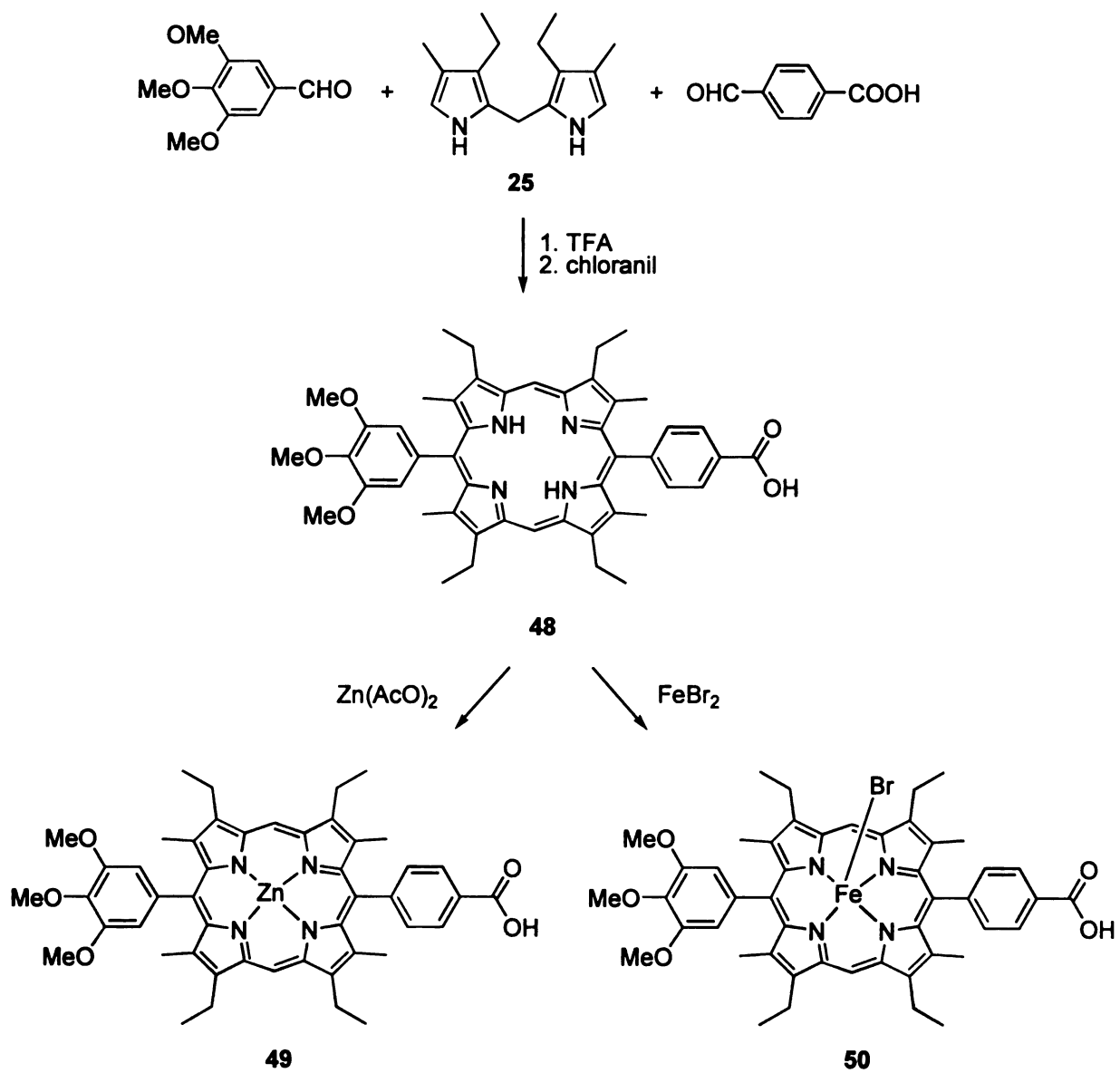
B. Porphyrin amidinium and carboxylic acid—coupling system

To introduce an amidinium group directly on the porphyrin ring, we initiated the synthesis of *meso*-formyloctaethylporphyrin, from which *meso*-cyano-octaethylporphyrin was made by using the Olah's method. However, our attempt to convert the nitrile to amidinium was unsuccessful, presumably due to the steric hindrance at the *meso* position. For this reason, we decided to shift the amidinium group to a β -position, where it was

less sterically encumbered. The synthetic strategy used here was to introduce an aldehyde group at β -position first. Then the aldehyde could be converted to a nitrile and then an amidinium group by using the methodology established previously. In addition, carboxylic acid derivatives could be synthesized from the aldehyde by oxidation, to generate another moiety for the proton interface. The first step in the synthesis of the porphyrin aldehyde was the synthesis of pyrrole **58** ([Scheme 10](#)). Ethyl bromoacetate reacted with 2,4-pentadione to give **57**, from which **58** was synthesized by employing Knorr's pyrrole condensation. Pyrrole **58** was brominated with bromine to give bromomethylpyrrole **59**, which condensed with ethyl 3,4-dimethylpyrrole-2-carboxylate to form dipyrromethane **60**. The ethyl acetate side chain of the dipyrromethane **60** was selectively reduced with diborane to form the hydroxyethyl derivative **61**. The ester groups of **61** was then saponified and decarboxylated by heating with sodium hydroxide in ethylene glycol to give compound **62**, which was one half of the target of porphyrin **66**.

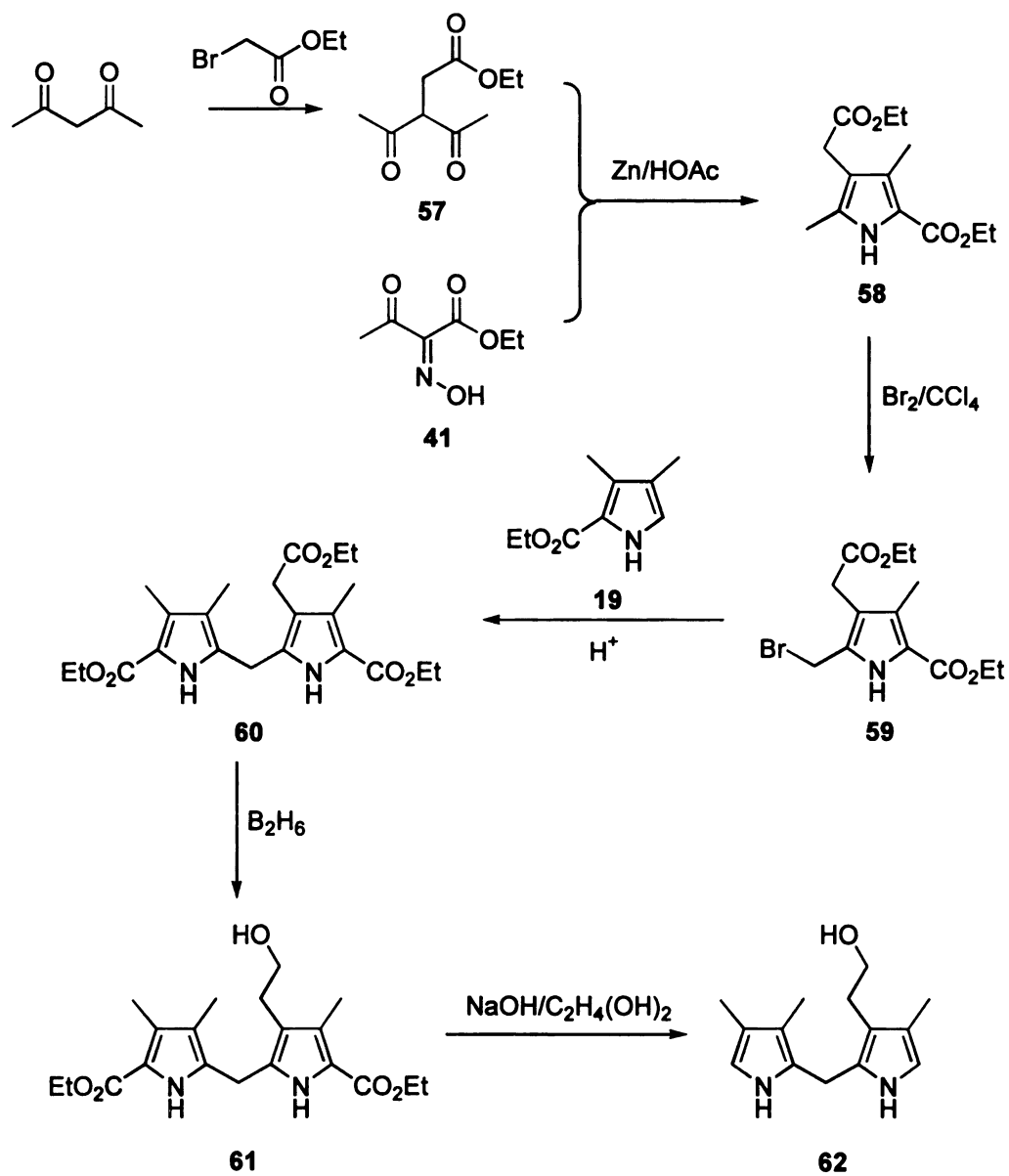
To synthesize the second half of porphyrin **66**, 3,4,5-trimethoxybenzaldehyde reacted with pyrrole **19** in the presence of an acid catalyst to give dipyrromethane **63** in 62% yield. Compound **63** was saponified and decarboxylated to form di- α free dipyrromethane **64**. After treatment with the Vilsmeier reagent, **64** was converted to its diformyl derivative **65**. Compound **62** and **65** were condensed in a "2+2" pattern under McDonald conditions to generate porphyrin **66** in 56% yield ([Scheme 11](#)).

The transformation of **66** to porphyrin aldehyde **70** was described in [Scheme 12](#). The hydroxyethyl porphyrin **66** was chlorinated with the Vilsmeier reagent to give chloroethyl porphyrin **67**. Vinyl porphyrin **68** was obtained by treating **67** with DBU in refluxing pyridine. In the previous study, Chang⁴⁹ found that the vinyl group could be

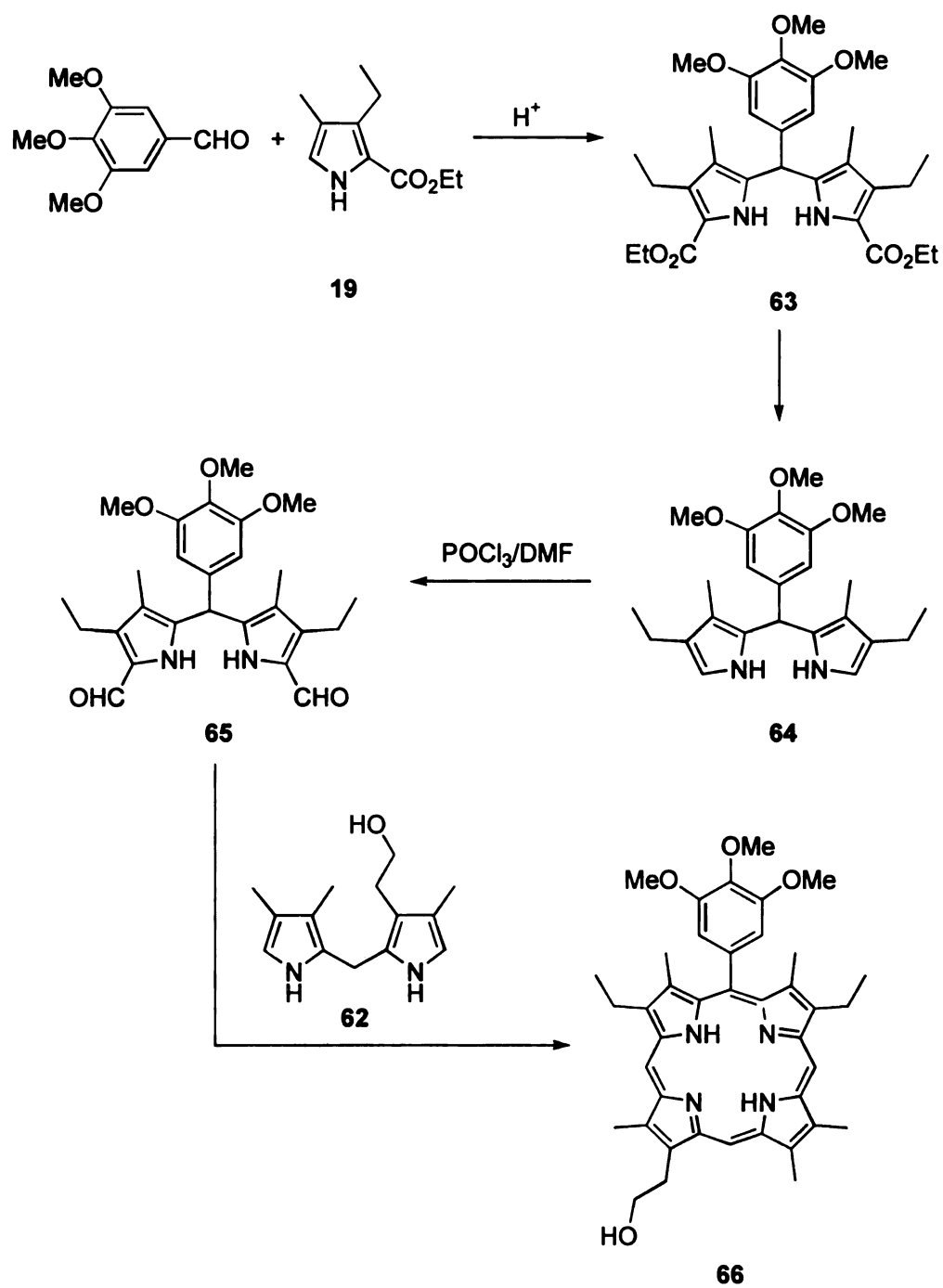


Scheme 8

Scheme 9



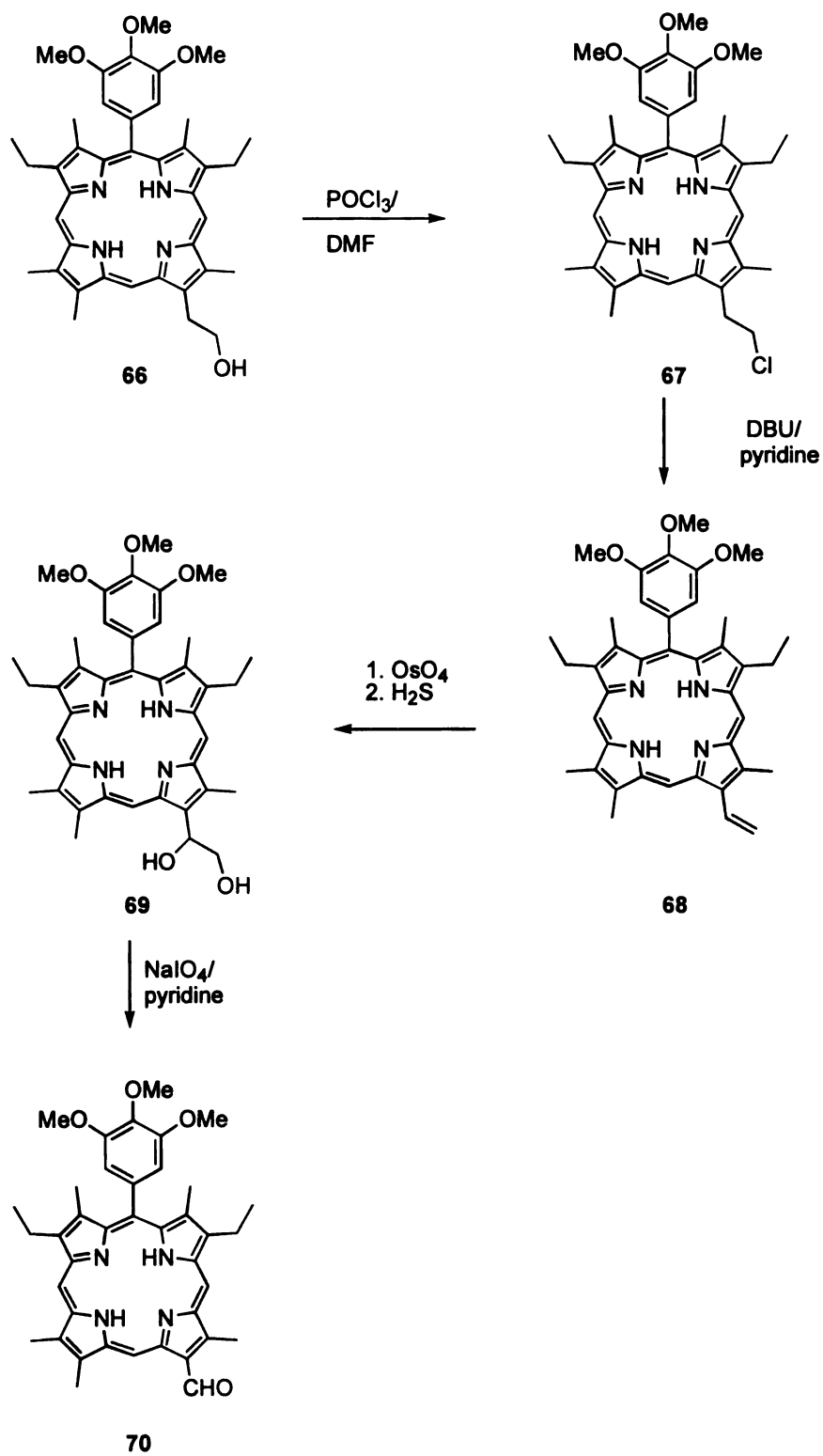
Scheme 10



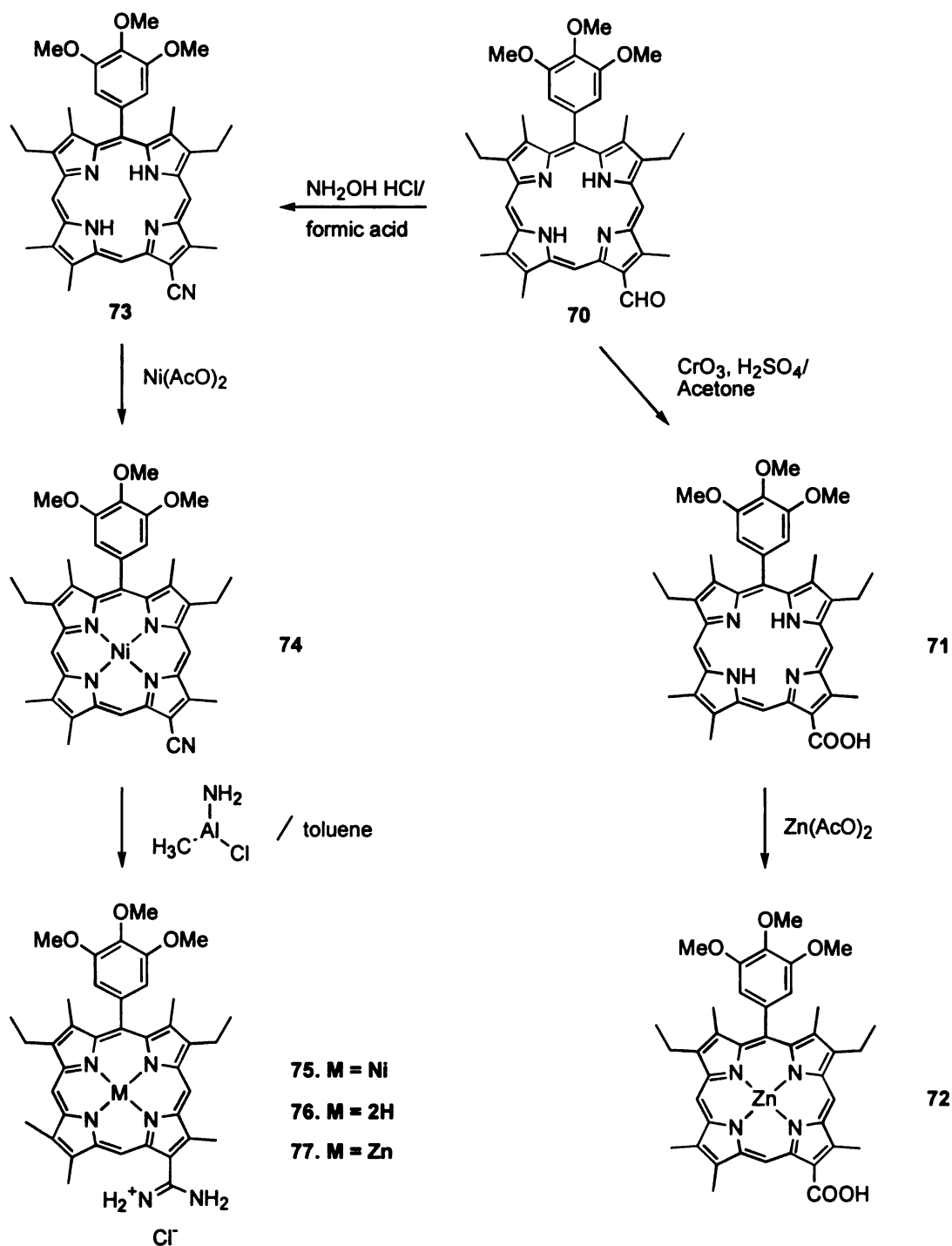
Scheme 11

conveniently converted to an aldehyde with osmium tetroxide/sodium periodate. In this case, the OsO₄ reaction was carried out in dichloromethane using one equivalent of osmium tetroxide (per porphyrin) in the presence of pyridine. This reaction had to be monitored carefully because prolonged reaction time caused side reactions, giving unidentified products. Maximum yields were obtained when the reaction was allowed to stir for 30 min. The resulting osmate ester was then treated with hydrogen sulfide to give porphyrin diol **69**. When the solution containing diol **69** in pyridine was treated with 5% sodium periodate, a precipitate formed and it was identified as porphyrin aldehyde **70**. The yield for the conversion from **69** to **70** was almost quantitative.

Both carboxylic acid porphyrin **71** and amidinium porphyrin **75** were derived from aldehyde **70** (Scheme 13). Oxidation of **70** with Jones' reagent⁵³ at 0 °C effected the conversion of aldehyde **70** to carboxylic acid **71**, as confirmed by both MS and NMR spectrum. Porphyrin **71** was then transformed to its zinc complex **72**. To make amidinium **75**, porphyrin **70** was first converted to porphyrin nitrile **73** by using hydroxylamine hydrochloride in refluxing formic acid. After nickel insertion, **74** was converted to **75** using ClAl(NH₂)CH₃. The amidinium porphyrin **75** was fully characterized by MS (FAB) and NMR, in which two characteristic peaks for NH protons of the amidinium group were observed at 6.82, 10.88 ppm with 1:1 ratio. Nickel porphyrin **75** was then converted to zinc complex **77** via free base **76** following the same procedure described previously. All porphyrins showed good solubility in CH₂Cl₂.



Scheme 12



Scheme 13

III. Properties

A. Coupling effects

UV-vis spectroscopy was used to probe the coupling between porphyrin chromophore and proton interface. The absorption spectrum of porphyrin amidinium **75** showed strong pH dependence. Significant spectral changes were observed upon protonation/deprotonation of the amidine group using acid/base. Figure 5 shows the spectral changes of **75** in the presence of various concentrations of DBU in CH_2Cl_2 . With the addition of this base, the porphyrin Soret band blue-shifted 7 nm (from 406 to 401 nm) and the Q band blue-shifted 9 nm (from 575 to 564 nm). Isosbestic points were maintained at 405 and 569 nm. Similar spectral changes were observed upon addition of other strong bases such as sodium methoxide and butyllithium. Furthermore, this process was found reversible and the original spectrum could be recovered when CH_2Cl_2 saturated with HClO_4 was added. The perturbation of the absorption profile upon protonation suggests that the porphyrinic chromophore of **75** is strongly coupled to the amidinium functional group and correspondingly the proton interface.

Conversely, when strong bases such as DBU were added to porphyrin **53**, which contained a phenyl spacer, only minor changes were observed (Figure 6). The conversion of amidinium to amidine had little effects on the electronic structure of the porphyrin. This independence of spectroscopic profile of **53** from the deprotonation of amidinium indicates that the porphyrinic chromophore is electronically decoupled from the amidinium group.

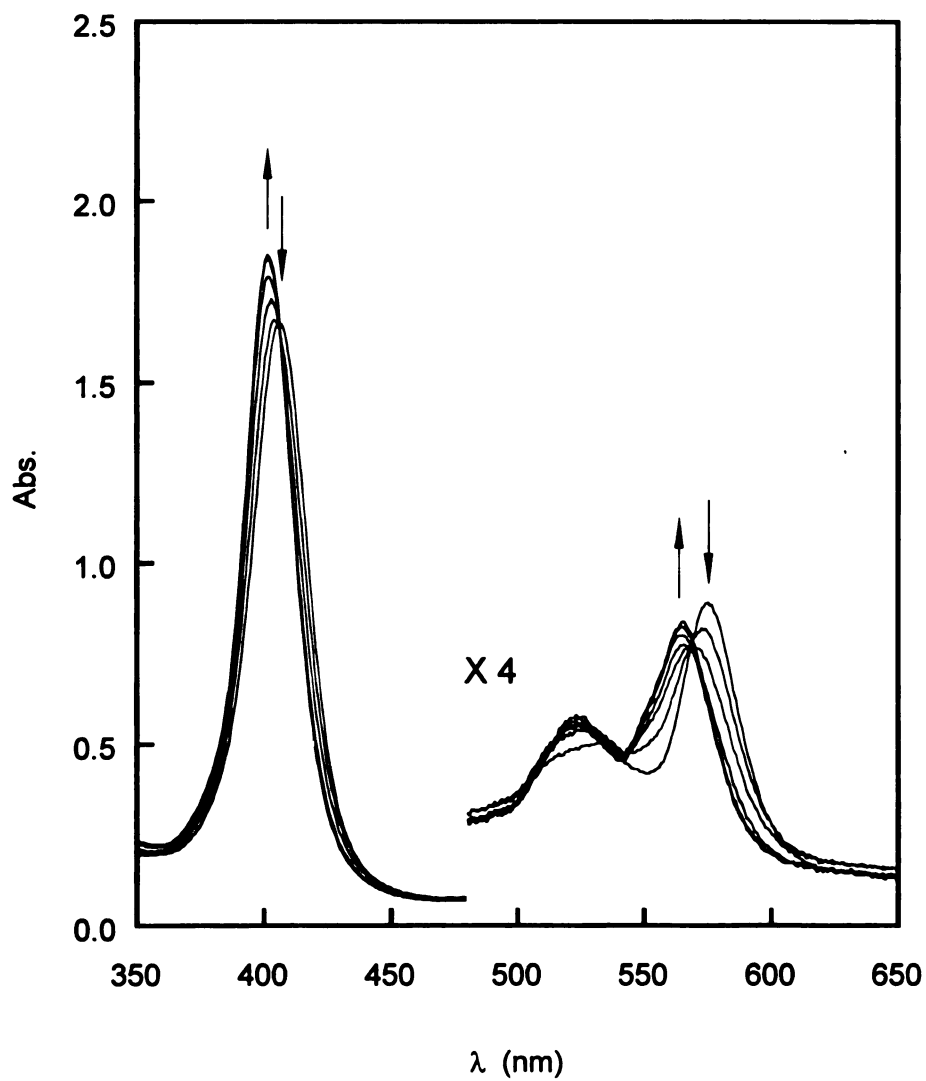


Figure 5. Absorption spectral changes of **75** upon addition of DBU in CH_2Cl_2 (The amount of DBU increase with arrows)

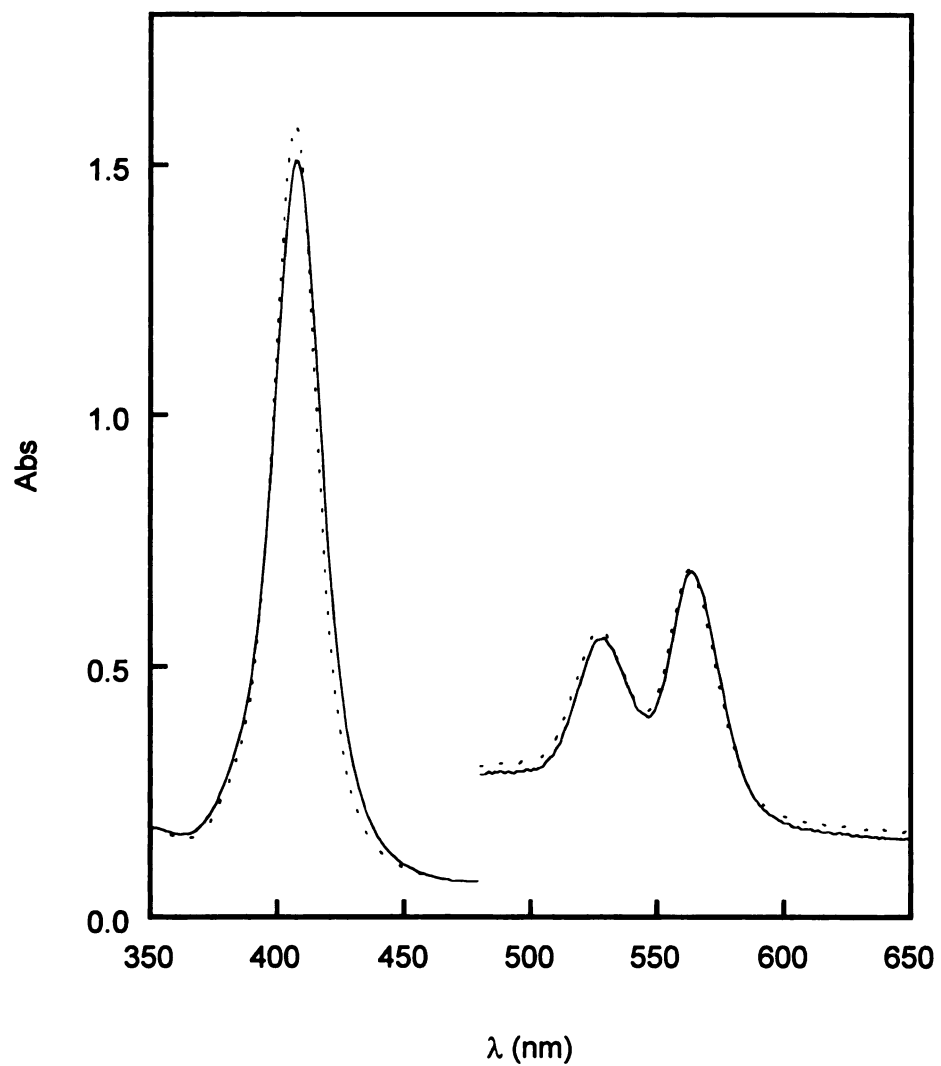


Figure 6. Absorption spectral of **53** in the absent (—) and the presence of 3.00 eq. DBU (·····) in CH_2Cl_2

B. IR studies

IR spectra were recorded for porphyrin amidinium **75** and its deprotonated form, namely, porphyrin amidine. Spectra are shown in Figure 7. In both cases, porphyrin ring vibrations remain unchanged, indicating that the blue shift of porphyrin spectra of **75** upon deprotonation is due to the electron withdrawing decrease of the amidine group and no redox change of the porphyrin π -system is involved. Previous IR and Raman spectroscopy studies⁵⁴ of amidine have established that the C=N stretching frequency is in the 1620-1700 cm^{-1} region. Accordingly, the peak at 1635 cm^{-1} (Figure 7b) is assigned to the C=N stretch of amidine. In the protonated form, the C=N stretching frequency of amidinium (Figure 7a) shifts to 1670 cm^{-1} . Similar changes in the C=N stretching frequency due to the protonation/deprotonation were also observed in other simple amidine compounds⁵⁵ (protonation of acetoamidine to acetoamidinium shifts the C=N stretching frequency from 1650 to 1690 cm^{-1}) and Schiff base compounds,⁵⁶ whose C=N stretching frequency displays 30-80 cm^{-1} blue shifts upon protonation. Theoretical calculations indicates that the protonation of nitrogen cause rehybridization of its orbitals. As a result, more nitrogen s-orbital participates in the formation of C-N bond, which gives a stronger C-N bond and higher force constant.⁵⁷ This diagnostic change in C=N stretching frequency of amidinium upon protonation/deprotonation should allow us to detect proton motion within the amidinium-carboxylate interface.

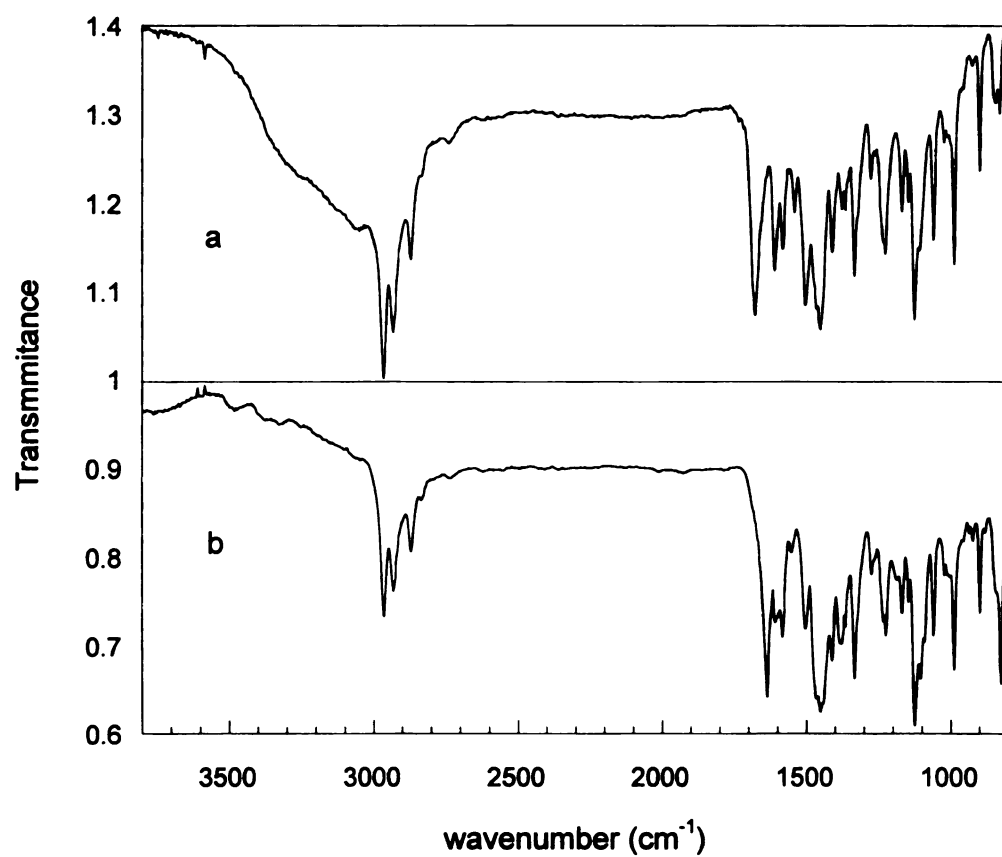


Figure 7. IR spectra of **75**. (a) protonation form, (b) deprotonation form

IV. Experimental

Materials and measurements. Reagents and solvents for synthesis were used as received unless otherwise stated. CH_2Cl_2 and DMF were distilled from CaH_2 . THF and toluene were freshly distilled from Na/benzophenone. Proton NMR spectra were recorded on Varian Gemini-300 in CDCl_3 (Cambridge Isotope laboratories) with the residual CHCl_3 as the internal standard set at 7.24 ppm. UV-vis spectra were measured on a Cary-17 spectrophotometer. Mass spectra were measured from a benchtop VG Trio-1 mass spectrometer. FAB-MS were obtained from a JEOL HX-110 HF double focusing spectrometer operating in the positive ion detection mode. Infrared spectra were obtained from coating samples on a KBr plate and recorded on a Nicolet IR/42 spectrometer. Analytical TLC was performed by using Eastman Kodak 13181 (100 μm thick) silica gel sheets. In column chromatography, 60-200 mesh silica gel was used.

4-Ethoxycarbonylbenzaldehyde 11

4-Carboxybenzaldehyde (15.0 g, 0.10 mol) was dissolved in ethanol (100 ml). Concentrated H_2SO_4 (1 ml) was added and the mixture was heated to reflux. After 1 h, the mixture was added to 200 g of ice and white precipitates formed. The mixture was neutralized by addition of sodium bicarbonate and the solid was collected by filtration and was washed with water and dried in air to give **11** in 67% yield (12 g, 0.067 mol). m.p. 65-67 °C; ^1H NMR (300 MHz, CDCl_3): δ 1.37 (3H, t, $\text{CO}_2\text{CH}_2\text{CH}_3$), 4.33 (2H, q, $\text{CO}_2\text{CH}_2\text{CH}_3$), 7.66 (4H, dd, aromatic), 10.5 (1H, CHO); MS found m/e 178, calcd. 178.06 for $\text{C}_{10}\text{H}_{10}\text{O}_3$.

4-Ethoxycarbonylbenzaldehyde glycol acetal 12

A 250-ml round-bottomed flask equipped with a reflux condenser was charged with **11** (8.9 g, 0.05 mol), ethylene glycol (31 g, 0.5 mol) and benzene (150 ml). *p*-Toluenesulfonic acid (0.15 g) was added and the mixture was heated to reflux until no more water was collected in the water collector. The reaction mixture was then cooled, washed with sodium bicarbonate solution, saturated sodium chloride solution and water, dried over sodium sulfate. The solvent was removed to give 9.5 g product (86% yield). ¹H NMR: δ 1.32 (3H, t, CO₂CH₂CH₃), 4.05 (4H, m, CH₂CH₂), 4.35 (2H, q, CO₂CH₂CH₃), 5.83 (1H, s, CH), 7.76 (4H, dd, aromatic); MS found *m/e* 222, calcd 222.09 for C₁₂H₁₄O₄.

4-hydroxymethylbenzaldehyde glycol acetal 13

A solution consisting of **12** (9.5 g, 0.043 mol) and lithium aluminum hydride (4.86 g, 0.128 mol) in 150 dry THF was stirred overnight at room temperature under nitrogen. Ethyl acetate (50 ml) was added dropwise to quench the reaction and the mixture was filtered to remove the solid residue. The filtrate was added to water and was extracted with methylene chloride several times. The organic layer was combined, dried over sodium sulfate and the solvent was removed to give 6.14 g product (81% yield). ¹H NMR (300 MHz, CDCl₃): δ 1.80 (1H, t, OH), 4.10 (4H, m, CH₂CH₂), 4.70 (2H, d, CH₂OH), 5.81 (1H, s, CH), 7.45 (4H, dd, aromatic); MS found *m/e* 180; calcd 180.08 for C₁₀H₁₂O₃.

Bis(5-ethoxycarbonyl-4-ethyl-3-methyl-2-pyrryl)(4-hydroxymethylphenyl)methane 20

A 250-ml round-bottomed flask equipped with a reflux condenser was charged with

acetal **12** (6.14g, 34.1 mmol), ethyl 3,4-dimethylpyrrole-2-carboxylate (12.33 g, 68.2 mmol), and 130 ml of absolute ethanol. A few drops of concentrated HCl were added, and the solution was refluxed under nitrogen with stirring. At the end of this time, TLC (silica gel, 20% EtOAc/hexane eluent) indicated the absence of starting material. The solvent was removed under reduced pressure, and the red oil was loaded onto a silica gel column. Elution with 20% EtOAc/hexane yielded the product as a pale yellow oil. Drying under high vacuum gave **20** as a pale yellow solid (11.5 g, 23.9 mmol) in 73% yield. ¹H NMR (300 MHz, CDCl₃): δ 1.10 (6H, t, CH₂CH₃), 1.31 (6H, t, CO₂CH₂CH₃), 1.79 (6H, s, CH₃), 2.72 (4H, q, CH₂CH₃), 4.24 (4H, q, CO₂CH₂CH₃), 4.70 (2H, d, CH₂OH), 5.48 (1H, s, CH₃), 7.33 (4H, dd, aromatic), 8.24 (2H, s, NH); MS (CI 70eV), m/e= 480, calcd 480.26 for C₂₈H₃₆N₂O₅.

Bis(4-ethyl-3-methyl-2-pyrryl)(4-hydroxymethylphenyl)methane 21

A 250-ml round-bottomed flask equipped with a reflux condenser was charged with **20** (11.5 g, 0.0239 mol), 120 ml of ethylene glycol, and 12 g of sodium hydroxide pellets. The reaction mixture was refluxed overnight under nitrogen. After cooling of the solution to room temperature, water was added and the precipitate was filtered off, washed with H₂O, and dried to afford the pure **21** (11.62 g, 0.022 mol) in 92.8%. ¹H NMR (300 MHz, CDCl₃): δ 1.17 (6H, t, CH₂CH₃), 1.79 (6H, s, CH₃), 2.42 (4H, q, CH₂CH₃), 4.68 (2H, s, CH₂OH), 5.49 (1H, d, CH), 7.21 (4H, dd, phenyl-H), 6.38 (2H, s, CH), 8.5 (2H, br, NH); MS found m/e= 336, calcd 336.22 for C₂₂H₂₈N₂O.

5, 5'-Diethoxycarbonyl-3, 3'-diethyl- 4, 4'-dimethyl-2, 2'-dipyrrolemethane 23

Lead tetraacetate (378 g, 0.69 mol) was slowly added with stirring, to a solution of ethyl 4-ethyl-3, 5-dimethylpyrrole-2-carboxylate (135 g, 0.69 mol) in HOAc (700 ml). The mixture was then warmed on a steam bath for 10 min before being poured into water (2 l). The precipitate was filtered, washed, and dried to give **22**, which was used directly for the next step without further purification.

The crude acetoxy compound was dissolved in 1500 ml of hot HOAc. The mixture was heated to reflux and water (300 ml) was added. The mixture was reflux for additional 10 min, poured into water (2.5 l) and left standing overnight, undisturbed. The precipitate was filtered, washed, and crystallized from methanol/water to give 115 g of the title compound (89%). m.p. 109-110 °C; ¹H NMR (300 MHz, CDCl₃): δ 1.05 (6H, t, CH₂CH₃), 1.30 (6H, t, CO₂CH₂CH₃), 2.25 (6H, s, CH₃), 2.40 (4H, q, CH₂CH₃), 3.85 (2H, s, CH₂), 4.25 (4H, q, CO₂CH₂CH₃), 8.95 (2H, br, NH); MS found m/e 374, calcd 374.22 for C₂₁H₃₀N₂O₄.

3,3'-Diethyl- 4,4'-dimethyl-2,2'-dipyrrolemethane 24

Dipyrrolylmethane diester **23** (11.1 g, 0.03 mol) from the last step was saponified and decarboxylated with sodium hydroxide in refluxing ethylene glycol under conditions described for **21**, to give 6.8 g of **24** (98%). ¹H NMR (300 MHz, CDCl₃): δ 1.10 (6H, t, CH₂CH₃), 2.05 (6H, s, CH₃), 2.45 (4H, q, CH₂CH₃), 3.85 (2H, s, CH₂), 6.38 (2H, s, α-H), 7.42 (2H, br, NH); MS (CI 70eV), m/e 230, calcd 230.18 for C₁₅H₂₂N₂.

3,3'-Diethyl-5,5'-diformyl- 4,4'-dimethyl-2,2'-dipyrrolemethane 25

A solution consisting of **24** (4.6 g, 0.020 mol) in DMF (30 ml) was cooled below 5 °C.

Benzoyl chloride (5 ml) was added dropwise over 10 minutes to the solution while maintaining the temperature below 5 °C. The solution was stirred at this temperature for 20 min, and then allowed to stir at room temperature for 1 hour. Aqueous ethanol (50 ml, 50%) containing sodium carbonate (10 g) was added and the mixture was warmed on a steam bath for 15 min. Water was added until all the sodium carbonate residue dissolved. After 4 hours at room temperature, the precipitate was collected and recrystallized from 95% ethanol to give **25** (4.4 g, 0.010 mol) in 77% yield. m.p. 205-206 °C; ¹H NMR (300 MHz, CDCl₃): δ 1.10 (6H, t, CH₂CH₃), 2.30 (6H, s, CH₃), 2.45 (4H, q, CH₂CH₃), 3.95 (2H, s, CH₂), 9.50 (2H, s, aldehyde), 10.50 (2H, br, NH); MS found m/e 286, calcd 286.17 for C₁₇H₂₂N₂O₂.

5-(4'-Hydroxymethylphenyl)-2,8,13,17-tetraethyl-3,7,12,18-tetramethylporphyrin **26**

A 500 ml round-bottomed flask was charged with **21** (1.018 g, 2.96 mmol), 5, 5'-diformyl-dipyrromethane **25** (1.0 g, 2.96 mmol), and 320 ml of THF:MeOH (2:1). The reaction mixture was purged with N₂, covered with foil, and 1.0 ml of HClO₄(aq) was added with stirring. The reaction was allowed to stir in the dark for 12 h, after which o-chloranil (1.2 g) was added and the reaction was stirred for an additional 12 h. The reaction mixture was poured into brine and extracted several times with methylene chloride. The organic layers were combined, washed with NaHCO₃(aq) and H₂O, and dried over Na₂SO₄. The solvent was removed on a rotary evaporator to give dark solid. After chromatography on silica gel (2% MeOH/CH₂Cl₂ eluent), the title compound (812 mg, 1.39 mmol) was isolated in 46.9% yield. m.p. >275 °C; UV-vis: λ_{max} 404, 503, 536, 569, 622 nm; ¹H NMR (300 MHz, CDCl₃): δ -3.50 (1H, s, NH), -3.35 (1H, s, NH), 1.72,

1.86 (6H each, t, CH_2CH_3), 2.42, 3.62 (6H each, s, CH_3), 4.1 (8H, m, CH_2CH_3), 5.18 (2H, s, CH_2), 7.88 (4H, m, aromatic), 9.92 (1H, s, *meso*), 10.14 (2H, s, *meso*); MS found m/e 584.2, calcd 584.35 for $\text{C}_{39}\text{H}_{44}\text{N}_4\text{O}$.

5-(4'-Formylphenyl)-2,8,13,17-tetraethyl-3,7,7,12,18-tetramethylporphyrin 27

A 250 ml round-bottomed flask was charged with porphyrin **26** (584 mg, 1.00 mmol), freshly distilled CH_2Cl_2 (100 ml), and PDC (1.01 g, 2.7 mmol). The reaction mixture was allowed to stir for 3 h under nitrogen, at which time TLC (2% MeOH/ CH_2Cl_2 eluent) indicated the complete conversion of starting material into product. The reaction mixture was poured into brine and extracted several times with CH_2Cl_2 . The organic layers were combined, washed several times with H_2O and dried (Na_2SO_4). After evaporation, the product was purified by chromatography on silica gel (2% MeOH/ CH_2Cl_2 eluent) to give the titled compound in 80% yield. m.p. >270 °C; UV-vis: λ_{max} 401, 505, 536, 569, 630 nm; ^1H NMR (300 MHz, CDCl_3): δ -3.30 (1H, s, NH), -3.15 (1H, s, NH), 1.72, 1.86 (6H each, t, CH_2CH_3), 2.43, 3.64 (6H each, s, CH_3), 4.05 (8H, m, CH_2CH_3), 8.40 (4H, m, aromatic), 9.96 (1H, s, *meso*), 10.18 (2H, s, *meso*), 11.95 (1H, s, aldehyde); MS found m/e 582, calcd 582.34 for $\text{C}_{39}\text{H}_{42}\text{N}_4\text{O}$.

5-(4'-cyanophenyl)-2,8,13,17-tetraethyl-3,7,7,12,18-tetramethylporphyrin 28

A 100-ml round-bottomed flask equipped with a reflux condenser was charged with porphyrin aldehyde **27** (232 mg, 0.40 mmol), hydroxyamine hydrochloride (200 mg, 1.4 mmol) and 10 ml of 95% formic acid. The reaction mixture was heated at reflux overnight under nitrogen atmosphere. The solution was cooled to room temperature and

poured into water. It was then neutralized with sodium bicarbonate before being extracted several times with methylene chloride. The organic layers were combined and washed with water twice. After drying over sodium sulfate, the solvent was removed on a rotary evaporator and the resulting solid was chromatographed on silica gel (dichloromethane eluent) to give **28** (198 mg, 0.34 mmol) in 85% yield. m.p. >270 °C; UV-vis: λ_{max} 402, 505, 536, 570, 630 nm; ^1H NMR (300 MHz, CDCl_3): δ -3.30, -3.15 (1H each, s, NH), 1.76, 1.82 (6H each, t, CH_2CH_3), 2.40, 3.62 (6H each, s, CH_3), 4.05 (8H, m, CH_2CH_3), 8.12 (4H, m, aromatic), 9.96 (1H, s, *meso*), 10.18 (2H, s, *meso*); MS found m/e 579, calcd 579.34 for $\text{C}_{39}\text{H}_{41}\text{N}_5$.

Nickel 5-(4'-cyanophenyl)-2,8,13,17-tetraethyl-3,7,7,12,18-tetramethylporphyrin **29**

A 100-ml round-bottomed flask equipped with a reflux condenser was charged with porphyrin **28** (115 mg, 0.2 mmol) and DMF (20 ml). The reaction mixture was refluxed until chelation was completed (monitored by both UV-vis and TLC, ca. 1 hours). Water was added, followed by dichloromethane. The organic layer was washed several times with water. After removal of solvent, the solid residue was chromatographed on silica (eluted with dichloromethane) to give **29** (116 mg, 0.18 mmol) in 91% yield. m.p. >270 °C; UV-vis: λ_{max} 399, 521, 556 nm; MS found m/e 635; calcd 635.26 for $\text{C}_{39}\text{H}_{39}\text{N}_5\text{Ni}$.

Nickel 5-(4'-amidiniumphenyl)-2,8,13,17-tetraethyl-3,7,7,12,18-tetramethylporphyrin chloride **30**

To a solution of porphyrin **29** (116 mg, 0.18 mmol) in dry toluene (15 ml), was added a solution of chloromethylaluminum amide (2.0 M in toluene, 1.0 ml). This solution was

heated at 80 °C for 48 h under argon atmosphere. The reaction mixture was cooled and the aluminum complex was decomposed by carefully pouring the solution into a slurry of silica gel (5 g) in chloroform. The mixture was stirred for 5 min and the silica gel was filtered. The filtercake was further washed with methanol. Evaporation of the filtrate and purification of the residue by chromatography on silica gel (25% methanol in dichloromethane) afforded the title compound (96 mg, 0.15 mmol) in 82% yield. m.p. >270 °C; UV-vis: λ_{max} 398.0, 521.0, 556.0 nm; ^1H NMR (300 MHz, DMSO- d_6): δ 1.58, 1.73 (6H each, t, CH_2CH_3), 2.23, 3.45 (6H each, s, CH_3), 3.85 (8H, m, CH_2CH_3), 8.15 (4H, m, aromatic), 9.26, 9.68 (2H each, s, NH_2 of amidinium), 9.70 (1H, s, *meso*), 9.76 (2H, s, *meso*); MS (FAB) found m/e 653.2 for (MH^+), calcd 653.29 for $\text{C}_{39}\text{H}_{43}\text{N}_6\text{Ni}$.

5-(4'-Amidiniumphenyl)-2,8,13,17-tetraethyl-3,7,7,12,18-tetramethylporphyrin chloride
31

Concentrated H_2SO_4 (2 ml) was added to nickel porphyrin **30** (80 mg, 0.122 mmol). The reaction mixture was stirred at room temperature for 1 h before diluted carefully with ice. The solution was then neutralized with Na_2CO_3 and the porphyrin was collected by filtration. The crude product was chromatographed on a silica (30% MeOH in CH_2Cl_2) afforded 72 mg of **31** (96%). m.p. >270 °C; UV-vis: λ_{max} 402, 501, 535, 570, 623 nm.

Zinc 5-(4'-amidiniumphenyl)-2,8,13,17-tetraethyl-3,7,7,12,18-tetramethylporphyrin chloride
32

Zinc chloride (0.1 g) in methanol was added to a solution of porphyrin **31** (20 mg, 0.0335 mmol) in 10 ml of DMF. The mixture was heated at 60°C until the zinc insertion was

complete (monitored by UV-vis). Then water was added, followed by CH_2Cl_2 . The organic layers was separated and washed with water several times and dried over Na_2SO_4 . After evaporation of solvent, the crude product was purified on TLC plate (20% MeOH in CH_2Cl_2) to give 20 mg of **32** (90%). m.p. $>270^\circ\text{C}$; UV-vis: λ_{max} 406, 536, 571 nm; ^1H NMR (300 MHz, DMSO-d_6): δ 1.58, 1.73 (6H each, t, CH_2CH_3), 2.23, 3.45 (6H each, s, CH_3), 3.85 (8H, m, CH_2CH_3), 8.20 (4H, m, aromatic), 9.40, 9.70 (2H each, s, NH_2 of amidinium), 9.75 (1H, s, meso), 9.80 (2H, s, meso); MS (FAB) found m/e 659.2 for (MH^+), calcd 659.28 for $\text{C}_{39}\text{H}_{43}\text{N}_6\text{Zn}$.

Iron (4'-amidiniumphenyl)-2,8,13,17-tetraethyl-3,7,12,18-tetramethylporphyrin bromide **33**

Iron(II) bromide (50 mg, 0.23 mmol) was added to a solution of porphyrin free base **30** (30 mg, 0.050 mmol) in anhydrous THF containing pyridine (10 drops). The mixture was refluxed under nitrogen for 1h. The solvent was removed under reduced pressure and the residue was chromatographed on a column of silica gel. The first and second fractions eluting from the column contained iron porphyrin and its μ -oxo dimer, respectively, and were combined. The solution was treated with 2 M HBr, dried over Na_2SO_4 and brought to dryness under vacuum to give iron porphyrin **33** (31 mg, 0.038 mmol) in 76% yield. UV-vis: λ_{max} 389, 511, 641 nm; MS (FAB) found 651.1 for (Fe-porphyrin + H), calcd 651.29 for $\text{C}_{39}\text{H}_{43}\text{N}_6\text{Fe}$.

Bis(5-ethoxycarbonyl-4-ethyl-3-methyl-2-pyrrolyl)(4-ethoxycarbonylphenyl)methane **34**

4-Carboxybenzaldehyde (1.5 g, 0.01 mol) was condensed with ethyl 3, 4-dimethylpyrrol-

2-carboxylate (3.6 g, 20.0 mol) under conditions described for **20**, yielding 3.8 g (69%) of the title compound. m.p. >270 °C; ¹H NMR (300 MHz, CDCl₃): δ 1.10 (6H, t, CH₂CH₃), 1.31 (6H, t, CO₂CH₂CH₃), 1.39 (6H, t, CO₂CH₂CH₃), 1.79 (6H, s, CH₃), 2.74 (4H, q, CH₂CH₃), 4.26 (4H, q, CO₂CH₂CH₃), 4.38 (4H, q, CO₂CH₂CH₃), 5.53 (1H, s, CH₃), 7.18, 8.10 (2H each, d, aromatic), 8.28 (2H, s, NH); MS found m/e 522, calcd 522.27 for C₃₀H₃₈N₂O₆.

Bis(4-ethyl-3-methyl-2-pyrrolyl)(4-carboxyphenyl)methane 35

Dipyrrolylmethane **34** (3.8 g, 6.88 mmol) was treated with sodium hydroxide in ethylene glycol under conditions described for **21**, yielding 2.16 g of the titled compound (90% yield). ¹H NMR (300 MHz, CDCl₃): δ 1.17 (6H, t, CH₂CH₃), 1.79 (6H, s, CH₃), 2.42 (4H, q, CH₂CH₃), 5.49 (1H, s, CH₃), 6.38 (2H, s, α-H of pyrrole), 7.12, 7.30 (2H each, d, aromatic), 8.50 (2H, s, NH); MS found m/e 350, calcd 350.20 for C₂₂H₂₆N₂O₂.

Zinc 5-(4'-carboxyphenyl)-2,8,13,17-tetraethyl-3,7,12,18-tetramethylporphyrin 36

A 500 ml round-bottomed flask was charged with **35** (1.05 g, 3.00 mmol), **25** (0.86 g, 3.00 mmol) and 300 ml of dry dichloromethane. The reaction mixture was purged with nitrogen, covered with alumna foil, and was added a solution of p-toluenesulfonic acid hydrate (2.0 g) in methanol (36 ml). The reaction was allowed to stir in the dark for 12 h, before adding a saturated solution of zinc acetate in methanol (32 ml). After 12 h, p-chloranil (1.2 g) was added and the reaction was stirred for an additional 12 h. The reaction mixture was neutralized with Na₂CO₃ and poured into brine and extracted several times with CH₂Cl₂. The organic layers were combined, washed with water and

dried with Na_2SO_4 . The solvent was evaporated on a rotary evaporator to give a dark solid. After chromatography on silica gel (4% $\text{MeOH}/\text{CH}_2\text{Cl}_2$ eluent), the product (960 mg, 1.45 mol) was isolated in 48% yield. m.p. $>270^\circ\text{C}$; UV-vis: λ_{max} 404, 534, 570 nm; ^1H NMR (300 MHz, $\text{CDCl}_3/\text{CD}_3\text{OD}$): δ 1.72, 1.81 (6H each, CH_2CH_3), 2.32, 3.62 (6H each, s, CH_3), 3.98 (8H, m, CH_2CH_3), 8.22 (4H, m, aromatic), 9.92 (1H, s, meso), 10.04 (2H, s, meso); MS found m/e 660, calcd 660.24 for $\text{C}_{39}\text{H}_{40}\text{N}_4\text{O}_2\text{Zn}$.

Iron 5-(4'-carboxyphenyl)-2,8,13,17-tetraethyl-3,7,12,18-tetramethylporphyrin 38

To a solution of zinc porphyrin **36** (132 mg, 0.2 mmol) in 10% $\text{MeOH}/\text{CH}_2\text{Cl}_2$ (30 ml) was added 10% $\text{HCl}(\text{aq})$. The mixture was stirred for 20 min and neutralized with saturated sodium bicarbonate solution. The organic layer was then washed with water and dried with Na_2SO_4 . The solvent was removed under reduced pressure to give 120 mg of free base **37**.

The porphyrin **37** (60 mg, 0.1 mmol) was treated with FeBr_2 in THF under condition described previously, giving 45 mg of iron(III) porphyrin **38** (70%). m.p. $>275^\circ\text{C}$; UV-vis: λ_{max} 389, 511, 641 nm; MS found m/e 652, calcd 652.25 for $\text{C}_{39}\text{H}_{40}\text{FeN}_4\text{O}_2$.

Nickel 5-(4'-carboxyphenyl)-2,8,13,17-tetraethyl-3,7,12,18-tetramethylporphyrin 39

Nickel insertion of **37** (60 mg, 0.1 mmol) was accomplished by using $\text{Ni}(\text{AcO})_2$ in DMF following the procedure described before, affording porphyrin **39** (53 mg, 0.080 mmol) in 80% yield. m.p. $>275^\circ\text{C}$; UV-vis: λ_{max} 400, 522, 558 nm; MS found m/e 654, calcd 654.25 for $\text{C}_{39}\text{H}_{40}\text{N}_4\text{NiO}_2$.

3-Acetylundecane-2-one 40

In a 3000 ml 3-necked flask were placed anhydrous potassium carbonate (75 g, 0.50 mol), potassium iodide (15 g, 0.09 mol), 2-butanone (100 ml), 2, 4-pentanedione (50 g, 0.50 mol) and 1-iodooctane (120 g, 0.50 mol). On heating to reflux, the reaction became violent and the heating had to be withdrawn. When the reaction had subsided, it was refluxed for 4 hours using hot water bath. The reaction mixture was diluted with acetone and the salts were filtered off and washed further with acetone. The filtrates were concentrated under vacuum and the oil was distilled under reduced pressure to give the title compound as light yellow oil (53 g, 0.25 mol, 43% yield). b. p. 110°C-112 °C/15 mmHg.

Ethyl 3,5-dimethyl-4-octylpyrrole-2-carboxylate 42

Ethyl acetoacetate (31.2 g, 0.20 mol) in glacial acetic acid (30 ml) was cooled in an ice bath. Sodium nitrite (14.0 g, 0.20 mol) in water (15 ml) was added dropwise over 1 hours with stirring. The resulting solution of ethyl α -oximinoacetoacetate **41** was added dropwise, along with zinc dust (326 g, 5.0 mol), to a stirred solution of **40** (42.0 g, 0.20 mol) in acetic acid (1200 ml) over 1 hour. The temperature was kept under 80 °C during the reaction process. After the addition, the reaction was allowed to stir for 0.5 h. Then the mixture was decanted in cold water and left overnight. The resulting solid was filtered off and washed with tap water. The filter cake was dissolved in dichloromethane and filtered to remove the zinc dust. The organic phase was evaporated in vacuo and the solid was crystallized from methanol/water to give product as white crystals (22.3 g, 0.08 mol, 40% yield). ¹H NMR (300 MHz, CDCl₃): δ 0.88 (3H, t, CH₃ of octyl), 1.25 (12 H,

m, CH₂ of octyl), 1.32 (3H, t, CO₂CH₂CH₃), 2.15, 2.25 (3H each, s, CH₃), 2.30 (2H, , t, CH₂), 4.32 (2H, q, CO₂CH₂CH₃), 8.50 (1H, s, NH); MS found m/e 279, calcd 279.22 for C₁₇H₂₉NO₂.

5,5'-Diethoxycarbonyl-4,4'-dimethyl-3,3'-dioctyl-2,2'-dipyrrolylmethane 44

Pyrrole **42** (22.3 g, 0.08 mol) from the last step was converted to **44** via its acetoxymethyl derivative **43** following the procedure described for making **23**, yielding 17.3 g of product (80% base on **42**). . m.p. 101-102 °C; ¹H NMR (300 MHz, CDCl₃): δ 0.85 (3H, t, CH₃ of octyl), 2.12 (3H, t, CO₂CH₂CH₃), 1.20 (12H, m, CH₂ of octyl), 2.20 (3H, s, CH₃), 2.25 (2H, t, CH₂ of octyl), 3.75 (2H, s, CH₂), 4.15 (2H, q, CO₂CH₂CH₃), 8.80 (2H, s, NH); MS found m/e 542, calcd 542.42 for C₃₃H₅₄N₂O₄.

4,4'-Dimethyl-3,3'-dioctyl-2,2'-dipyrrolylmethane 45

Dipyrrolylmethane **43** (16.2 g, 0.30 mol) from the last step was saponified and decarboxylated with sodium hydroxide in refluxing ethylene glycol using conditions described for **21**, generating 9.8 g of product (82%). ¹H NMR (300 MHz, CDCl₃): δ 0.82 (3H, t, CH₃ of octyl), 1.30 (12H, m, CH₂ of octyl), 2.00 (3H, s, CH₃), 2.38 (2H, t, CH₂ of octyl), 3.78 (2H, s, CH₂), 6.34 (2H, s, α-H of pyrrole), 7.34 (2H, s, NH); MS found m/e 398, calcd 398.37 for C₂₇H₄₆N₂.

5,5'-Diformyl-4,4'-dimethyl-3,3'-dioctyl-2,2'-dipyrrolylmethane 46

Dipyrrolylmethane **45** (4.0 g, 0.01 mol) was formylated with the Vilsmeier reagent generated in situ by addition of POCl₃ to DMF using conditions described for **25**, to

afford 4.1 g of the title compound (88%). m.p. 157-158 °C; ^1H NMR (300 MHz, CDCl_3): δ 0.82 (3H, t, CH_3 of octyl), 1.30 (12H, m, CH_2 of octyl), 2.25 (3H, s, CH_3), 2.40 (2H, t, CH_2 of octyl), 3.90 (2H, s, CH_2), 9.50 (2H, s, aldehyde), 10.64 (2H, s, NH); MS (CI 70 eV), m/e 454, calcd 454.36 for $\text{C}_{29}\text{H}_{46}\text{N}_2\text{O}_2$.

Zinc 5-(4'-carboxyphenyl)-2,8-diethyl-3,7,12,18-tetramethyl-13,17-dioctylporphyrin 47

Condensation of **45** (1.37 g, 3.00 mmol) with **25** (0.86 g, 3.00 mmol) using conditions described for **36** afforded 620 mg dioctylporphyrin **47** (25%). m.p. >275 °C; UV-vis: λ_{max} 403, 534, 571 nm; ^1H NMR (300 MHz, $\text{CDCl}_3/\text{CD}_3\text{OD}$): δ 0.85 (6H, t, CH_3 of octyl), 1.40 (24H, m, CH_2 of octyl), 1.72 (6H, t, CH_2CH_3), 2.32, 3.62 (6H each, s, CH_3), 3.98 (4H, m, CH_2CH_3), 4.05 (4H, t, CH_2 of octyl), 8.22 (4H, m, aromatic), 9.92 (1H, s, *meso*), 10.04 (2H, s, *meso*); MS found m/e 830, calcd 828.43 for $\text{C}_{51}\text{H}_{64}\text{N}_4\text{O}_2\text{Zn}$.

5-(4'-Carboxyphenyl)-2,8,12,18-tetraethyl-20-(3',4',5'-trimethoxyphenyl)-3,7,13,17-tetramethylporphyrin 48

A 100 ml round-bottomed flask was charged with 4-carboxybenzaldehyde (0.75 g, 5.0 mmol), dipyrromethane **25** (2.30 g, 10.0 mmol), and 3,4,5-trimethoxybenzaldehyde (1.00 g, 5.0 mmol) in freshly distilled dichloromethane (200 ml). The reaction mixture was purged with nitrogen, covered with foil, and trifluoroacetic acid (0.4 ml) was added with stirring. The reaction was allowed to stir in the dark for 12 h. Before being neutralized by the addition of sodium acetate (2.5 g). After which p-chloranil (1.5 g, 6.1 mmol) was added and the reaction stirred for an additional 12 h. The solvent was removed under reduced pressure to give a dark solid. Chromatography on silica gel

(dichloromethane first, then 4% methanol in dichloromethane), first eluted 5, 15-bis(3',4',5'-trimethoxyphenyl)porphyrin, followed by desired porphyrin **48** (0.98 g, 26%). m.p. >275 °C; UV-vis: λ_{max} 408, 506, 540, 573, 625; ^1H NMR (300 MHz, CDCl_3): δ - 2.25 (2H, s, NH), 1.85 (12H, m, CH_2CH_3), 2.50, 2.65 (6H each, s, CH_3), 3.90 (6H, s, *m*- OCH_3), 4.00 (8H, m, CH_2CH_3), 4.20 (3H, s *p*- OCH_3), 7.32 (2H, s, aromatic), 8.25, 8.55 (2H each, d, aromatic), 10.25 (2H, s, *meso* proton); MS found *m/e* 764, calcd 764.39 for $\text{C}_{48}\text{H}_{52}\text{N}_4\text{O}_5$.

Zinc 5-(4'-carboxyphenyl)-2,8,12,18-tetraethyl-20-(3',4',5'-trimethoxyphenyl)-3,7,13,17-tetramethylporphyrin **49**

Saturated zinc acetate in methanol (0.5 ml) was added to a solution of free base **48** (76 mg, 0.1 mmol) in dichloromethane (20 ml). The mixture was heated reflux for 20 min and then the solution was washed with water and dried over sodium sulfate. After evaporation of solvent, the residue was chromatographed on silica gel (4% methanol in dichloromethane) to give 80 mg of zinc porphyrin **49** (96%). m.p. >275 °C; UV-vis: λ_{max} 411, 539, 573; MS found *m/e* 826, calcd 826.32 for $\text{C}_{48}\text{H}_{50}\text{N}_4\text{O}_5\text{Zn}$.

Iron 5-(4'-carboxyphenyl)-2,8,12,18-tetraethyl-20-(3',4',5'-trimethoxyphenyl)-3,7,13,17-tetramethylporphyrin **50**

The iron insertion was accomplished by using the FeBr_2/THF method described previously, yielding iron porphyrin **51** in 75% yield. m.p. >275 °C; UV-vis: λ_{max} 390, 512, 642 nm; MS found *m/e* 818, calcd 818.31 for $\text{C}_{48}\text{H}_{50}\text{N}_4\text{O}_5\text{Fe}$.

5-(4'-Cyanophenyl)-2,8,12,18-tetraethyl-20-(3',4',5'-trimethoxyphenyl)-3,7,13,17-tetramethylporphyrin 51

Cross condensation of 4-cyanobenzaldehyde (0.65 g, 5.0 mmol), dipyrromethane **25** (2.30 g, 10.0 mmol), and 3,4,5-trimethoxybenzaldehyde under conditions described previously afforded 1.34 g porphyrin **51** (36%). m.p. >275 °C; ¹H NMR (300MHz, CDCl₃): δ -2.30 (2H, s, NH), 1.85 (12H, m, CH₂CH₃), 2.40, 2.65 (6H each, s, CH₃), 3.90 (6H, s, *m*-OCH₃), 4.00 (8H, m, *p*-CH₂CH₃), 4.20 (3H, s OCH₃), 7.30 (2H, s, aromatic), 8.00, 8.20 (2H each, d, aromatic), 10.25 (2H, s, *meso* proton); MS found 745, calcd 745.40 for C₄₈H₅₁N₅O₃.

Nickel 5-(4'-cyanophenyl)-2,8,12,18-tetraethyl-20-(3',4',5'-trimethoxyphenyl)-3,7,13,17-tetramethylporphyrin 52

Free base **51** (370 mg, 0.5 mmol) was treated with nickel acetate under condition described previous, yielding 315 mg of nickel porphyrin **52** (78%). m.p. >275 °C; UV-vis: λ_{max}: 407, 527, 563; MS found m/e 801, calcd 801.32 for C₄₈H₄₉N₅NiO₃.

Nickel 5-(4'-amidiniumphenyl)-2,8,12,18-tetraethyl-20-(3',4',5'-trimethoxyphenyl)-3,7,13,17-tetramethylporphyrin chloride 53

Nickel porphyrin **52** (160 mg, 0.20 mmol) was treated with chloromethylaluminum amide (1 ml, 1.0 mmol) under conditions described before, giving 147 mg of porphyrin amidinium chloride **53** (86%). m.p. >275 °C; UV-vis: λ_{max} 408, 528, 563; ¹H NMR (300 MHz, CDCl₃): δ 1.5, 1.55 (6H each, t, CH₂CH₃), 2.10, 2.35 (6H each, s, CH₃), 3.56, 3.64 (4H each, q, CH₂CH₃), 3.80 (6H, s, *m*-OCH₃), 4.21 (3H, s *p*-OCH₃), 7.08 (2H, s,

aromatic), 8.04, 8.20 (2H each, d, aromatic), 8.32, 10.02 (2H each, s, NH of amidinium), 9.40 (2H, s, *meso* proton); MS (FAB) found m/e 819.3 (MH^+), calcd 819.35 for $C_{48}H_{53}N_6O_3Ni$.

Zinc 5-(4'-amidiniumphenyl)-2,8,12,18-tetraethyl-20-(3',4',5'-trimethoxyphenyl)-3,7,13,17-tetramethylporphyrin chloride 55

Porphyrin **53** was demetallated using concentrated sulfuric acid under conditions described previously to give free base **54**. The zinc insertion of the free base was accomplished by using the $ZnCl_2$ /DMF method described previously, giving zinc porphyrin **55** in 95% yield. m.p. >275 °C; UV-vis: λ_{max} 411, 539, 573; MS (FAB) found m/e 825.2 (MH^+), calcd 825.35 for $C_{48}H_{53}N_6O_3Zn$.

Iron 5-(4'-amidiniumphenyl)-2,8,12,18-tetraethyl-20-(3',4',5'-trimethoxyphenyl)-3,7,13,17-tetramethylporphyrin chloride 56

Free base **54** (22.0 mg, 0.030 mmol) was treated with $FeBr_2$ in THF under conditions described previously, affording 18.0 mg of iron porphyrin **56** (73%). m.p. >275 °C; UV-vis: 390, 512, 642; MS (FAB) found 817.5 (MH^+), calcd 817.35 for $C_{48}H_{53}N_6O_3Fe$.

Ethyl 3-acetyl-4-oxopentanoate 57

In a 3-l 3-necked flask were placed anhydrous potassium carbonate (415.08 g, 3 mol), potassium iodide (90.3 g, 0.54 mol), 2-butanone (100 ml), 2, 4-pentanedione (308 ml, 3 mol) and ethyl chloroacetate (367.5 g, 3 mol). On heating to reflux, the reaction became violent and the heating was withdrawn. When the reaction subsided, it was refluxed for 4

hours. The reaction mixture was diluted with acetone and the salts were filtered off and washed further with acetone. The filtrates were concentrated in vacuo and the oil was distilled under reduced pressure to give the product as light yellow oil (236 g, 1.3 mol, 43% yield). b.p. 140°C-145°C/15mmHg; ^1H NMR (300 MHz, CDCl_3): two tautomers was observed: 1) for keto: δ 1.12 (3H, t ($J = 7.5$ Hz), $\text{CO}_2\text{CH}_2\text{CH}_3$), 2.15 (6H, s, CH_3), 2.74 (2H, d ($J = 8.0$ Hz), CH_2), 4.00 (1H, t ($J = 8.0$ Hz), CH), 4.01 (2H, q ($J = 7.5$ Hz), $\text{CO}_2\text{CH}_2\text{CH}_3$), 2) for enol form: δ 1.11 (3H, t ($J = 7.5$ Hz), $\text{CO}_2\text{CH}_2\text{CH}_3$), 2.04 (6H, s, CH_3), 3.14 (s, 2H, CH_2), 4.01 (2H, q ($J = 7.5$ Hz), $\text{CO}_2\text{CH}_2\text{CH}_3$); MS (CI 70 eV), m/e 186, calcd 186.09 for $\text{C}_9\text{H}_{14}\text{O}_4$.

Ethyl 4-ethoxycarbonylmethyl-3,5-dimethyl pyrrole-2-carboxylate 58

Ethyl acetoacetate (237.6 g, 1.50 mol) in glacial acetic acid (300 ml) was cooled in an ice bath, sodium nitrite (103.8 g, 1.50 mol) in water (145 ml) was added dropwise over 2 hours with stirring. The resulting solution of ethyl α -oximinoacetoacetate was added dropwise, along with zinc dust (326 g, 5.0 mol), to a stirred solution of ethyl 3-acetyl-4-oxopentanoate (279 g, 1.50 mol) in acetic acid (1200 ml) over 1 hour. The temperature was kept under 80 °C during the reaction process. After the addition, the reaction was allowed to stir for 0.5 hour. Then the mixture was decanted to pour into cold water and left standing overnight. The resulting solid was filtered off and washed with tap water. The filter cake was dissolved in dichloromethane and filtered to remove zinc dust. The organic phase was evaporated in vacuo and the solids were recrystallized from methanol/water to give the pyrrole as yellowish crystal (177.1 g, 0.70 mol, 46% yield). m.p. 116-117 °C; ^1H NMR (300 MHz, CDCl_3): δ 1.21 (3H, t, $\text{CO}_2\text{CH}_2\text{CH}_3$), 1.32 (3H, t,

CO₂CH₂CH₃), 2.21, 2.25(3H each, s, CH₃), 3.34 (2H, s, CH₂), 4.13 (2H, q, CO₂CH₂CH₃), 4.25 (2H, q, CO₂CH₂CH₃), 8.82 (1H, s, NH); MS found m/e 253, calcd 253.13 for C₁₃H₁₉NO₄.

Ethyl 5-bromomethyl-4-ethoxycarbonyl methyl-3-methyl pyrrole-2-carboxylate 59

In a 500-ml Erlenmyer flask, ethyl 4-ethoxycarbonylmethyl-3,4-dimethyl pyrrole-2-carboxylate (12.7 g, 0.050 mol) was dissolved in carbon tetrachloride (70 ml) and was heated to 50 °C. A solution of bromine (8.0 g, 0.050 mol) in carbon tetrachloride (32 ml) was added dropwise. After addition was complete, a precipitate was formed and the mixture turned reddish color. It was kept stirring at 50 °C for 2 more hours and then refrigerated for overnight. The precipitate was collected by filtration and the resulting solid was recrystallized from chloroform/hexane to give the product (8.77 g, 0.026 mol) in 53% yield. ¹H NMR (300 MHz, CDCl₃): δ 1.23 (3H, t, CO₂CH₂CH₃), 1.34 (3H, t, CO₂CH₂CH₃), 2.27 (3H, s, CH₃), 3.46 (2H, s, CH₂), 4.13 (2H, q, CO₂CH₂CH₃), 4.32 (2H, q, CO₂CH₂CH₃), 4.55 (2H, s, CH₂Br), 9.44 (1H, s, NH); MS found m/e 331, calcd:331.06 for C₁₃H₁₈NO₄Br.

3-Ethoxycarbonyl methyl-5,5'-diethoxycarbonyl-3',4,4'-trimethyl-2,2'-dipyrrylmethane 60

A 250-ml round-bottomed flask was charged with 2-ethoxycarbonyl-3,4-dimethyl pyrrole (3.34 g, 0.020 mol), concentrated HCl (0.30 ml) and methanol (32 ml). Pyrrole **59** (6.6 g, 0.020 mol) in 60 ml methanol was added dropwise while heating to 60 °C. Once addition was completed, it was refluxed for 10 min and a precipitate formed. The

reaction mixture was then refrigerated for 2 h. The precipitate was collected by suction filtration and washed with small amount methanol to give the title compound (6.68 g, 0.016 mol) in 80% yield. ^1H NMR (300 MHz, CDCl_3): δ 1.30 (3H, t, $\text{CO}_2\text{CH}_2\text{CH}_3$), 1.34 (6H, t, $\text{CO}_2\text{CH}_2\text{CH}_3$), 2.02, 2.25, 2.29 (3H each, s, CH_3), 3.71 (2H, s, $\text{CH}_2\text{CO}_2\text{CH}_2\text{CH}_3$), 4.88 (2H, s, CH_2), 4.26 (6H, m, $\text{CO}_2\text{CH}_2\text{CH}_3$), 9.15, 9.98 (1H each, s, NH); MS found m/e 418, calcd: 418.21 for $\text{C}_{22}\text{H}_{30}\text{N}_2\text{O}_6$.

5,5'-Diethoxycarbonyl-3-(2-hydroxyethyl)-3',4,4'-trimethyl-2,2'-dipyrrylmethane 61

With stirring, boron trifluoride etherate (5.1 ml) was added dropwise to a mixture containing dipyrromethane **60** (6.27 g, 0.015 mol) and sodium borohydride (1.14 g, 0.030 mol) in dry THF (20 ml) under nitrogen atmosphere. After the addition was complete, the reaction was stirred for 0.5 h. Acetic acid (2 ml) was added dropwise, followed by water until hydrogen evolution ceased. The product was extracted into dichloromethane (30 ml) and washed several times with water. The solvent was removed under vacuo and the resulting solid was crystallized with methanol/water to give the title compound (4.76 g, 0.013 mol) in 84% yield. m.p. 79-80 °C; ^1H NMR (300 MHz, CDCl_3): δ 1.32, 1.33 (3H each, t, $\text{CO}_2\text{CH}_2\text{CH}_3$), 1.86 (1H, t, $\text{CH}_2\text{CH}_2\text{OH}$), 2.02, 2.25, 2.29 (3H each, s, CH_3), 2.72 (2H, t, $\text{CH}_2\text{CH}_2\text{OH}$), 3.81 (2H, m, $\text{CH}_2\text{CH}_2\text{OH}$), 3.86 (2H, s, CH_2), 4.26 (4H, m, $\text{CO}_2\text{CH}_2\text{CH}_3$), 8.60, 9.65 (1H each, s, NH); MS found m/e 376, calcd 376.20 for $\text{C}_{20}\text{H}_{28}\text{N}_2\text{O}_5$.

3-(2'-Hydroxyethyl)-3',4,4'-trimethyl-2,2'-dipyrrylmethane 62

A 100-ml round-bottomed flask equipped with a reflux condenser was charged with

dipyrrylmethane **61** (4.76 g, 0.013 mol), 60 ml of ethylene glycol, and 5g of sodium hydroxide. The reaction mixture was refluxed for overnight under nitrogen. Upon cooling of the solution to room temperature, water was added and the precipitate was filtered off, washed with water, and dried to afford the pure α -free dipyrrylmethane (2.82 g, 0.012 mol) in 94% yield. ^1H NMR (300 MHz, CDCl_3): δ 1.70 (1H, br, $\text{CH}_2\text{CH}_2\text{OH}$), 1.98, 2.00, 2.02 (3H each, s, CH_3), 2.70 (2H, t, $\text{CH}_2\text{CH}_2\text{OH}$), 3.81 (2H, m, $\text{CH}_2\text{CH}_2\text{OH}$), 3.80 (2H, s, CH_2), 6.36, 6.37 (1H each, s, α -H), 7.51, 8.94 (1H each, s, NH); MS found m/e 232.2, calcd 232.16 for $\text{C}_{14}\text{H}_{20}\text{N}_2\text{O}$.

Bis(5-ethoxycarbonyl-4-ethyl-3-methyl-2-pyrryl)(3,4,5-trimethoxyphenyl)methane 63

A 250-ml round-bottomed flask equipped with a reflux condenser was charged with 3,4,5-trimethoxybenzylaldehyde (6.66 g, 34.1 mmol), pyrrole **19** (12.33 g, 68.2 mmol), and 130 ml of absolute ethanol. A few drops of concentrated HCl were added, and the stirred solution was refluxed overnight under nitrogen. At the end of this time, TLC (silica gel, 20% EtOAc/hexane eluent) indicated the absence of the starting material. The solvent was removed *in vacuo*, and the red oil was loaded onto a silica gel column. Elution with 20% EtOAc/hexane yielded the title compound as pale yellow oil. Drying under high vacuum gave the dipyrrylmethane as a pale yellow solid (11.5 g, 21.3 mmol) in 62% yield. ^1H NMR (300 MHz, CDCl_3): δ 1.10 (6H, t, CH_2CH_3), 1.31 (6H, t, $\text{CO}_2\text{CH}_2\text{CH}_3$), 1.79 (6H, s, CH_3), 2.72 (4H, q, CH_2CH_3), 3.75 (6H, s, *m*- OCH_3), 3.85 (3H, s, *p*- OCH_3), 4.24 (4H, q, $\text{CO}_2\text{CH}_2\text{CH}_3$), 5.48 (1H, s, CH), 7.25 (2H, aromatic), 8.24 (2H, s, NH) ppm; MS found m/e 540, calcd 540.28 for $\text{C}_{30}\text{H}_{40}\text{N}_2\text{O}_7$.

Bis(4-ethyl-3-methyl-2-pyrryl)(3,4,5-trimethoxyphenyl)methane 64

Dipyrrylmethane **63** was saponified and decarboxylated with sodium hydroxide in ethylene glycol under conditions described before, affording the pure α -free dipyrrylmethane (7.83 g, 0.0198 mol) in 92.8%. ^1H NMR (300 MHz, CDCl_3): δ 1.10 (6H, t, CH_2CH_3), 1.79 (6H, s, CH_3), 2.40 (4H, q, CH_2CH_3), 3.70 (6H, s, *m*- OCH_3), 3.80 (3H, s, *p*- OCH_3), 5.38 (1H, s, CH), 6.30 (2H, aromatic), 6.35 (2H, s, α -H), 7.34 (2H, s, NH); MS found *m/e* 396, calcd 396.24 for $\text{C}_{24}\text{H}_{32}\text{N}_2\text{O}_3$.

Bis(4-ethyl-5-formyl-3-methyl-2-pyrryl) (3,4,5-trimethoxyphenyl)methane 65

Formylation of dipyrrylmethane **64** (5.5 g, 0.0139 mol) was effected with POCl_3 in DMF under conditions described previously to give the title compound (5.0 g, 0.0110 mol) in 79.5% yield. m.p. 155-156 °C; ^1H NMR (300 MHz, CDCl_3): δ 1.18 (6H, t, CH_2CH_3), 1.82 (6H, s, CH_3), 2.70 (4H, q, CH_2CH_3), 3.70 (6H, s, *m*- CH_3), 3.85 (3H, s, *p*- CH_3), 5.45 (1H, s, CH), 6.28 (2H, aromatic), 8.90 (2H, s, NH), 9.50 (2H, s, aldehyde); MS *m/e* 452.4, calcd 452.23 for $\text{C}_{26}\text{H}_{32}\text{N}_2\text{O}_5$.

2,8-Diethyl-13-hydroxyethyl-5-(3',4',5'-trimethoxyphenyl)-3,7,12,17,18-pentamethyl-porphyrin 66

A 500-ml round-bottomed flask was charged with **65** (1.356 g, 3.00 mmol), **62** (0.696 g, 3.00 mmol), and 320 ml of THF:MeOH (2:1). The reaction mixture was purged with nitrogen and covered with foil, Perchloric acid (70%, 1 ml) was added and the solution was allowed to stir in the dark for 12 hours. At the end of this time, o-chloranil (1.2 g, 4.72 mmol) was added and the mixture was stirred for an additional 12 h. The reaction

mixture was poured into brine and extracted several times with methylene chloride. The organic layers were combined, washed with sodium bicarbonate, water, and dried over sodium sulfate. The solvent was removed under reduced pressure to give a dark solid. After chromatography on silica gel (2% MeOH / CH₂Cl₂ eluent), porphyrin **66** was isolated (920 mg, 1.43 mmol) in 47.8% yield. m.p. >275 °C; UV-vis: λ_{max} 404, 501, 536, 569, 622 nm; ¹H NMR (300 MHz, CDCl₃): δ -3.10 (2H, s, NH), 1.78 (6H, t, CH₂CH₃), 2.40, 2.42, 3.60, 3.62, 3.66 (3H each, s, CH₃), 3.92 (6H, s, *m*-OCH₃), 4.1 (4H, m, CH₂CH₃), 4.20 (3H, s, *p*-OCH₃), 4.32 (2H, t, CH₂CH₂OH), 4.50 (2H, m, CH₂CH₂OH), 7.32 (2H, s, aromatic), 9.92, 10.16, 10.18 (1H each, s, *meso*); MS found m/e 646, calcd 646.35 for C₄₀H₄₆N₄O₄.

13-(2'-Chloroethyl)-2,8-diethyl-5-(3',4',5-trimethoxyphenyl)-3,7,12,17,18-pentamethyl-porphyrin **67**

Benzoyl chloride (5 ml) was added dropwise over 10 minutes to a solution consisting of porphyrin **66** (798 mg, 1.24 mmol) in DMF (30 ml), while maintaining the temperature below 5 °C. The solution was allowed to stir at this temperature for 20 min and then heated on a steam bath for 20 min. Aqueous ethanol (50%, 50 ml) containing sodium carbonate (10 g) was added and the mixture was warmed on the steam bath for 15 min. Water was added until all sodium carbonate residue had dissolved and the porphyrin precipitated. The precipitate was collected and recrystallized from CH₂Cl₂/methanol to give **67** (728 mg, 1.10 mmol) in 88% yield. m.p. >275 °C; UV-vis: λ_{max} 404, 502, 536, 569, 624 nm; ¹H NMR (300 MHz, CDCl₃): δ -3.24, -3.22 (1H each, s, NH), 1.78 (6H, t, CH₂CH₃), 2.60, 2.62, 3.60, 3.62, 3.64 (3H each, s, CH₃), 3.92 (6H, s, *m*-OCH₃), 4.05 (4H,

m, $\underline{\text{CH}_2\text{CH}_3}$), 4.20 (3H, s, $p\text{-OCH}_3$), 4.32 (2H, t, $\underline{\text{CH}_2\text{CH}_2\text{OH}}$), 4.50 (2H, t, $\text{CH}_2\underline{\text{CH}_2\text{Cl}}$), 7.34 (2H, s, aromatic), 9.84, 10.16, 10.19 (1H each, s, *meso*); MS found m/e 664, calcd 664.32 for $\text{C}_{40}\text{H}_{45}\text{ClN}_4\text{O}_3$.

2,8-Diethyl-5-(3',4',5'-trimethoxyphenyl)-3,7,12,17,18-pentamethyl-13-vinylporphyrin

68

A 250-ml round-bottomed flask equipped with a reflux condenser was charged with chloroethylporphyrin **67** (665 mg, 1.0 mmol), pyridine (60 ml), and DBU (3.5 ml). The reaction mixture was refluxed for 30min under nitrogen. Upon cooling of the solution to room temperature, the reaction mixture was poured into water and extracted several times with methylene chloride. The organic layers were combined, washed with hydrochloric acid (5%), saturated sodium bicarbonate solution and water. After drying over sodium sulfate, the solvent was removed under reduced pressure and the residue was chromatographed on silica gel (dichloromethane eluent). The porphyrin obtained was further recrystallization from dichloromethane/methanol to afford the title compound (504 mg, 0.80mmol) in 80% yield; m.p. >275 °C; UV-vis: λ_{max} 406, 506, 541, 574, 629 nm; ^1H NMR (300 MHz, CDCl_3): δ -3.32, -3.22 (1H each, s, NH), 1.75 (6H, t, $\text{CH}_2\underline{\text{CH}_3}$), 2.60, 2.64, 3.60, 3.62, 3.64 (3H each, s, CH_3), 3.92 (6H, s, $m\text{-OCH}_3$), 4.00 (4H, m, $\underline{\text{CH}_2\text{CH}_3}$), 4.18 (3H, s, $p\text{-OCH}_3$), 6.12 (1H, d, $\text{cis-CH}=\underline{\text{CH}_2}$), 6.40 (1H, t, $\text{trans-CH}=\underline{\text{CH}_2}$), 7.32 (2H, s, aromatic), 8.24 (1H, dd, $\underline{\text{CH}}=\text{CH}_2$), 10.02, 10.10, 10.20 (1H each, s, *meso*); MS found m/e 628, calcd 628.34 for $\text{C}_{40}\text{H}_{44}\text{N}_4\text{O}_3$.

2,8-Diethyl-13-(1',2'-dihydroxyethyl)-5-(3',4',5'-trmethoxyphenyl)-3,7,12,17,18-

pentamethyl-porphyrin 69

Osmium tetroxide (254 mg, 1.0 mmol) was added to the mixture of vinylporphyrin (610 mg, 0.97 mmol), dichloromethane (100 ml) and pyridine (1 ml). The reaction mixture was stirred for about 30 min until the TLC showed completion of the reaction. Methanol was added and H₂S was bubbled through the mixture for 10 min. The solvent was removed on steam bath in the hood and the resulting residue chromatographed on silica gel (4% methanol/dichloromethane eluent) to give the title compound (550 mg, 0.84 mmol) in 88% yield. m.p. >275 °C; UV-vis: λ_{max} 404, 502, 538, 570, 623 nm; ¹H NMR (300 MHz, CDCl₃): δ -3.45, 3.25 (1H each, s, NH), 1.75 (6H, m, CH₂CH₃), 2.60, 2.64, 3.50 (3H each, s, CH₃), 3.60 (6H, s, CH₃), 3.92 (6H, s, *m*-OCH₃), 4.02 (4H, m, CH₂CH₃), 4.20 (3H, s, *p*-OCH₃), 4.58 (2H, m, CH(OH)CH₂OH), 6.18 (1H, m, CH(OH)CH₂OH), 7.32 (2H, s, aromatic), 10.02, 10.10, 10.18 (1H each, s, *meso*); MS found m/e 644 (M⁺-H₂O), calcd 644.33 for C₄₀H₄₄N₄O₄

2,8-Diethyl-13-formyl-5-(3',4',5'-trimethoxyphenyl)-3,7,12,17,18-pentamethylporphyrin 70

An aqueous sodium periodate (5%, 20 ml) solution was added to a solution of porphyrin diol **69** (550 mg, 0.84 mmol) in pyridine (50 ml). The mixture was heated on steam bath for 0.5 h. Upon cooling, water (50 ml) was added and a precipitate formed. The precipitate was collected and recrystallized from dichloromethane/methanol to give **70** (510 mg, 0.81 mmol) in 96% yield. m.p. >275 °C; UV-vis: λ_{max} 417, 519, 560, 584, 640 nm; ¹H NMR (300 MHz, CDCl₃): δ -3.22 -2.92 (1H each, s, NH), 1.75 (6H, m, CH₂CH₃), 2.56, 2.64, 3.60 (3H each, s, CH₃), 3.90 (6H, s, CH₃), 3.94 (6H, s, *m*-OCH₃), 4.06 (4H, m,

CH₂CH₃), 4.20 (3H, s, *p*-OCH₃), 7.32 (2H, s, aromatic), 10.00, 10.20, 10.70 (1H each, s, *meso*), 11.40 (1H, s, aldehyde); MS found *m/e* 630, calcd 630.32 for C₃₉H₄₂N₄O₄.

13-Carboxy-2,8-diethyl-5-(3',4',5'-trimethoxyphenyl)-3,7,12,17,18-pentamethylporphyrin 71

Jones reagent (CrO₃/H₂SO₄, 5 eq.) was added to a stirred solution of porphyrin aldehyde **70** (126 mg, 0.20 mmol) in acetone (30 ml) at 0 °C. The reaction was monitored by TLC until the starting porphyrin disappeared. Ice (30 g) was added and the solution was neutralized with aqueous saturated sodium bicarbonate solution. The mixture was extracted with dichloromethane three times and the organic layers were combined, washed with water and dried over sodium sulfate. After evaporation of the solvent, the residue was chromatographed on a silica gel to give the product (81 mg, 0.12 mmol) in 60% yield. *m.p.* >275 °C; UV-vis: λ_{max} 411, 512, 551, 580, 632 nm; ¹H NMR (300 MHz, CDCl₃): δ -3.55 -3.20 (1H each, s, NH), 1.80 (6H, m, CH₂CH₃), 2.56, 2.64, 3.60, 3.62, 3.85 (3H each, s, CH₃), 3.92 (6H, s, *m*-OCH₃), 4.10 (4H, m, CH₂CH₃), 4.20 (3H, s, *p*-OCH₃), 7.32 (2H, s, aromatic), 10.00, 10.10, 10.20 (1H each, s, *meso*); MS (FAB), *m/e* 646.4, calcd 646.32 for C₃₉H₄₂N₄O₅.

Zinc 13-carboxy-2,8-diethyl-5-(3',4',5'-trimethoxyphenyl)-3,7,12,17,18-pentamethylporphyrin 72

The insertion of zinc into porphyrin **71** was carried out with Zn(OAc)₂ in CHCl₃-MeOH as described previously, yielding 80 mg of porphyrin **72** (90%). *m.p.* >275 °C; UV-vis: λ_{max} 419, 548, 592 nm; MS (FAB), *m/e* 708.3; calcd 708.23 for C₃₉H₄₀N₄O₅Zn.

5-(3',4',5'-Trimethoxyphenyl)-2,8-diethyl-13-cyano-3,7,12,17,18-pentamethylporphyrin
73

A 100-ml round-bottomed flask equipped with a reflux condenser was charged with porphyrin aldehyde **70** (126 mg, 0.20 mmol), hydroxyamine hydrochloride (100 mg, 1.4 mmol) and 5 ml of 95% formic acid. The reaction mixture was refluxed under nitrogen overnight. Upon cooling of the solution to room temperature, the reaction mixture was poured into water. It was neutralized with aqueous saturated sodium bicarbonate solution before extracted several times with methylene chloride. The organic layers were combined and washed with water twice. After dried over sodium sulfate, the solvent was removed on a rotary evaporator and the resulting solid was chromatographed on silica gel (dichloromethane eluent) to give the title compound (119 mg, 0.19 mmol) in 95% yield. m.p. >275 °C; UV-vis: λ_{max} 410, 514, 552, 557, 629 nm; ¹H NMR (300 MHz, CDCl₃): δ -3.50, -3.20 (1H each, s, NH), 1.75 (6H, m, CH₂CH₃), 2.56, 2.70, 3.62, 3.64, 3.85 (3H each, s, CH₃), 3.90 (6H, s, *m*-OCH₃), 4.10 (4H, m, CH₂CH₃), 4.20 (3H, s, *p*-OCH₃), 7.30 (2H, s, aromatic), 10.00, 10.08, 10.20 (1H each, s, meso); MS found *m/e* 627.3, calcd 627.32 for C₃₉H₄₁N₅O₃.

Nickel 13-cyano-5-(3',4',5'-trimethoxyphenyl)-2,8-diethyl -3,7,12,17,18-pentamethyl-
porphyrin **74**

Nickel acetate was added to a solution of porphyrin nitrile free base (119 mg, 0.19 mmol) in DMF (15 ml) and the mixture refluxed until chelation was complete (monitored by both UV-vis and TLC, ca. 1 hours). Water was added and the solution was extracted

with dichloromethane. The organic layer was washed several times with water. After removal of solvent, the solid residue was chromatographed on silica (eluted with dichloromethane) to give **74** (120 mg, 0.17 mmol) in 92% yield. m.p. >275 °C; UV-vis λ_{max} 406, 532, 574; ^1H NMR (300 MHz, CDCl_3): δ 1.62 (6H, m, CH_2CH_3), 2.42 (6H, s, CH_3), 3.40 (6H, s, CH_3), 3.70 (3H, s, CH_3), 3.88 (4H, m, CH_2CH_3), 3.90 (6H, s, *m*- OCH_3), 4.14 (3H, s, *p*- OCH_3), 7.10 (2H, s, aromatic), 9.56 (1H, s, meso), 9.64 (1H, s, meso), 9.66 (1H, s, meso); MS found m/e 683, calcd 683.24 for $\text{C}_{39}\text{H}_{39}\text{N}_5\text{O}_3\text{Ni}$.

Nickel 13-amidinium-5-(3',4',5'-trimethoxyphenyl)-2,8-diethyl-3,7,12,17,18-pentamethylporphyrin chloride **75**

Porphyrin nitrile **74** (120 mg, 0.17 mmol) and dry toluene (20 ml) were placed in a Schlenk tube. After the system was purged with argon three times, chloromethylaluminum(III) amide (1 M, 1 ml) was introduced by syringe. The reaction mixture was stirred at 80 °C for 3 days under an argon atmosphere. Then the reaction mixture was added to mixture of silica (5 g) and chloroform (20 ml). After stirring for 0.5 h, the mixture was filtered and washed with dichloromethane. The solid mixture was loaded on a silica gel pad and eluted with 15% methanol in dichloromethane to give the title compound (116 mg, 0.16 mmol) in 93% yield. m.p. >275 °C; UV-vis: λ_{max} 406, 530, 574 nm; ^1H NMR (300 MHz, CDCl_3): δ 1.54 (3H, t, CH_2CH_3), 1.62 (3H, t, CH_2CH_3), 2.40, 2.44, 3.05, 3.08, 3.48 (3H each, s, CH_3), 3.56 (2H, q, CH_2CH_3), 3.75 (2H, q, CH_2CH_3), 3.90 (6H, s, *m*- OCH_3), 4.12 (3H, s, *p*- OCH_3), 6.82 (2H, br, axial NH of amidinium), 7.10 (2H, s, aromatic), 9.24 (2H, s, *meso*), 9.60 (1H, s, *meso*), 10.88 (2H, s, equatorial NH of amidinium). MS (FAB), m/e (MH^+) 701.2, calcd 701.28 for $\text{C}_{39}\text{H}_{42}\text{N}_6\text{O}_3$.

Zinc 3-amidinium-5-(3',4',5'-trimethoxyphenyl)-2,8-diethyl -3,7,12,17,18-pentamethyl-porphyrin 77

Concentrated sulfuric acid (2 ml) was added to a solution of the nickel complex **75** (50 mg, 0.068 mmol) in dichloromethane (10 ml). The mixture was stirred until all the porphyrin was extracted into the sulfuric acid layer. Ice (20 g) was added, followed by saturated aqueous sodium bicarbonate. After neutralization, the organic layer was collected, washed with water and dried over sodium sulfate. The solvent was removed under reduced pressure to give the free base **76**. m.p. >275 °C; UV-vis: λ_{max} : 407, 510, 547, 574, 626 nm.

To the above free base, zinc chloride (40 mg) and DMF (15 ml) was added. The mixture was heated until chelation was complete (monitored by both UV-vis and TLC, ca. 10min). After cooling to the room temperature, water was added to the mixture and it was extracted with dichloromethane. The organic layers were washed with water several times. After removal of the solvent, the solid residue was chromatographed on silica gel (eluted with 15% methanol in dichloromethane) to give **77** (44 mg, 0.060mmol) in 88% yield. m.p. >275 °C; UV-vis: λ_{max} : 414, 546, 589 nm; MS (FAB), m/e 707.2 (MH⁺), calcd 706.27 for C₃₉H₄₂N₆O₃Zn.

Chapter III

Characterization of Amidinium-Carboxylate Salt Bridge

This Chapter describes the characterization of the amidinium-carboxylate salt bridge formed by porphyrin amidinium and benzoate utilizing X-ray crystallography. The binding strength of this salt bridge formed by various porphyrins and aromatics has been measured by ^1H NMR and UV-vis spectroscopies. ET rates measured by using fluorescence quenching technique are also presented.

I. Crystal Structure

The complex formed by porphyrin amidinium **75** and benzoate consists of two crystallographically independent molecular complexes. Their structures are shown by the ORTEP drawing in Figure 8 and Figure 9, respectively. Crystal data and refinement parameters are given in Table 1. The data for selected bond distances and angles for both structures are given in Table 2. Table 3 lists atomic coordinates of all atoms.

Both structures show that an amidinium-carboxylate salt bridge is formed between porphyrin amidinium **75** and benzoate. In one structure (Figure 8), two internal

protons (HN5a and HN6a) of the amidinium group form the hydrogen bond with oxygen atoms (O4 and O5) of carboxylate and O \cdots H distances are 1.800(5) and 1.874(5) Å, respectively. The bond angles for N6-C34-N5 and O4-C40-O5 are 118.0(7) and 121.9(7)°, respectively. The two N-O distances are 2.81 and 2.76 Å. These relatively short hydrogen bond distances indicate significant stability of the salt bridge and relatively strong hydrogen bonding. The amidinium group rotates by 42° with respect to the plane of the porphyrin ring (defined by the four pyrrole nitrogen atoms) due to the steric interaction of the *meso*-proton. The salt bridge twists by 5.4° (dihedral angle defined by the planes of the CN₂ and CO₂ atoms of the salt bridge). The four Ni-N bond lengths in porphyrin **75** [1.927(6), 1.924(6), 1.928(6), 1.900(6)] are typically short, resulting in a deformation of the macrocycle ring of **75** from planarity. The normal radius of the cavity in an undistorted metalloporphyrin has been estimated to be 2.01 Å,⁵⁸ whereas the usual Ni-N bond length found in diamagnetic nickel(II) square-planar complexes is ca. 1.85 Å.⁵⁹ Hence, the porphinato-core must contract from the ideal situation to accommodate a low-spin nickel(II) atom. It has been postulated^{58,60} that 1.96 Å is the smallest radius the porphyrin cavity may have in order to maintain a planar structure and this is supported by experimental results. For example, in nickel(II) 2,4-diacetyldeuteroporphyrin-IX dimethyl ester,⁶¹ the Ni-N distance is 1.960(8) and this compound is essentially planar. In the nickel(II) OEP,⁶² the Ni-N distance is 1.929(3) and the porphyrin ring has severe warping.

The overall structural features of the salt bridge in the other independent structure are similar (Figure 9). The O \cdots H bond distances are 1.854(6) and 1.838(6) Å. The N-O distances are 2.78 and 2.79 Å. The amidinium group of this structure rotates 61.8° out of

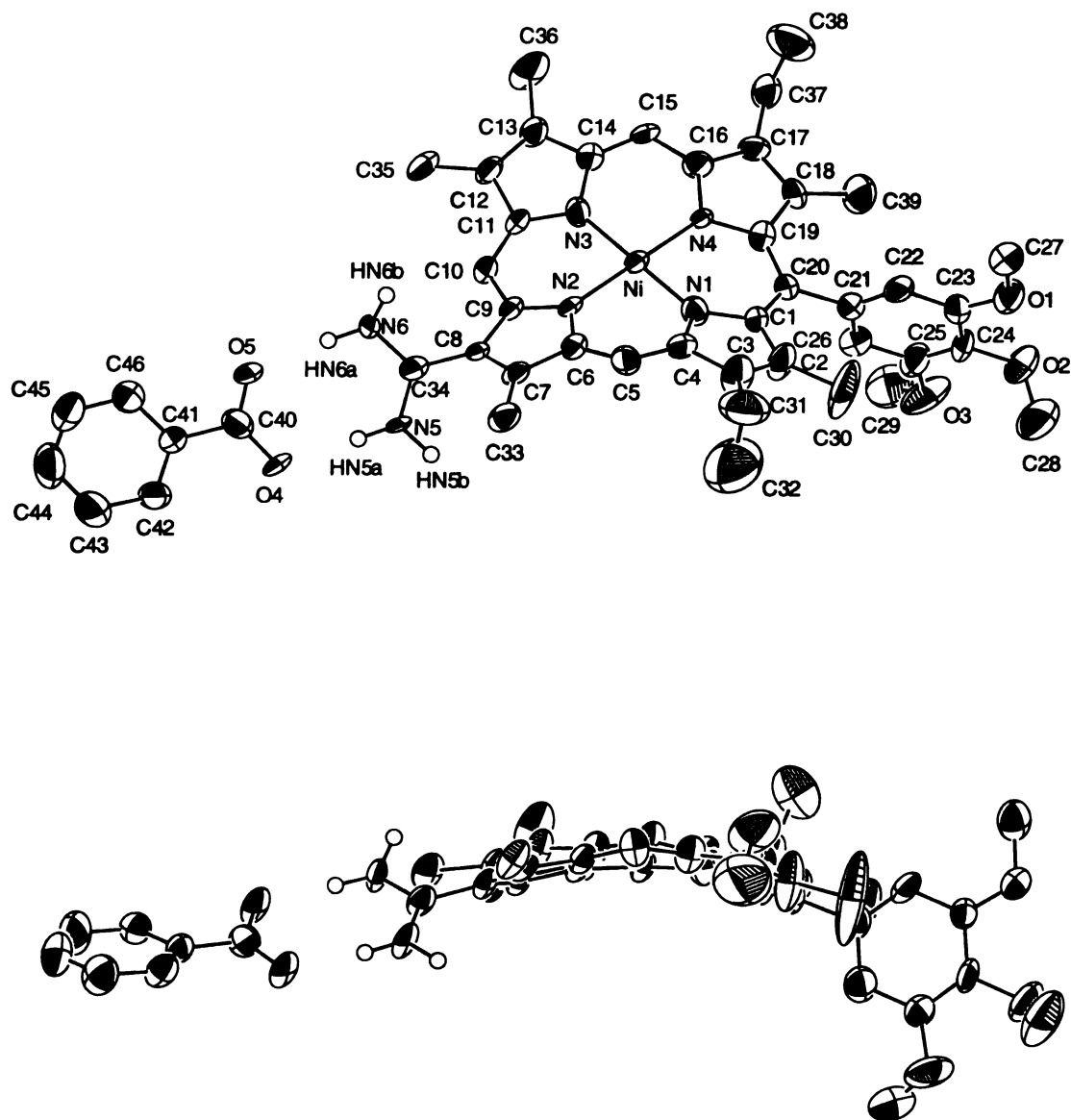


Figure 8. Top and side views of the ORTEP diagrams of the crystal structure of the salt-bridged supramolecular assembly formed by association of **75** with benzoate (structure 1)

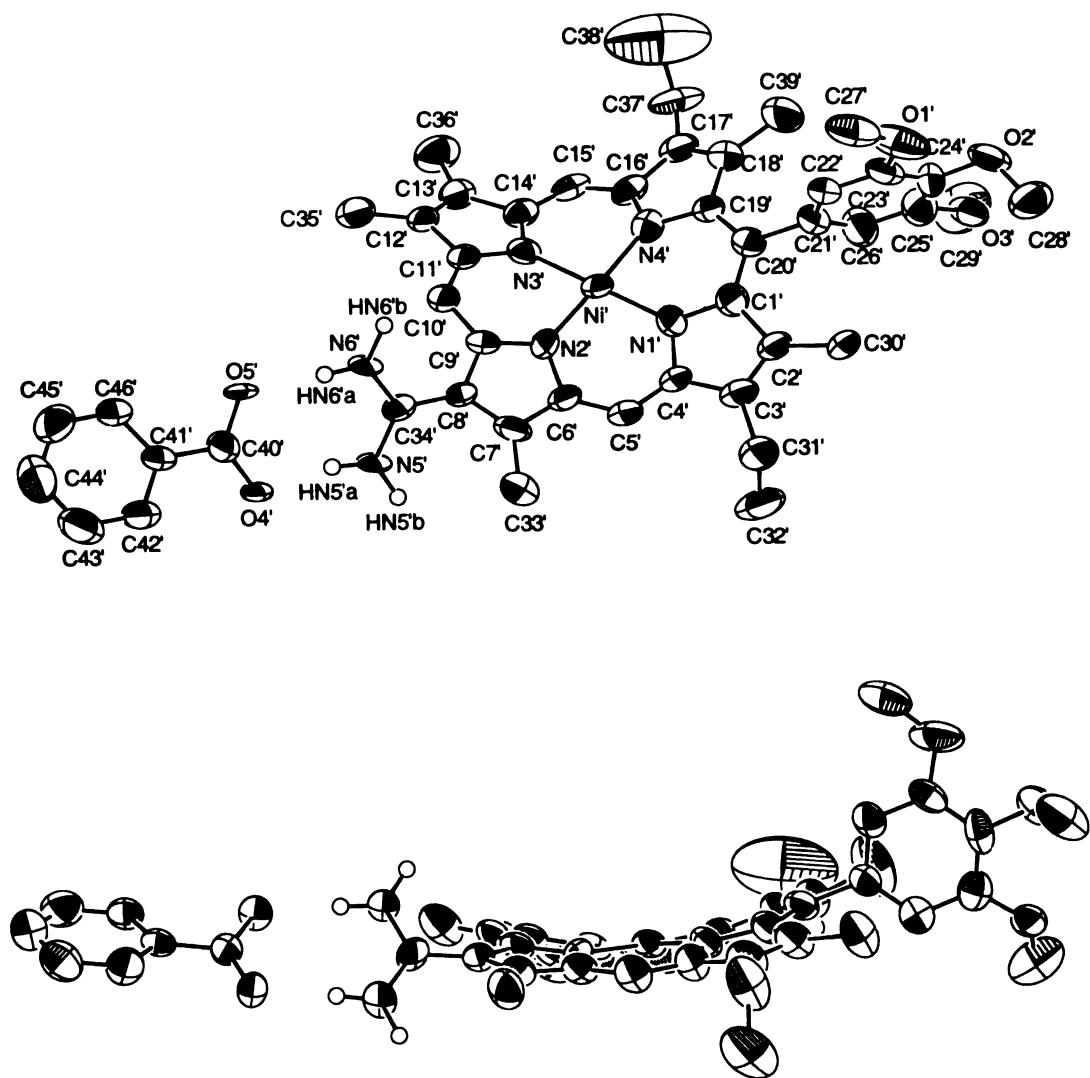


Figure 9. Top and side views of the ORTEP diagrams of the crystal structure of the salt-bridged supramolecular assembly formed by association of **75** with benzoate (structure **2**)

Table 1. Crystal Data and Conditions for Crystallographic Data Collection and Structure Refinement

Formula	Ni O ₅ N ₆ C ₄₆ H ₄₈
Formular weight	822.11
Diffractometer used	Nonius
Space Group	Triclinic $P\bar{1}$
a (Å)	15.497(3)
b (Å)	16.268(3)
c (Å)	19.483(7)
α (°)	113.589(23)
β (°)	109.687(22)
γ (°)	93.435(14)
V (Å ³)	4128.8(18)
Z	4
Dcalc. (g · cm ⁻³)	1.323
λ (Å)	0.7107
F(000)	1732.
Unit cell detn: #;(2 θ range.)	25;(19.00 - 24.24 °)
Scan type	$\theta/2\theta$
Scan width (degree)	2(0.80+0.35tan(θ))
Scan Speed (degree/min)	3.30-8.24
(2 θ) _{max}	45.0
h k l ranges	(-16; 16) (0; 17) (-20; 19)
μ (cm ⁻¹)	5.219
Crystal size (mm)	0.05 × 0.50 × 1.50
Transmission	0.795; 1.000
Temperature (K)	298
# of meas. reflns.	10777
# of obsd relfns. (I>2.0 σ (I))	5300
# of unique reflns.	10761
Rf; Rw	0.065; 0.058
GoF	2.06
Refinement program	NRCVAX
# of atoms	212
# of refined params..)	1045 (5300 out of 10761 reflns
Minimize function	Sum(w Fo-Fc ²)
Weights scheme	1/[σ^2 (Fo)]
The weight modifier K in KFo ² is	0.000100
(δ/σ) _{max}	0.0087
Residual in final D-map (e/ Å ³)	-0.400; 0.630

NOTE :

$$R_f = \Sigma(F_o - F_c) / \Sigma(F_o)$$

$$R_w = [\Sigma(w(F_o - F_c)^2) / \Sigma(wF_o^2)]^{1/2}$$

$$GoF = [\Sigma(w(F_o - F_c)^2) / (\text{No. of reflns} - \text{No. of params.})]^{1/2}$$

Table 2. Selected Bond Distances and Bond Angles and Their Estimated Standard Deviations for Porphyrin Amidinium Benzoate

Structure 1		Structure 2	
Bond Distance (Å)			
Ni-N1	1.927(6)	Ni'-N1'	1.925(7)
Ni-N2	1.924(6)	Ni'-N2'	1.942(7)
Ni-N3	1.928(6)	Ni'-N3'	1.915(7)
Ni-N4	1.900(6)	Ni'-N4'	1.931(7)
N5-C34	1.301(10)	N5'-C34'	1.311(11)
N5-Hn5a	0.938(6)	N5'-Hn5'a	0.923(7)
N5-Hn5b	0.980(6)	N5'-Hn5'b	0.986(7)
N6-C34	1.349(10)	N6'-C34'	1.328(11)
N6-Hn6a	0.957(6)	N6'-Hn6'a	0.934(7)
N6-Hn6b	0.942(7)	N6'-Hn6'b	0.983(7)
C40-C41	1.475(12)	C40'-C41'	1.487(12)
C40-O4	1.264(10)	C40'-O4'	1.261(10)
C40-O5	1.270(10)	C40'-O5'	1.254(10)
O4-Hn5a	1.874(5)	O4'-Hn5'a	1.838(6)
O5-Hn6a	1.800(5)	O5'-Hn6'a	1.854(6)
Bond Angle (deg)			
C34-N5-Hn5a	125.3(7)	C34'-N5'-Hn5'a	117.7(7)
C34-N5-Hn5b	117.7(7)	C34'-N5'-Hn5'b	120.3(7)
C34-N6-Hn6a	118.3(7)	C34'-N6'-Hn6'a	116.2(7)
C34-N6-Hn6b	101.4(6)	C34'-N6'-Hn6'b	122.1(7)
Hn5a-N5-Hn5b	116.9(6)	Hn5'a-N5'-Hn5'b	122.1(7)
Hn6a-N6-Hn6b	128.3(7)	Hn6'a-N6'-Hn6'b	121.6(7)
N5-C34-N6	118.0(7)	N5'-C34'-N6'	118.8(8)
N5-C34-C8	120.5(7)	N5'-C34'-C8'	120.0(8)
N6-C34-C8	121.5(7)	N6'-C34'-C8'	121.2(7)
C41-C40-O4	119.7(7)	C41'-C40'-O4'	117.3(8)
C41-C40-O5	118.4(7)	C41'-C40'-O5'	118.5(7)
O4-C40-O5	121.9(7)	O4'-C40'-O5'	124.2(8)
C40-C41-C46	120.0(8)	C40'-C41'-C46'	121.5(8)
C40-O4-Hn5a	115.9(5)	C40'-O4'-Hn5'a	119.5(6)
C40-O5-Hn6a	124.8(5)	C40'-O5'-Hn6'a	111.2(5)
N5-Hn5a-O4	176.0(5)	N5'-Hn5'a-O4'	175.2(6)
N6-Hn6a-O5	177.5(4)	N6'-Hn6'a-O5'	165.6(6)

Table 3. Atomic Parameters x,y,z and Beq.

	x	y	z	Beq
Ni	0.49612(8)	0.11872(8)	0.39834(6)	2.98(7)
N1	0.4896 (4)	0.1182 (5)	0.2976 (4)	3.4 (5)
N2	0.6305 (4)	0.1333 (4)	0.4361 (3)	2.6 (4)
N3	0.5035 (4)	0.1218 (5)	0.5001 (4)	3.2 (5)
N4	0.3632 (4)	0.1023 (5)	0.3605 (3)	2.9 (4)
N5	0.9165 (5)	0.0620 (5)	0.5291 (4)	4.2 (5)
N6	0.8870 (5)	0.1539 (5)	0.6382 (4)	4.1 (5)
C1	0.4114 (6)	0.0844 (7)	0.2233 (5)	4.2 (6)
C2	0.4407 (7)	0.0956 (9)	0.1643 (5)	6.9 (9)
C3	0.5314 (7)	0.1397 (8)	0.2030 (6)	6.3 (8)
C4	0.5644 (6)	0.1503 (6)	0.2858 (5)	4.1 (6)
C5	0.6562 (6)	0.1718 (6)	0.3363 (5)	3.8 (6)
C6	0.6880 (6)	0.1571 (6)	0.4023 (5)	3.2 (6)
C7	0.7827 (5)	0.1549 (5)	0.4445 (4)	2.8 (5)
C8	0.7835 (5)	0.1298 (6)	0.5019 (4)	3.0 (5)
C9	0.6895 (5)	0.1189 (5)	0.4981 (4)	2.5 (5)
C10	0.6636 (6)	0.1053 (6)	0.5548 (5)	2.9 (5)
C11	0.5761 (6)	0.1130 (6)	0.5574 (4)	2.9 (5)
C12	0.5531 (6)	0.1239 (6)	0.6279 (5)	3.4 (6)
C13	0.4672 (6)	0.1376 (6)	0.6094 (5)	4.0 (6)
C14	0.4335 (6)	0.1355 (6)	0.5296 (5)	3.6 (6)
C15	0.3450 (6)	0.1350 (7)	0.4877 (5)	4.2 (6)
C16	0.3105 (6)	0.1132 (6)	0.4062 (5)	3.7 (6)
C17	0.2123 (6)	0.0855 (6)	0.3564 (5)	4.3 (7)
C18	0.2025 (6)	0.0537 (6)	0.2774 (5)	3.9 (6)
C19	0.2972 (6)	0.0691 (6)	0.2806 (5)	3.5 (6)
C20	0.3222 (6)	0.0545 (6)	0.2146 (5)	3.8 (6)
C21	0.2455 (6)	0.0069 (6)	0.1285 (5)	4.1 (6)
C22	0.2011 (6)	0.0546 (6)	0.0915 (5)	3.9 (6)
C23	0.1332 (6)	0.0084 (6)	0.0117 (5)	3.7 (6)
C24	0.1136 (6)	0.0869 (6)	-0.0250 (5)	3 (6)

Table 3 (cont'd)

C25	0.1535 (7)	-0.1355 (7)	0.0137 (5)	5.3 (7)
C26	0.2253 (7)	-0.0879 (7)	0.0939 (5)	5.7 (7)
C27	0.1017 (7)	0.1450 (7)	0.0019 (6)	5.8 (8)
C28	0.0788 (9)	-0.1528 (10)	-0.1647 (7)	10.1 (11)
C29	0.1271 (8)	-0.2790 (7)	0.0166 (7)	8.1 (9)
C30	0.3858 (8)	0.0642 (14)	0.0741 (7)	15.1 (17)
C31	0.5931 (8)	0.1911 (8)	0.1721 (7)	9.5 (10)
C32	0.6343 (13)	0.1246 (11)	0.1379 (9)	14.8 (16)
C33	0.8625 (6)	0.1797 (7)	0.4241 (5)	4.5 (6)
C34	0.8640 (6)	0.1143 (6)	0.5571 (5)	3.6 (6)
C35	0.6196 (6)	0.1219 (6)	0.7028 (5)	4.4 (7)
C36	0.4109 (7)	0.1557 (8)	0.6615 (6)	7.1 (9)
C37	0.1342 (6)	0.0892 (7)	0.3869 (5)	5.1 (7)
C38	0.1023 (8)	0.1771 (9)	0.4006 (7)	8.3 (11)
C39	0.1083 (7)	0.0140 (8)	0.2059 (6)	6.9 (9)
C40	1.1051 (6)	0.0832 (6)	0.7042 (5)	4.1 (6)
C41	1.1957 (6)	0.0833 (6)	0.7620 (5)	3.6 (6)
C42	1.2678 (6)	0.0597 (6)	0.7381 (5)	4.3 (6)
C43	1.3546 (7)	0.0646 (7)	0.7944 (6)	6.1 (8)
C44	1.3690 (7)	0.0952 (8)	0.8754 (6)	6.9 (8)
C45	1.2976 (8)	0.1172 (8)	0.8974 (6)	7.7 (9)
C46	1.2114 (7)	0.1136 (7)	0.8438 (5)	6.1 (8)
O1	0.0850 (4)	0.0480 (4)	-0.0329 (3)	5.0 (4)
O2	0.0430 (5)	-0.1340 (5)	-0.1046 (3)	6.5 (5)
O3	0.1272 (6)	-0.2305 (5)	-0.0277 (4)	8.7 (6)
O4	1.0834 (4)	0.0390 (4)	0.6284 (3)	4.4 (4)
O5	1.0513 (4)	0.1289 (4)	0.7326 (3)	5.0 (4)
Ni'	-0.42867(9)	0.62335(8)	-0.16357(7)	3.73(7)
N1'	-0.5304 (5)	0.6045 (5)	-0.1320 (4)	4.2 (5)
N2'	-0.3359 (5)	0.6314 (5)	-0.0635 (4)	3.8 (5)
N3'	-0.3282 (5)	0.6434 (5)	-0.1954 (4)	3.7 (4)
N4'	-0.5190 (5)	0.6123 (5)	-0.2652 (4)	3.8 (5)
N5'	-0.0662 (5)	0.5682 (5)	0.0393 (4)	6.1 (5)

Table 3 (cont'd)

N6'	-0.0491 (5)	0.6991 (6)	0.1506 (4)	6.8 (6)
C1'	-0.6259 (6)	0.5786 (6)	-0.1767 (5)	4.5 (6)
C2'	-0.6762 (6)	0.5846 (7)	-0.1242 (5)	5.0 (7)
C3'	-0.6108 (7)	0.6110 (7)	-0.0495 (5)	5.7 (7)
C4'	-0.5206 (6)	0.6240 (6)	-0.0526 (5)	4.3 (7)
C5'	-0.4369 (6)	0.6405 (7)	0.0097 (5)	4.8 (7)
C6'	-0.3510 (6)	0.6422 (6)	0.0066 (5)	4.2 (6)
C7'	-0.2657 (6)	0.6459 (6)	0.0679 (5)	4.6 (6)
C8'	-0.1984 (6)	0.6355 (6)	0.0363 (5)	4.4 (6)
C9'	-0.2443 (6)	0.6270 (6)	-0.0450 (5)	3.8 (6)
C10'	-0.1969 (6)	0.6231 (6)	-0.0960 (5)	4.5 (6)
C11'	-0.2370 (6)	0.6341 (6)	-0.1655 (5)	4.3 (6)
C12'	-0.1863 (6)	0.6477 (6)	-0.2105 (5)	4.7 (6)
C13'	-0.2426 (6)	0.6737 (6)	-0.2637 (5)	4.7 (6)
C14'	-0.3327 (6)	0.6673 (6)	-0.2557 (5)	3.8 (6)
C15'	-0.4128 (7)	0.6715 (6)	-0.3100 (5)	4.7 (7)
C16'	-0.5005 (6)	0.6392 (6)	-0.3177 (5)	4.0 (6)
C17'	-0.5847 (7)	0.6125 (7)	-0.3891 (5)	4.7 (7)
C18'	-0.6530 (7)	0.5660 (7)	-0.3824 (5)	5.1 (7)
C19'	-0.6145 (6)	0.5715 (6)	-0.3009 (5)	4.0 (6)
C20'	-0.6658 (6)	0.5542 (6)	-0.2614 (5)	4.2 (6)
C21'	-0.7690 (6)	0.5110 (6)	-0.3053 (5)	4.1 (6)
C22'	-0.8337 (7)	0.5611 (7)	-0.3204 (6)	5.8 (7)
C23'	-0.9289 (7)	0.5192 (7)	-0.3601 (6)	5.3 (7)
C24'	-0.9564 (6)	0.4269 (7)	-0.3830 (5)	5.4 (8)
C25'	-0.8916 (6)	0.3761 (6)	-0.3692 (5)	4.7 (6)
C26'	-0.7953 (6)	0.4174 (6)	-0.3303 (5)	4.7 (7)
C27'	-0.9890 (10)	0.6290 (9)	-0.3963 (8)	9.9 (12)
C28'	-1.1007 (8)	0.3877 (8)	-0.3772 (7)	9.1 (10)
C29'	-0.8596 (8)	0.2287 (7)	-0.3866 (6)	7.9 (9)
C30'	-0.7794 (7)	0.5671 (8)	-0.1441 (6)	6.6 (8)
C31'	-0.6237 (8)	0.6316 (9)	0.0281 (6)	8.1 (9)
C32'	-0.6090 (9)	0.7330 (9)	0.0798 (7)	11.1 (11)
C33'	-0.2601 (7)	0.6592 (7)	0.1510 (6)	5.9 (8)

Table 3 (cont'd)

C34'	-0.1025 (6)	0.6344 (7)	0.0761 (5)	5.2 (7)
C35'	-0.0880 (7)	0.6366 (8)	-0.1963 (6)	7.0 (8)
C36'	-0.2214 (8)	0.7006 (8)	-0.3218 (6)	7.4 (9)
C37'	-0.5923 (9)	0.6300 (7)	-0.4611 (6)	7.4 (9)
C38'	-0.5834 (19)	0.5494 (14)	-0.5269 (11)	23.3 (28)
C39'	-0.7495 (8)	0.5159 (10)	-0.4497 (6)	9.5 (11)
C40'	0.1674 (6)	0.6368 (6)	0.1889 (5)	4.4 (6)
C41'	0.2655 (6)	0.6301 (6)	0.2279 (5)	3.9 (6)
C42'	0.3191 (7)	0.5984 (6)	0.1819 (5)	5.0 (7)
C43'	0.4101 (7)	0.5942 (7)	0.2187 (6)	6.9 (8)
C44'	0.4508 (7)	0.6179 (8)	0.2998 (7)	7.4 (9)
C45'	0.3993 (8)	0.6528 (8)	0.3476 (6)	7.3 (8)
C46'	0.3077 (7)	0.6578 (7)	0.3106 (5)	5.6 (7)
O1'	-0.9995 (5)	0.5614 (6)	-0.3783 (5)	9.1 (7)
O2'	-1.0509 (4)	0.3828 (5)	-0.4250 (4)	7.6 (6)
O3'	-0.9245 (5)	0.2838 (4)	-0.3967 (4)	7.0 (5)
O4'	0.1253 (4)	0.5883 (4)	0.1130 (3)	6.1 (4)
O5'	0.1311 (4)	0.6885 (5)	0.2332 (3)	6.7 (5)
HN5a	0.971	0.051	0.561	4
HN5b	0.898	0.031	0.47	4
HN6a	0.944	0.146	0.672	4.3
HN6b	0.864	0.208	0.646	4.3

Beq is the Mean of the Principal Axes of the Thermal Ellips

the porphyrin plane accompanied by a more twisted salt bridge interface (25.9° between the CN_2 and the carboxylate planes). We believe that such variabilities in the solid state accentuate the high degree of rotational freedom of the salt bridge, which is also anticipated to occur in solution.

II. Determination of Association Constants

A. Proton NMR

In the course of determining the association constant of the amidinium-carboxylate salt bridge, we observed that the resonance of NH_2 protons of the amidinium group became broad when the carboxylate was added and eventually collapsed into the base line. This hindered the accurate determination of the chemical shift of the proton involved in the formation of salt bridge. It is believed that the broadening of NH peak is caused by the coupling of ^{14}N nucleus, which has a spin number I of 1. The coupling between the proton and nitrogen are determined by exchange rate of the proton on the nitrogen atom and the electrical quadrupole moment of the ^{14}N nucleus. If the exchange is rapid, the NH proton(s) is decoupled from the nitrogen atom and the NH peak is therefore a sharp singlet. Such is the case for the unbound amidinium group. If the NH exchange rate is slow, the NH peak becomes broad because the quadrupole moment of the nitrogen nucleus induces a moderately longer lifetime for the spin state of the nitrogen. The proton thus sees three spin states of the nitrogen nucleus ($I = 1$) which are changing at a moderate rate and the proton responds by giving a broad peak. This is what we observed for the bound amidinium, in which the formation of hydrogen bond locks the protons within the interface and slows the exchange of NH protons.

Acid is known to accelerate the proton exchange rate and has been introduced in our titration experiments to improve the resolution of NH peaks. The conjugated acid of the carboxylate was selected in order to avoid bringing other counter-ions. The binding studies were carried out in DMSO- d_6 . With the present of acid, the resolution of the protons of NH was found to be enhanced dramatically. Figure 10 shows the 1H NMR spectral changes resulting from the association of porphyrin **75** to benzoate in DMSO- d_6 . Without the addition of benzoate, protons of amidinium group of porphyrin amidinium **75** displayed two sharp peaks at 9.77 and 9.98 ppm. The addition of benzoic acid did not have effect on the chemical shifts of the NH protons. Nevertheless, when tetrabutylammonium benzoate was added, the peak at 9.77 ppm was found shift down field (> 4 ppm). This shift was believed due to the formation of hydrogen bonds with carboxylate and consequently, this peak was assigned as the internal NH protons of the amidinium group. The peak at 9.98 ppm shifted up field slightly (< 0.5 ppm) and it was assigned as the external NH protons of amidinium group. The chemical shift of the *meso*-proton remained unchanged during the titration, which clearly excluded the possibility that the interaction between the porphyrin and benzoate was due to π - π stacking.⁶³

Similar changes were observed when porphyrin amidinium **75**, porphyrin phenyl amidinium **43** were titrated with 3,5-dinitrobenzoate (3,5-DNB) or benzoate. In all spectra, internal NH protons of the amidinium group shifted downfield upon the formation the hydrogen bond, while the external NH proton of amidinium group only changed slightly. In all cases, no π - π interaction was observed. To obtain the association constant, the chemical shift of the internal proton of the amidinium group was plotted

against the concentration of benzoate to give corresponding titration curves. A typical titration curve is shown in Figure 11. The association constant was then fitted by using the non-linear least square method described by Wilcox.⁶⁸ Table 4 lists association constants of the salt bridge in DMSO- d_6 determined by NMR titration.

We observed that porphyrin effect had little influence on the binding constants of the same carboxylate. However, it was found when benzoate was replaced by 3,5-dinitrobenzoate (DNB), the association constant decreased dramatically due to the electron-withdrawing effect of the nitro groups.

Wilcox⁶⁴ observed that meta and para-substituents on N-octyl-N'-arylthiourea had large effects on binding when hydrogen bonds were formed with sulfonate. The binding strength increased when electron-withdrawing groups were presented on the proton donor. In their case, the N-H bonds become more positive due to the electron withdrawing group and NH proton become more acidic, which causes the increase of binding strength. Obviously, Our results showed another aspect of the substituents effects and complemented the earlier results.

In order to investigate the stoichiometry of the complex formed by amidinium-carboxylate salt bridge, Job's method of continuous variation⁶⁵ was applied. In this method, solutions containing various concentration ratios of porphyrin amidinium and carboxylate were prepared in such a manner as to keep the total concentration of the samples constant. This dictated that a 1:1 complex would reach a maximum value when the concentration of amidinium was equal to benzoate, while the concentration of a 2:1 complex would reach a maximum value when the concentration of amidinium was twice that of benzoate. In our study, the chemical shift of the internal amidinium proton was

recorded at each ratio. The concentration of the complex was represented by the product of the chemical shift changes (relative to unbound amidinium) and the mole fraction of amidinium according to the approach of Newcomb.⁶⁶ Plotting of the concentration vs. the mole fraction of amidinium, resulted in a Job's plot. This plot, as shown in Figure 12, revealed that the relative amidinium-carboxylate complex concentration approached a maximum when the mole fraction of amidinium was approximately 0.5. This confirmed the formation of 1:1 complex between amidinium-carboxylate in solution, which agreed with the stoichiometry in solid state that was observed in the crystal structure.

In less polar solvents such as dichloromethane and chloroform, the association constant was found to greatly increase. A difficulty encountered in the determination of association constants was that unreliable results were obtained by NMR titration. Wilcox⁶⁸ has indicated that the optimal concentration for determination association constants should be $1/K_a$. The concentration limit for ^1H NMR is greater than $\text{ca. } 10^{-4} \text{ M}$ and thus this method is restricted to measure association constant below 10^5 M^{-1} . Thus, UV-vis spectroscopy was applied to determine the association constants.

B. UV-vis

The conjugation between porphyrin and amidinium in porphyrin amidinium **75** allowed a quantitative assessment of the strength of the amidinium-carboxylate hydrogen bond by using UV-vis spectroscopy. Specifically, similar to the ^1H NMR titration, addition of increasing quantities of benzoate into a solution of porphyrin amidinium **75** in dichloromethane produced noticeable change in the porphyrin absorption spectrum (Figure 13). The absorption increased at 403 and 570 nm and decreased at 406 and 574 nm. The set of absorption spectra contained isosbestic points at 408 and 571 nm. The

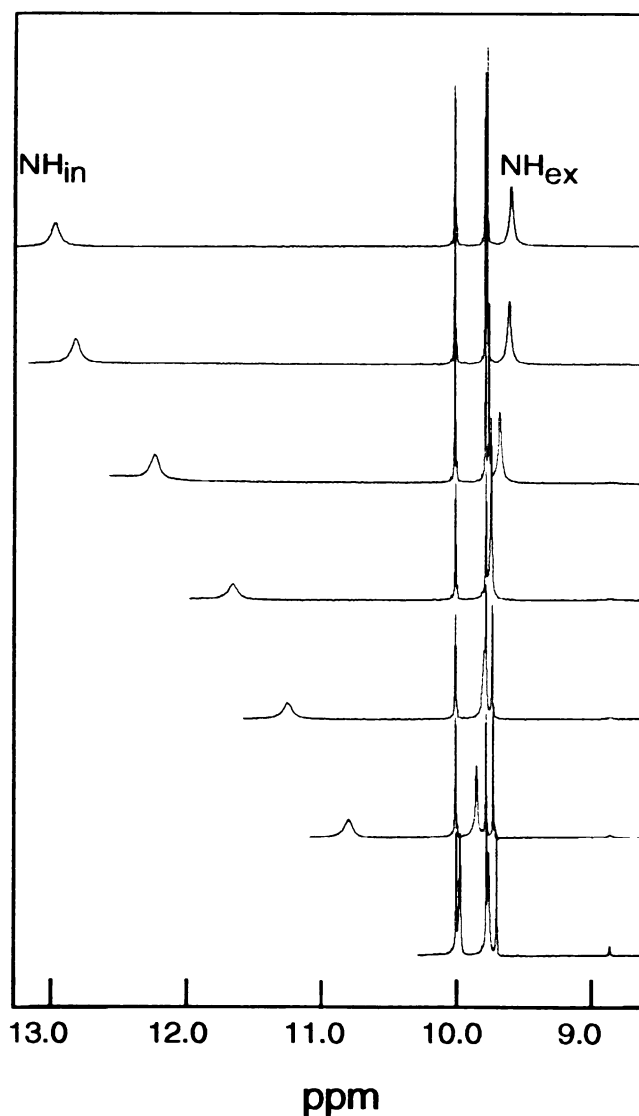


Figure 10. Selected ^1H NMR spectra of **75** (2.06 mM) with 1 eq. of benzoic acid in the absence of and in the presence of 1.78, 3.56, 5.35, 7.13, 8.92, 10.70, and 12.48 mM (bottom to top) of tetrabutylammonium benzoate in DMSO-d_6 at room temperature. The spectral range captures the amidinium protons internal (NH_{in}) and external (NH_{ex}) to the salt bridge interface and the three *meso* protons of the porphyrin ring.

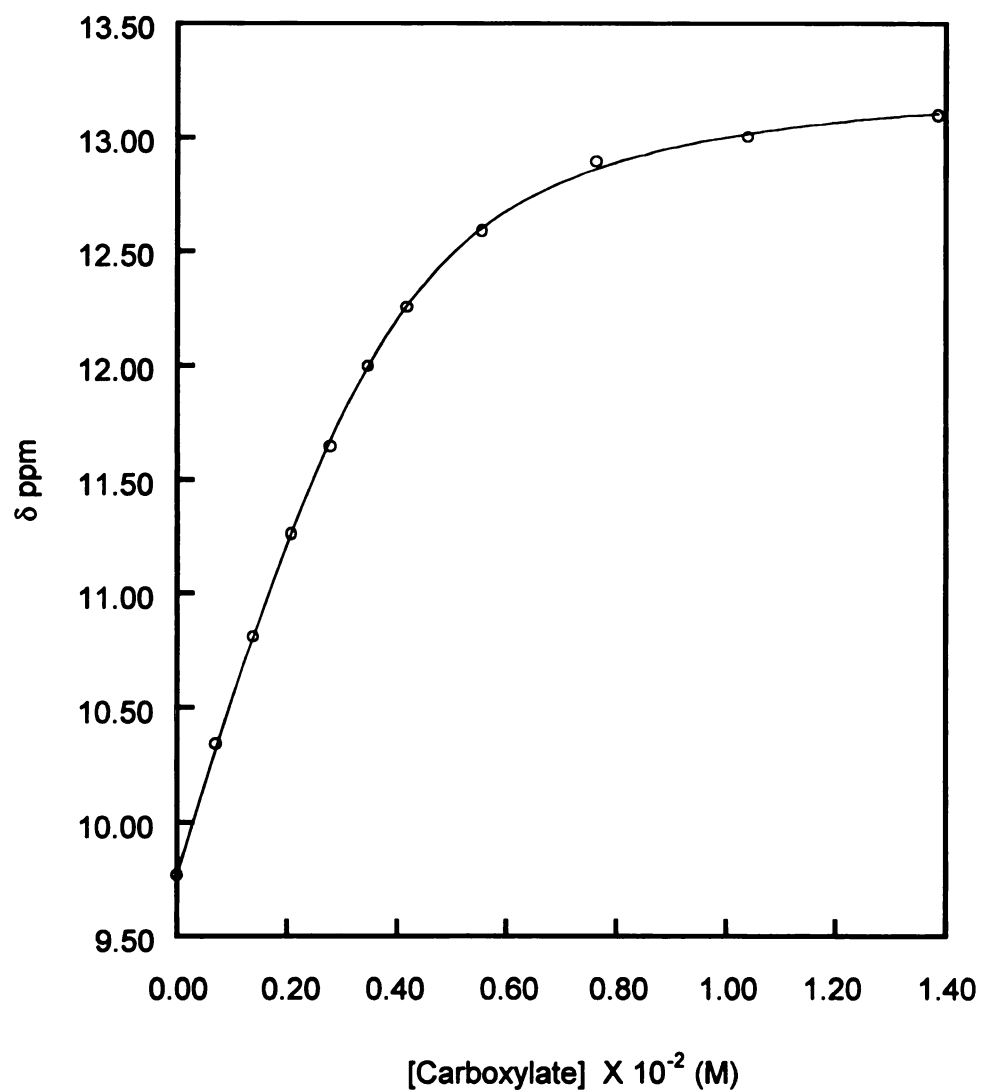


Figure 11. Plot of the chemical shift of internal protons of the amidinium versus the concentration of tetrabutylammonium benzoate.

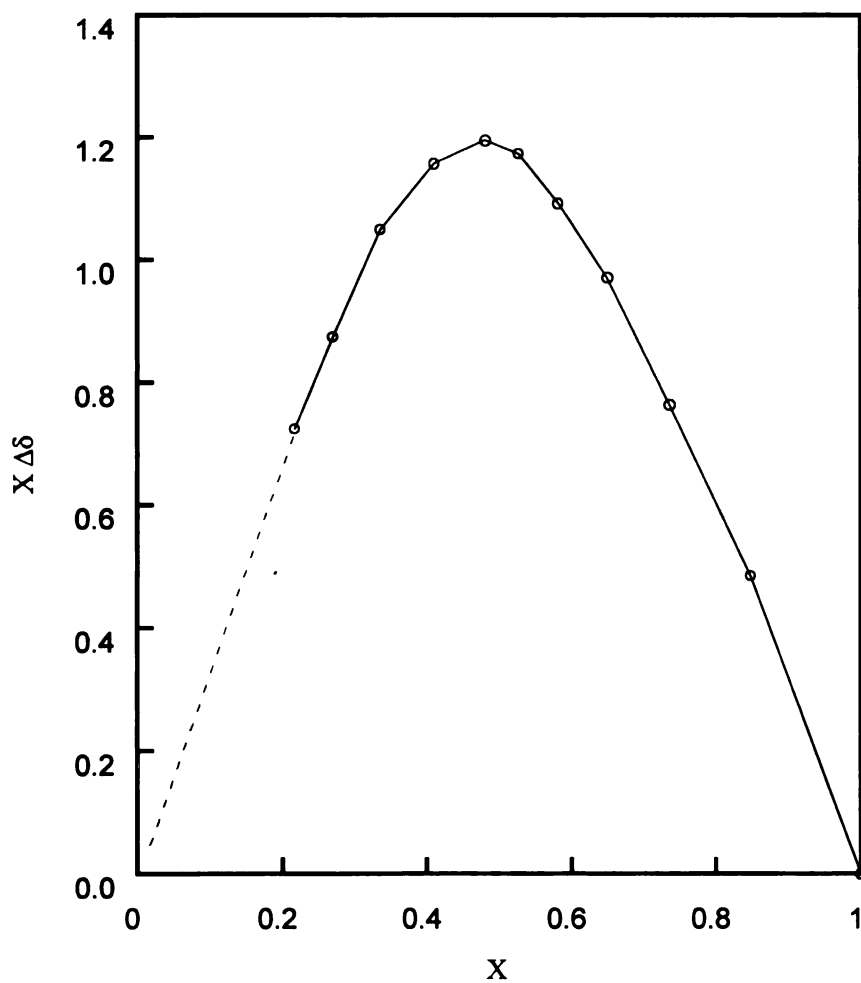


Figure 12. Job plot of the supramolecular complex formed by **75** and benzoate. The total concentration was kept at 3.5 mM and the systems were monitored by ^1H NMR (using the internal proton of amidinium) in DMSO at room temperature.

Table 4. Association Constants (K_a) and Energies (ΔG^0) of Amidinium-Carboxylate Salt Bridge in DMSO Determined by NMR Titration. Association Energies are determined by $\Delta G^0 = -RT \ln K_a$

Amidinium	Carboxylate	K_a (M^{-1})	ΔG^0 (kcal)
75	benzoate	1550 ± 87	-4.37
75	3, 5-DNB	$250 \pm$	-3.29
53	benzoate	1750 ± 95	-4.45
53	3, 5-DNB	134 ± 7	-2.90
53	49	1800 ± 170	-4.46

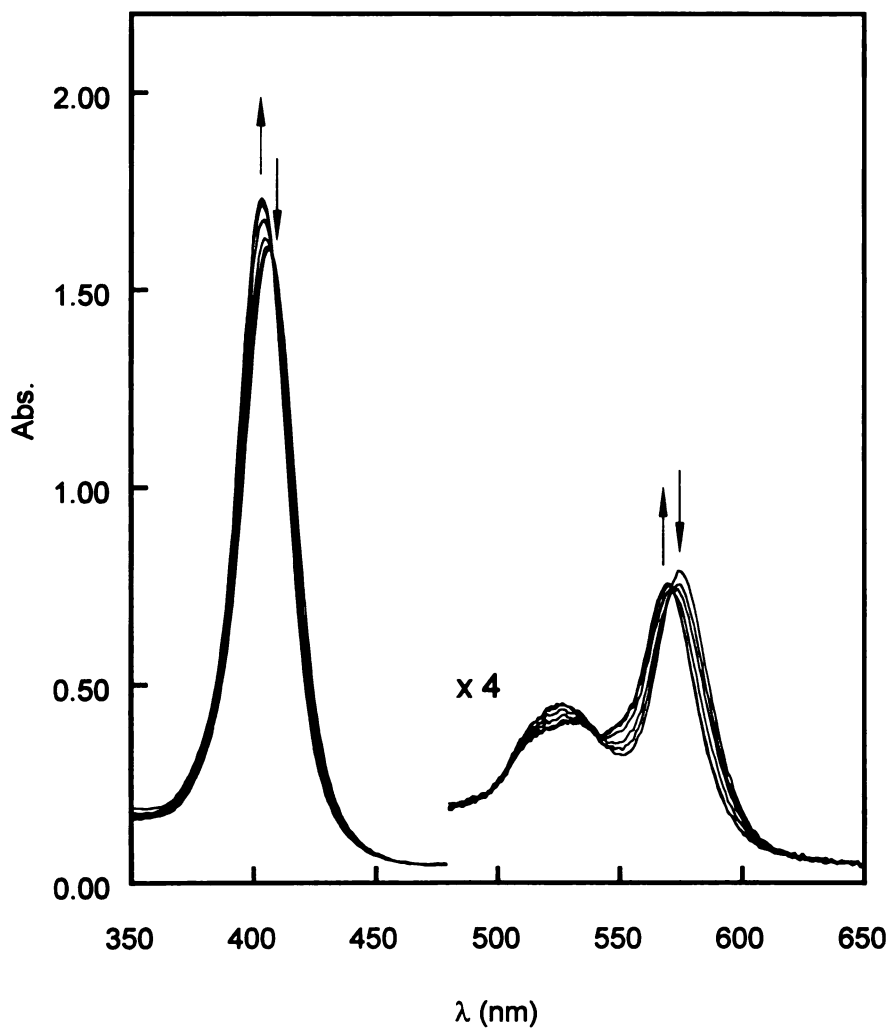


Figure 13. Selected UV-vis spectra of **75** (5.50 μM) in the presence of 0.0, 1.36, 2.71, 4.07, 5.42, 6.78 and 9.48 μM (increase with arrows) of tetrabutylammonium benzoate in dichloromethane.

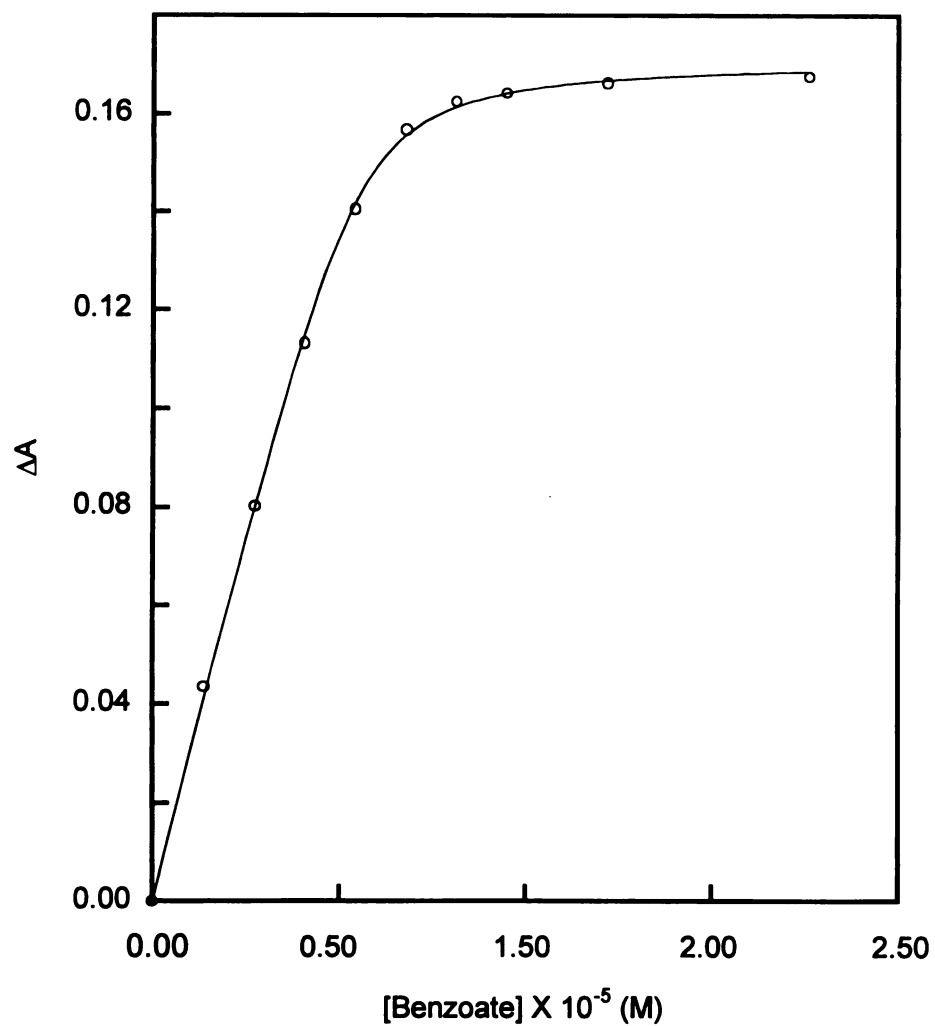


Figure 14. Plot of the absorption change of 75 at 398 nm versus the concentration of tetrabutylammonium benzoate

binding isotherm was determined by plotting the absorption change at 398 nm against the concentration of carboxylate (Figure 14). From the plot, the association constant was determined using the method described previously.

Table 5 lists the association constants measured under various conditions by UV-vis spectroscopic method. To compare this methodology with NMR, we studied the salt bridge formed by the same complex in DMSO. Initially, the titration was performed without the presence of an acid and the association constant was found to be $1.1(1) \times 10^4$, which was much higher than that obtained from the NMR titration. At this point, we decided to measure the association constant under comparable conditions to the NMR titration. Consequently, with 1 eq. of benzoic acid present, the association constant was found to be $3.2(3) \times 10^3 \text{ M}^{-1}$. The result was consistent with that determined by NMR [$K_a = 1.55(9) \times 10^3 \text{ M}^{-1}$]. Obviously, the presence of benzoic acid decreased the observed porphyrin carboxylate binding, presumably due to the competitive binding from the acid.

The significant increase of association constants in dichloromethane compared with that in DMSO shows a strong solvent effect on the stability of salt bridge. The change of solvent causes 3.7 kcal change in association energy. This is believed due to the different dielectric constants of these two solvents. The association energy of hydrogen bond is generally determined by the overlap of orbitals, solvation energy and Coulombic interaction.⁶⁷ In salt bridge, the primary interaction within salt bridge is Coulombic interaction, which is expressed by equation 3.1:

$$E = \frac{q_+ \times q_-}{\epsilon r} \quad (3.1)$$

where E is Coulombic energy, q_+ and q_- are the positive charges associated with the hydrogen bond, ϵ is dielectric constant of solvent and r is the distance between the

Table 5. Association Constants (K_a) and Energies (ΔG°) of Complexes Formed by **75** and Various Carboxylates. The Association Constants Are Determined Using UV-vis and the Association Energies Are Given by: $\Delta G^\circ = -RT\ln K_a$

Entry	Carboxylate	Solvent	Conjugated Acid (eq.)	K_a (M^{-1})	ΔG° (kcal)
1	Benzoate	CH_2Cl_2	0	$(5.7 \pm 1.2) \times 10^6$	-9.26
2	3, 5-DNB	CH_2Cl_2	0	$(7.6 \pm 1.4) \times 10^5$	-8.06
3	Benzoate	DMSO	0	$(1.1 \pm 0.1) \times 10^4$	-5.54
4	Benzoate	DMSO	1	$(3.2 \pm 0.3) \times 10^3$	-4.80

positive and negative charge. The dielectric constant of DMSO is 47.24, while that for CH_2Cl_2 is 8.93. For the same salt bridge, charges are the same and the bond distance shouldn't vary too much in these two solvents. Consequently, the Coulombic interaction in DMSO is weakened because of the large ϵ and the total hydrogen bond energy of the salt bridge is lower compare to that in CH_2Cl_2 .

The UV-vis titration method is limited to porphyrin amidinium **75**, in which the amidinium group is electronically coupled to the porphyrin. For porphyrin phenyl **43**, in which the amidinium group is decoupled from the porphyrin, no spectral change can be detected upon the formation of salt bridge. Hence, its association constant in dichloromethane can only be referred from that obtained in DMSO. We have demonstrated previously by NMR titration that porphyrin amidinium **43** has similar binding properties as those of porphyrin amidinium **75** in DMSO. Therefore, it is reasonable to estimate that the association constant of the salt bridge formed by porphyrin phenyl **43** and carboxylate in CH_2Cl_2 is also in a similar range of $10^5 - 10^6 \text{ M}^{-1}$, depending upon which benzoate is used.

III. PCET Studies

The ET rates have been measured in dichloromethane by using fluorescence quenching techniques. The fluorescence of **77** and **72** was quenched by the addition of electron acceptors 3,5-DNB and 3,5-dinitrobenzamidine (3,5-DNBA), respectively. All lifetime quenching measurements showed a biexponential decay in which one lifetime component was concentration dependent and the other was concentration independent. The concentration-dependent rate constant was assigned to the bimolecular ET processes and the concentration-independent rate constant was attributed to ET for the

associated pairs.

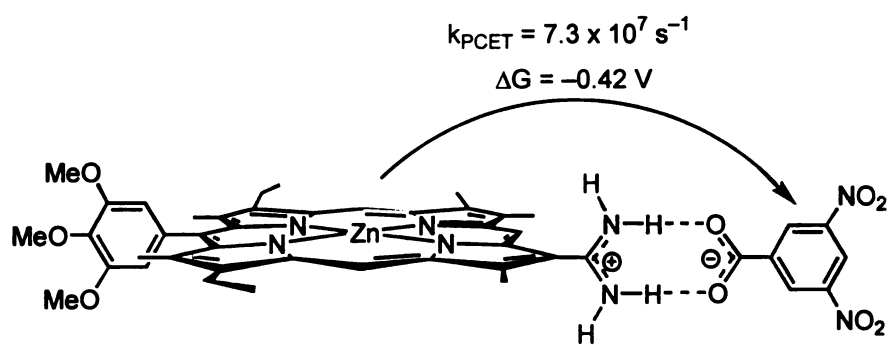
Figure 15 summarizes the unimolecular ET rates calculated from the decay kinetics and driving force of the ET reaction for the corresponding coupled system. In ZnPor (COOH-Am) DNB (72—3,5-DNBA), the salt bridge is aligned in such way, that the protons are located on the acceptor side and only the electron should transfer. The intermolecular electron transfer from zinc porphyrin **72** to 3,4-DNBA is $2.0 \times 10^9 \text{ s}^{-1}$, which is comparable to the ET through the carboxylic acid dimer.²² In ZnPor(Am-COOH)DNB (77—3,5-DNB), the proton interface is switched, both an electron and proton may traverse the proton interface. In this case, the intermolecular ET rate is significantly slow ($k_{\text{et}} = 6.4 \times 10^7$) although it possessed a similar driving force as ZnPor(COOH-Am)DNB. This dramatic difference in rates for ZnPor(Am-COOH)DNB and ZnPor(COOH-Am)DNB may have several origins. First, the electron transfer is in the direction of the permanent dipole of the salt bridge. The presence of an internal electric field contained within the electron transfer pathway may alter the driving force of reaction. Secondly, the proton may shift within the salt bridge and cause significant additional contribution to the Frank-Condon factor.

Determination of the ET rates in decoupled systems, using the method described previously, yielded the rate constants shown in Figure 16. As with ZnPor(Am-COOH)DNB and ZnPor(COOH-Am)DNB, ZnPorPh(Am-COOH)PhPorFe(III) and ZnPorPh(COOH-Am)PhPorFe(III) are assembled through a salt bridge. Therefore, the internal electric field is retained between the donor and acceptor, but the proton interface is decoupled from the porphyrin in a Franck Condon sense by the introduction of a phenyl spacer. In this case, switching the proton interface has little effect on the

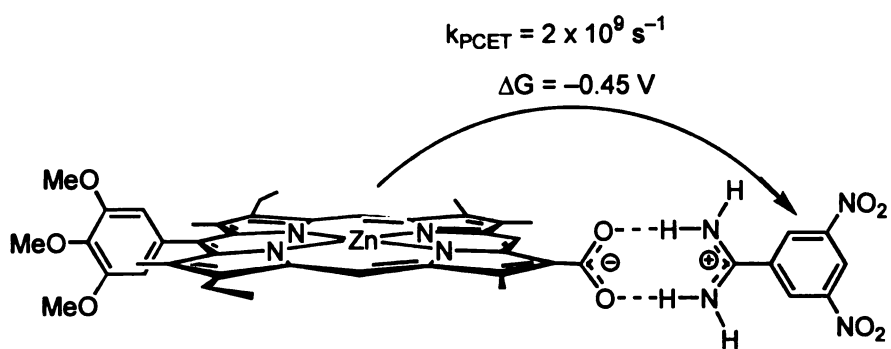
observed ET rates in these systems. These preliminary PCET studies reveal that proton shifting may be responsible for the observed slow ET process in the coupled systems. Nevertheless, because the distances between the donor and acceptor are different in these two systems, the effect of the permanent dipole associated with the salt bridge is not easy to address. Therefore the new systems based on purpurin and chlorin molecules have been designed and will be discussed in the next Chapter.

IV. Conclusions

This study has demonstrated that the electron donor/acceptor pairs juxtaposed by the amidinium-carboxylate salt bridge can be formed through self-assembly in solution. Hydrogen bond distances within amidinium-carboxylate salt bridge are in the range from 2.70 to 2.80 Å, indicating a very stable salt bridge in the solid state. In solution, the stability of the salt bridge is retained, as revealed by strong binding in DMSO despite its high dielectric constant.

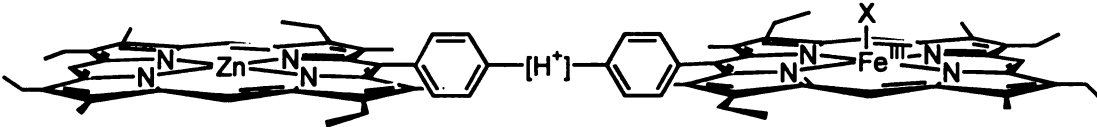


ZnPor(Am-COOH)DNB



ZnPor(COOH-Am)DNB

Figure 15. Summary of ET rates in coupling system



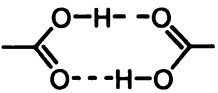
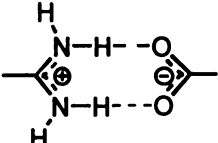
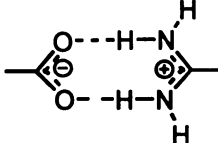
		$k_{\text{PCET}} / \text{s}^{-1}$	$\Delta G / \text{V vs SCE}$
ZnPorPh(COOH)2PhPorFe(III)		0.76×10^9	-1.11
ZnPorPh(Am-COOH)PhPorFe(III)		1.4×10^9	-1.14
ZnPorPh(COOH-Am)PhPorFe(III)		2.1×10^9	-1.04

Figure 16. Summary of ET rates in decoupling systems

V. Experimental

A. Crystallography

The single crystal suitable for crystallographic study was grown in acetonitrile using a 1:1 mixture of nickel porphyrin amidinium chloride and tetrabutylammonium benzoate. The crystal used for analysis was of the approximate dimension $0.05 \times 0.50 \times 1.50$ mm. Data collection was performed on a Nonius diffractometer at room temperature using graphite-monochromated Mo K α radiation. The unit cell parameters were determined by a least square fit of 25 machine-centered reflections having 2θ values in the range of 19.00-24.44°. The intensity data were reduced and corrected for Lorentz and polarization factors using the applied programs. The crystal structure was solved by direct methods using the NRCVAX program package and 1045 parameters were refined to $R = 0.065$ ($R_w = 0.058$). All non-hydrogen atoms were refined anisotropically. The hydrogen atoms were placed at calculated positions with fixed isotropic thermal parameters.

B. Binding studies

1. ^1H NMR

^1H NMR binding studies were performed on a VXMR 500MHz NMR spectrometer using DMSO- d_6 (Cambridge Isotope). ^1H NMR binding studies consisted of incremental additions of small volumes (1-2 ul) of a concentrated guest solution to a large volume (700 ul) of a host solution. The total volume change was less than 5%. After each addition of titrant (the guest solution), the ^1H NMR spectrum of the system was recorded. Changes in the spectrum of the host were plotted against the concentration

of the added guest. The guest concentration was known from the amount of guest solution added and the resulting volume change. The resulting data points were fitted using KaleidaGraph and the Wilcox's titration equation.⁶⁸ to determine the association constants.

2. Ultraviolet-Visible Absorption Spectroscopy Study

The UV-vis absorption experiments were performed with a Cary-17 spectrometer. The experiments were carried out in spectral grade dichloromethane distilled over calcium hydride or DMSO distilled under reduced pressure over barium oxide. A quartz cuvette capable of holding 5 ml of sample and possessing a stopper was employed in all of the binding studies. The binding study consisted of incremental additions of small volume (2-5 μ l) of a concentrated guest solution to large volume (5 ml) of a host solution. The total volume change was less than 1%. After each addition of guest, the spectrum was recorded and the changes in absorbency intensities were recorded. The concentration of the guest in the cuvette at each addition was calculated based on the guest's stock solution concentration. Changes in the absorbency intensity were plotted against the guest concentration to obtain the binding isotherm. The association constants were then determined using the same method described for the NMR binding study.

Chapter IV

Purpurin and Chlorin

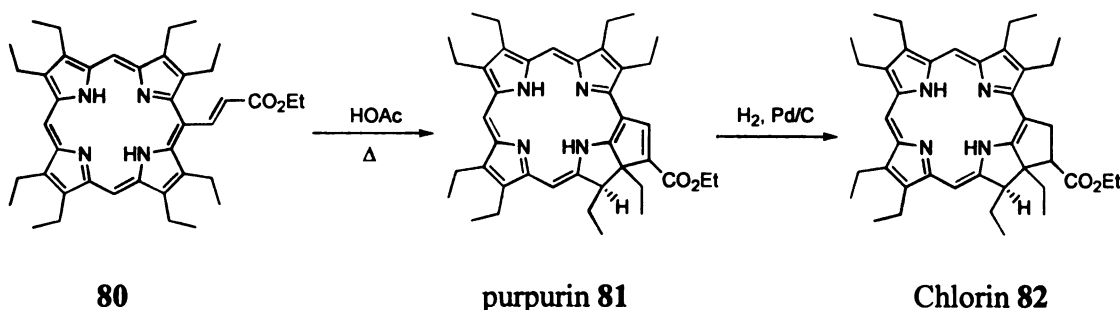
— Synthesis and Electron Transfer

I. Introduction

PCET studies of the porphyrin systems of Chapter III disclose that amidinium-carboxylate salt bridge internal to the ET pathway can profoundly regulate ET rates. While the results are striking, the system is not an optimally designed one. The method of decoupling the proton interface from the porphyrin has been achieved through the introduction of a phenyl spacer at the *meso* position. This modification changes the distance between donor and acceptor as well as the position where the proton interface is attached. Such changes may also alter the effect of the permanent dipole of the salt bridge on ET. Therefore, it is not appropriate to compare the coupled system to the decoupled system. Thus, the challenge of this project is to couple and decouple the ET chromophore from the salt bridge in a system sharing the same structural features.

In the course of total synthesis of chlorophyll *a*, Woodward et al.⁶⁹ discovered

that when porphyrin *meso*-acrylic ester was refluxed in acetic acid under inert atmosphere, an equilibrium was established between the porphyrin and purpurin, with an equilibrium constant of 1.7. This cyclization, aided by steric crowding and the electron-withdrawing power of the ester group,⁷⁰ was repeated by Fuhrhop⁷¹ and Morgan⁷² to convert *meso*-acrylic OEP **80** to the corresponding purpurin ester. Morgan further demonstrated that the double bond of the cyclopentenyl ring of purpurin ester **81** could be selectively reduced to a single bond to form chlorin **82** by hydrogenation in the presence of a catalytic amount of Pd/C (Scheme 14).



Scheme 14

Such purpurin/chlorin structures are particularly attractive to us. In purpurin **81**, the double bond of the cyclopentenyl ring enables chromophore conjugation with the external functional group. In chlorin **82**, such conjugation is interrupted by the reduction of the double bond to a single bond. Unlike the porphyrin systems, the number of bonds between the chromophore and proton interface will remain the same, as does the distance. The conversion between the purpurin and chlorin thus provides an ideal way to modulate the coupling or decoupling of the chromophore and proton interface. For our studies, the ester group should be replaced with either an amidinium or a carboxylic acid group. This

Chapter describes the synthesis and PCET studies of purpurin and chlorin analogous of **81** and **82**.

II. Results and Discussion

A. Synthesis

1. Purpurin and chlorin carboxylic acid

In Scheme 15, the synthesis was initiated from nickel octaethyl-porphyrin (OEP). According to the method of Morgan,⁷² nickel OEP was converted to nickel *meso*-formyl OEP **78** with the Vilsmeier reagent. Porphyrin aldehyde **78** was treated with (carbethoxymethylene)triphenylphosphorane to give nickel *meso*-[β -(ethoxycarbonyl)vinyl]octaethylporphyrin **79**. Subsequent demetallation with concentrated sulfuric acid (to yield the porphyrin **81**) and cyclization in refluxing glacial acetic acid under nitrogen afforded the corresponding (ethoxycarbonyl)octaethylpurpurin **81** in 72% yield. The use of free base was essential for the cyclization because the initial step of the cyclization involved the protonation of porphyrin nitrogen.⁷³ Evidences supporting the formation of **81** were given by mass spectrometry, which indicated a product isomeric with the reactant, and by the ¹H NMR spectrum of **81**. The signals associated with the acrylate protons in **81** (doublets at δ 10.40, 6.20 ppm) were no longer present in the spectrum of cyclized product, which instead contained a singlet at δ 9.40 ppm attributable to the olefinic proton of the cyclopentenyl ring. Of the four *meso* protons, one was shifted upfield approximately 1 ppm, which was indicative of its placement adjacent to a reduced pyrrole ring.⁷⁴ In addition, both methyl and methylene resonances of a peripheral ethyl group exhibited upfield shifts of approximately 1 ppm, consistent with their

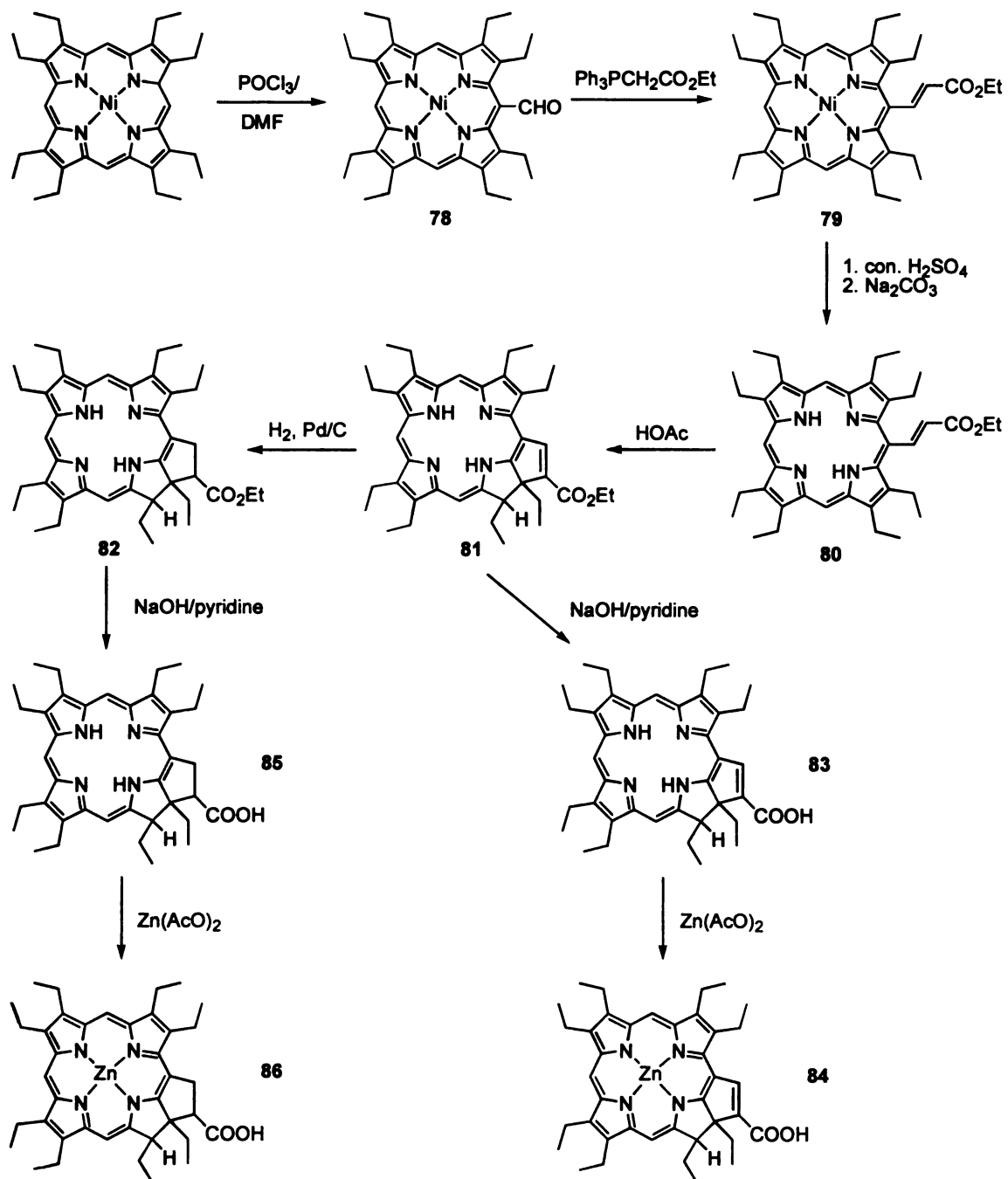
presence on a nonplanar reduced pyrrolic ring.⁷⁵ Finally, the visible spectrum of the **81** gave a purpurin-type spectrum, with the absorption of band I appearing at 695 nm.

The conversion of purpurin **81** to **82** was based on the method described by Morgan.⁷² Catalytic hydrogenation of **81** with 10% Pd/C resulted in the reduction of this molecule to the porphyrinogen as evidenced by loss of the color in the resulting solution. Filtration to remove the catalyst followed by vigorous stirring in the presence of air quickly reoxidized the macrocycle to give a deep blue/green solution from which the product **82** was isolated in 71% yield. The formation of the product as **82** was based on the mass spectrum (confirming addition of 1 mole of hydrogen), the visible spectrum, which resembled that of a chlorin⁷⁶ (λ_{max} 662 nm), and the ¹H NMR spectrum, which confirmed the integrity of the carbon skeleton but lacked the signal attributable to a cyclopentenyl proton.

Initial difficulties were encountered when ester **81** was hydrolyzed with sodium hydroxide in ethanol. However, when the reaction was carried in pyridine, the hydrolysis went smoothly. Both **81** and **82** were hydrolyzed by this method and were converted to **83** and **85**, respectively. Corresponding zinc complexes **84** and **86** were then obtained by regular zinc insertion procedures (ZnCl₂/DMF).

2. Purpurin and chlorin amidinium

The synthetic strategy used to derive the amidinium compound is similar to that described previously for making porphyrin amidinium **75**. Thus, the first step of the synthesis of **92** was to make purpurin nitrile **89**. As described in Scheme 16, diethyl cyanomethyl-phosphonate was treated with 1 eq. of sodium hydride to generate a Wittig



Scheme 15

reagent, which reacted with nickel *meso*-formyloctaethylporphyrin **78** to give nickel *meso*-(β -cyanoethenyl)-octaethylporphyrin **87** in 87% yield. After demetallation with concentrated sulfuric acid, free base **88** was obtained. In **88**, the steric effect and electron withdrawing properties of the porphyrin were similar to that of porphyrin **80**. Therefore, we expected that **87** should undergo similar cyclization to give the corresponding purpurin **89**. To accomplish the cyclization, **88** was refluxed in glacial acetic acid under nitrogen. After purification by column chromatography and crystallization, a purple crystalline product was obtained. Its UV-vis spectrum was similar to that of **81** with the absorption band I appearing at 692 nm. The mass spectrum indicated that the product was isomeric with the reactant **88**. Also in the ^1H NMR spectrum, signals associated with vinyl protons in **88** (doublets at δ 10.06, 5.58 ppm) were no longer present in the spectrum of product **89**, which contained instead a singlet at δ 9.20 ppm attributable to the olefinic proton of the cyclopentenyl ring. One *meso* proton as well as both methyl and methylene resonances of a peripheral ethyl group exhibited upfield shifts of approximately 1 ppm, which was similar to that observed in **81**. In addition, the IR spectrum revealed a peak at 2235 cm^{-1} , providing the evidence for the presence of a nitrile group in the product.

With the purpurin nitrile in hand, the conversion of **89** to **92** was achieved using the methodology described in Chapter II. Purpurin **89** was refluxed with nickel acetate in DMF to give the nickel complex **91**, which was then treated with chloromethylaluminum amide to effect the conversion of **91** to **92**. Spectral data supported the formation of amidinium **92**. Two broad NH peaks appeared at 8.80 and 8.96 ppm in the proton NMR of **92**, indicating of the formation of the amidinium group. Also, the nitrile stretching

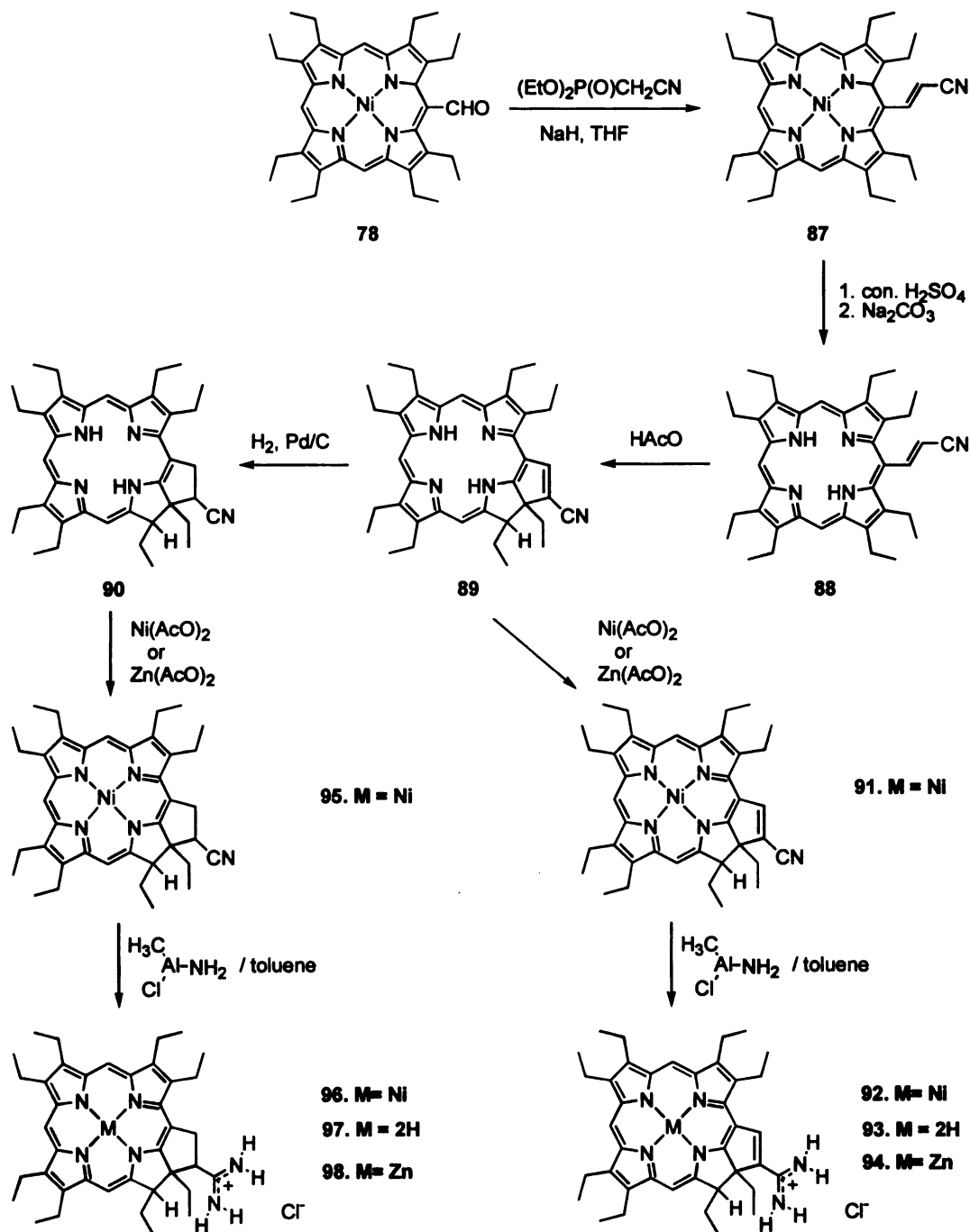
band (2235 cm^{-1}) was no longer present in the IR spectrum of **92**, and instead was replaced by a band at 1653 cm^{-1} , which is attributable to the C=N stretching of the amidinium group.

Catalytic hydrogenation of **89** with 10% Pd/C resulted in reduction of the molecule to the porphyrinogen, which was vigorously stirred in the presence of air to reoxidize the macrocycle to give **90** in 75% yield. The formation of the product as **82** is based on its mass spectrum (confirming addition of 1 mole of hydrogen), the chlorin type visible spectrum⁷⁷ (λ_{max} 662 nm), and its ^1H NMR spectrum, which confirmed the integrity of the carbon skeleton but lacked the signal attributable to a cyclopentenyl proton. After nickel insertion, **95** was converted to amidinium **96** with $\text{ClAl}(\text{NH}_2)\text{CH}_3$ using the methodology described previously in 93% yield. Both NMR and MS gave satisfactory results. Later it was found that chlorin amidinium **96** could be directly derived from purpurin amidinium **92**. When **92** was hydrogenated with 10% Pd/C, it was converted to **96**. This demonstrated that amidinium group was stable to hydrogenation.

After demetallation with concentrated sulfuric acid (to yield free bases), **92** and **96** were converted to corresponding zinc complexes **94** and **98**, respectively, using zinc chloride in DMF.

B. Coupling vs. Decoupling

In order to determine the electronic coupling between the chromophore and the proton interface in purpurin and chlorin complexes, we utilized the same methodology described in Chapter II by examining the pH dependence of their absorption spectrum. Figure 17 shows the spectral changes associated with deprotonation of purpurin amidinium **92** in CH_2Cl_2 . The arrows indicate the spectral shifts observed upon addition



Scheme 16

of DBU in CH_2Cl_2 to **92**. It can be seen that the deprotonation of the amidinium group of **92** results in blue shifts in the visible absorption maxima along with the sharpening of the Soret band. The set of absorption spectra contains isosbestic points at 434, 620 and 658 nm. This process was also found reversible and the original spectra could be recovered by the addition of CH_2Cl_2 saturated with 70% of HClO_4 . The perturbation of the absorption profile upon deprotonation of amidinium suggests that the purpurinic chromophore of **92** is strongly coupled to the amidinium group that constitutes interface.

Such changes were not observed in chlorin **96** upon deprotonation of the amidinium group. Figure 18 shows the spectra of **96** in the presence of various concentrations of DBU in CH_2Cl_2 . It can be seen that deprotonation of amidinium group of **96** results in no significant shift of the spectra. Compared to **92**, the lack of change in the absorption profile upon deprotonation of chlorin **96** thus suggests that the chlorinic chromophore of **96** is decoupled to the amidinium and correspondingly to the interface.

C. Binding Studies

The abilities of the purpurin and chlorin amidinium to form a salt bridge with benzoate in DMSO were studied using ^1H NMR. Upon stepwise addition of benzoate, the internal protons of amidinium exhibited downfield shift due to the formation of hydrogen bond with oxygen of the benzoate. Figure 19 shows the NMR spectra of purpurin amidinium **92** in the presence of various concentration of tetrabutylammonium benzoate in DMSO-d_6 . Consistent with the porphyrin system, the chemical shift of the *meso* proton remains unchanged and excludes the possibility that the interaction between the porphyrin and benzoate is due to π - π stacking. The association constants determined by this method for these systems are listed in Table 6. As in the previous porphyrin

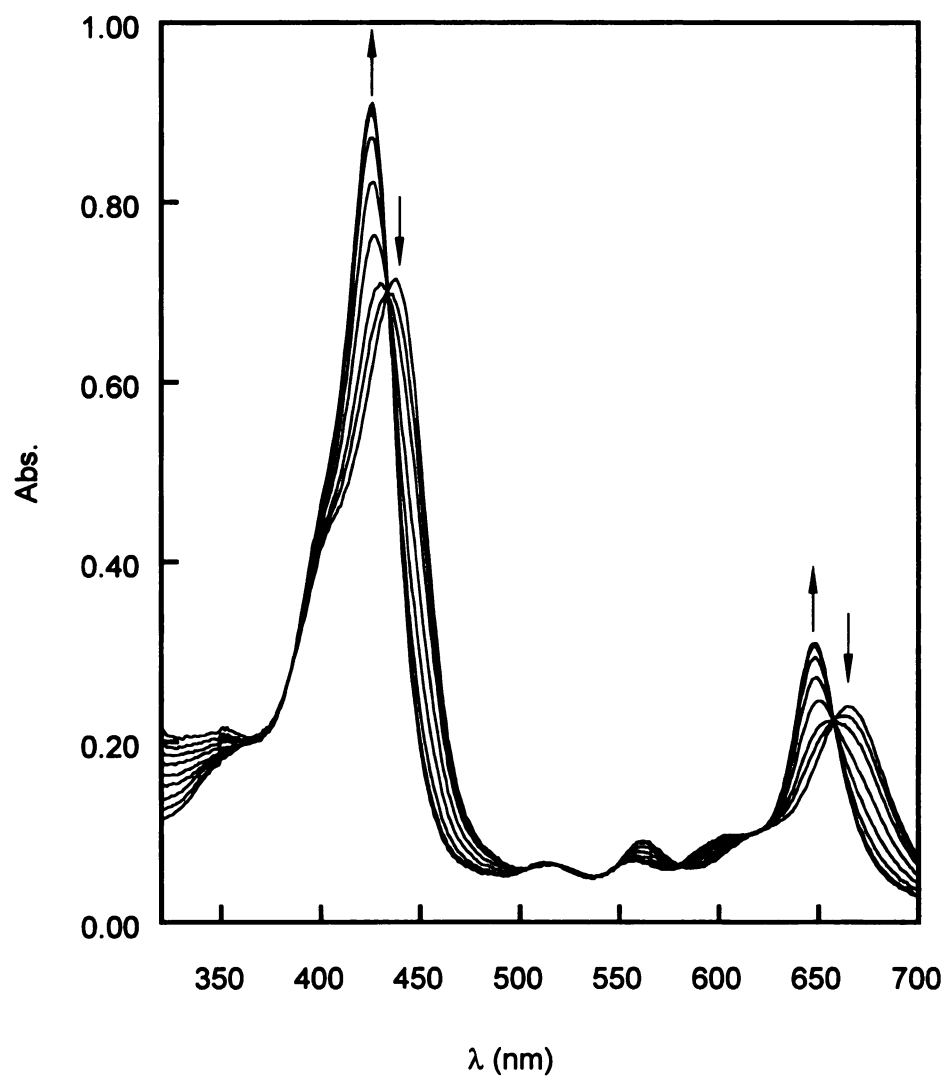


Figure 17. Absorption spectra of purpurin 92 (0.81 μM) in the presence of 0.00, 0.20, 0.40, 0.60, 0.80, 1.00, 1.40, 1.80, 2.40 eq. of DBU in CH_2Cl_2 . The arrows represent the increasing of DBU.

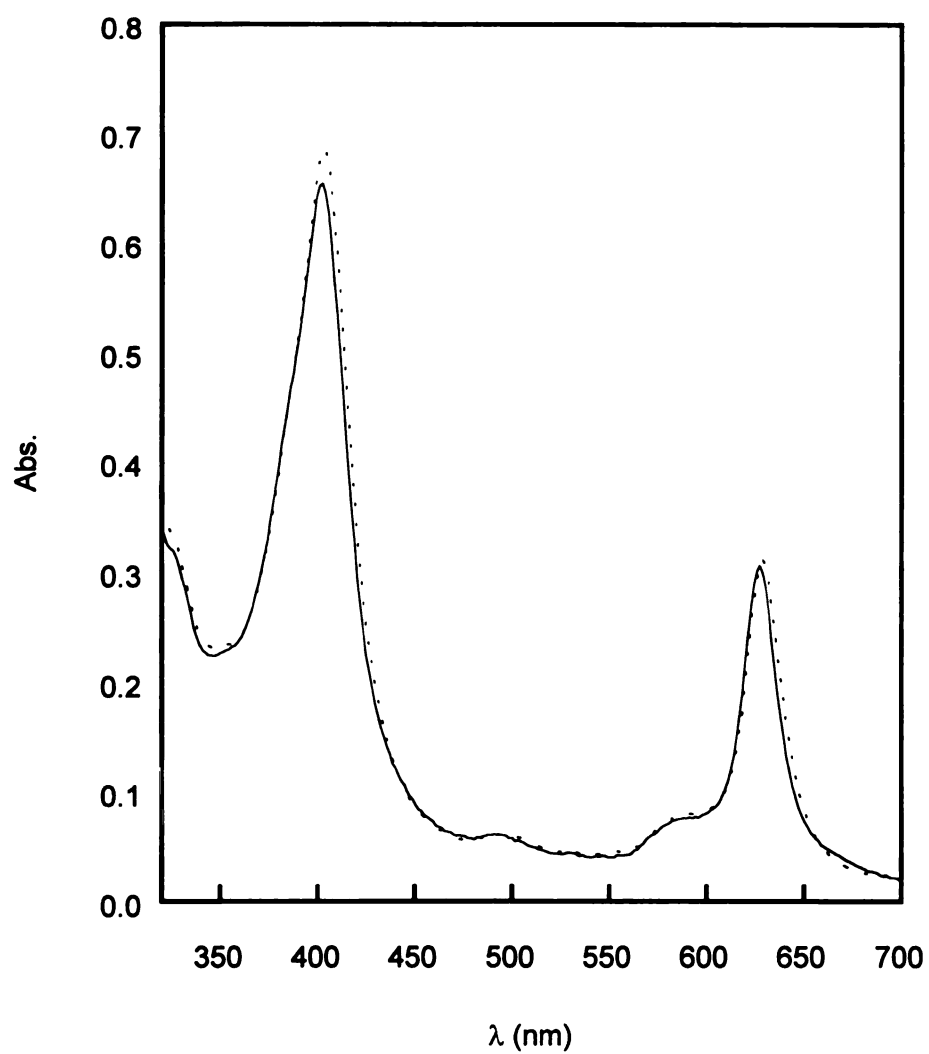


Figure 18. Absorption spectra of chlorin **96** (0.93 μM) in the absent (—) and present of 3.00 (.....) eq. of DBU in CH_2Cl_2 .

systems, these association constants are too large to be determined by NMR titration using CH_2Cl_2 as solvent. Thus, UV-vis was used to monitor the formation of salt bridge. However, this method is only applicable to purpurin **92**, in which the chlorinic chromophore is coupled to the amidinium. The binding constants determined by this method are also listed in Table 6. For the case of **96**, the lack of spectral shifts obviated the determination of association constant by UV-vis.

D. PCET Studies

The C=C double bond in purpurin **84** and **94** and the C—C single bond in **86** and **98** allow us to turn on and off the coupling between the chlorinic chromophore and the proton interface, respectively. Thus, this unique structural feature of the purpurins and chlorins provides us an opportunity to study proton-coupling effects. The PCET model systems are shown in Figure 23. The supramolecular complexes, $\text{ZnPur}(\text{Am-COOH})\text{DNB}$ (**94**—3,5-DNB), $\text{ZnPur}(\text{COOH-Am})\text{DNB}$ (**84**—3,5-DNB), $\text{ZnChl}(\text{Am-COOH})\text{DNB}$ (**98**—DNBA), and $\text{ZnChl}(\text{COOH-Am})\text{DNB}$ (**86**—3,5-DNBA) feature (purpurin and chlorin) zinc donors and dinitroaromatic acceptors separated by a fixed distance ensured by the external five member ring, which locks the salt bridge. The number of bonds along the electron transfer pathway is also fixed, ensuring that modification only impacts the coupling between the chromophore and proton interface, as well as the directionality of proton transfers. Table 7 lists the D—A separation of these systems.

The ET studies were performed in an analogous manner as described chapter III. Photoexcitation of **84**, **94**, **86** and **98** in CH_2Cl_2 produced the highly reducing singlet excited state molecules having intrinsic fluorescent lifetime of 0.95, 0.91, 1.46 and 0.98 ns.

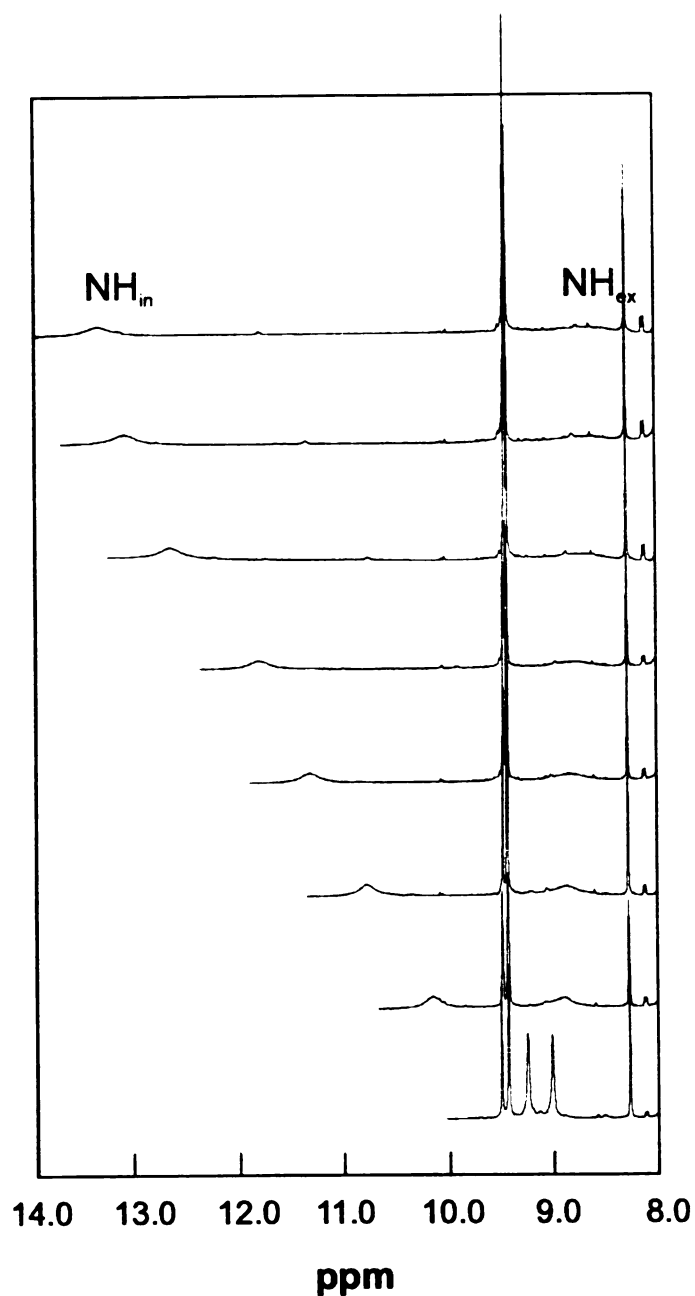


Figure 19. Selected ^1H NMR spectra of **96** (3.86 mM) with 1 eq. of benzoic acid in the absence of and in the presence of 1.00, 1.69, 2.38, 3.08, 5.16, 7.23, and 10.00 mM (bottom to top) of tetrabutylammonium benzoate in DMSO-d_6 at room temperature. The spectral range captures the amidinium protons internal (NH_{in}) and external (NH_{ex}) to the salt bridge interface and the three *meso* protons of the purpurin as well as olefinic proton of the cyclopentenyl ring.

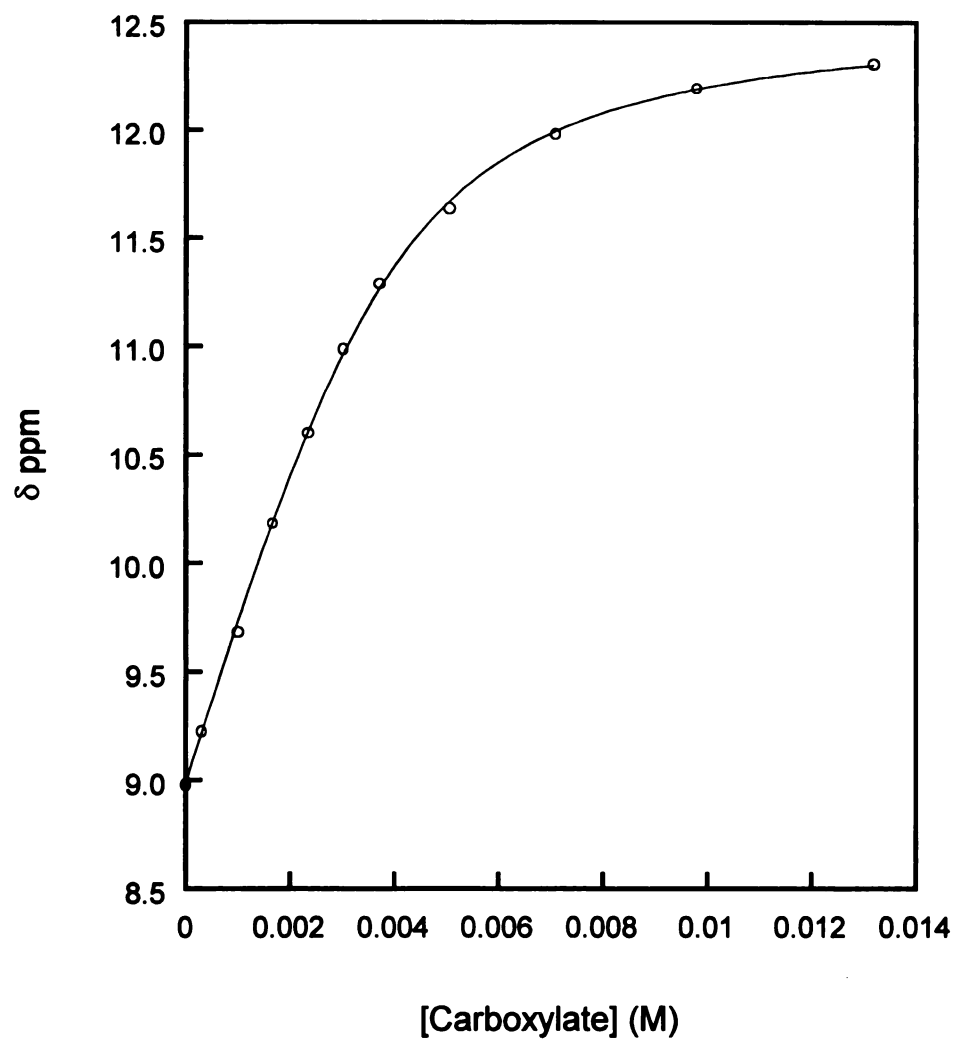


Figure 20. Plot of the chemical shift of internal protons of the amidinium versus the concentration of tetrabutylammonium benzoate

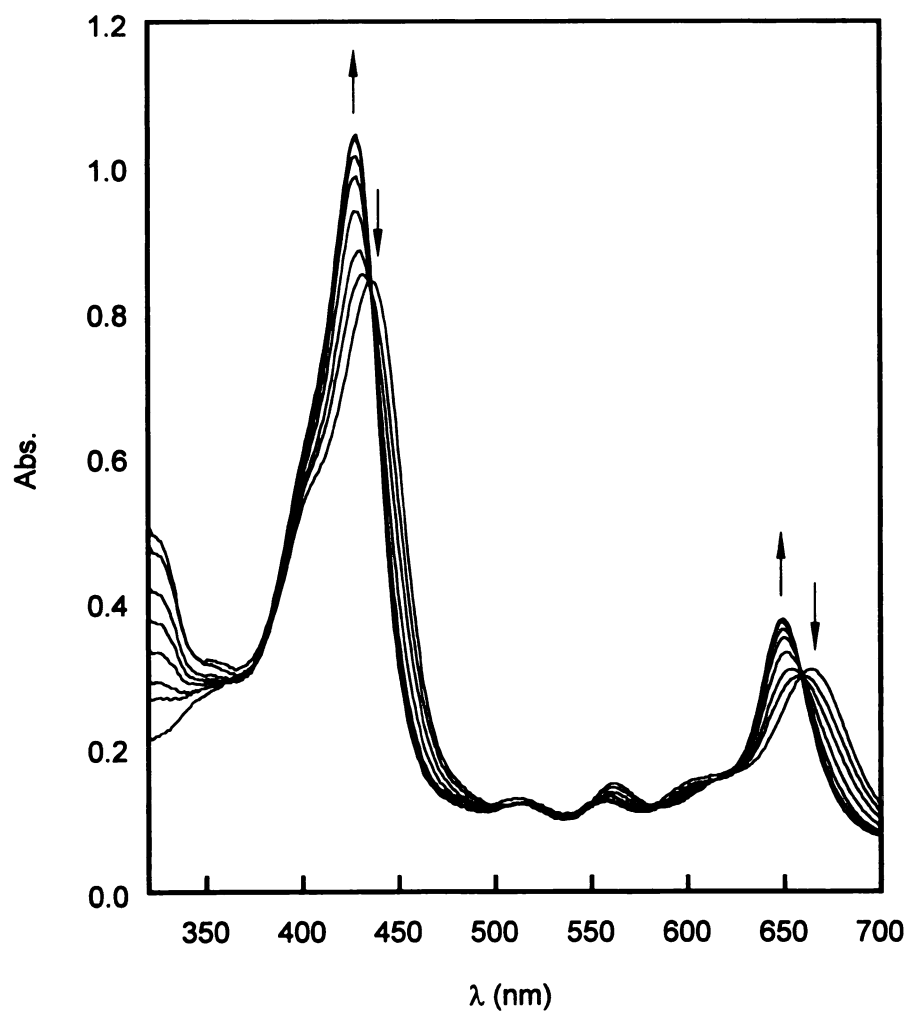


Figure 21. Selected UV-vis spectra of **92** (2.74 μM) in the presence of 0.0, 0.63, 1.26, 1.88, 2.51, 3.14, 4.40, 5.65 and 7.54 μM (increase with arrows) of tetrabutylammonium benzoate in dichloromethane.

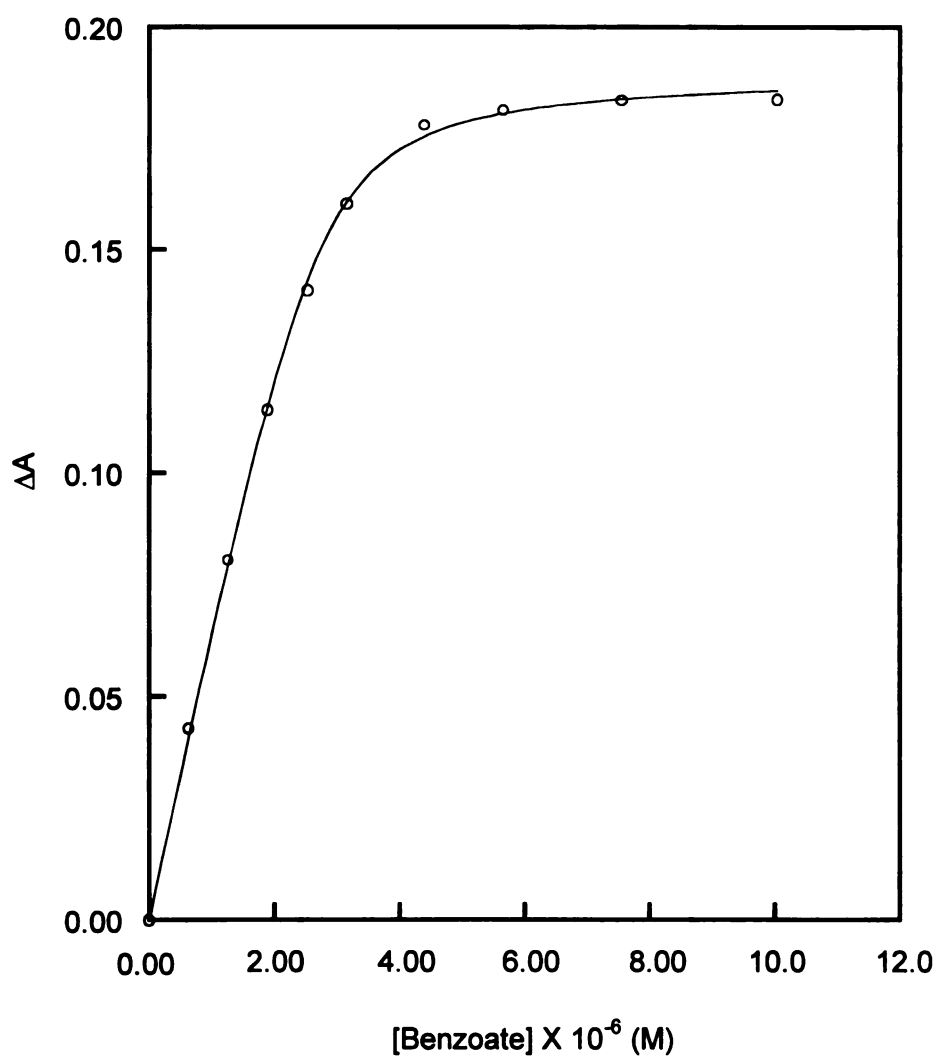


Figure 22. Plot of the absorption change of **92** at 420 nm versus the concentration of tetrabutylammonium benzoate

Table 6. Association Constants (K_a) and Energies (ΔG^0) for Purpurin and Chlorin Systems

Amidinium	Carboxylate	Solvent	K_a (M^{-1})	ΔG^0 (Kcal)
Purpurin amidinium 92	Benzoate	DMSO	$(1.80 \pm 0.17) \times 10^3$	-4.44
		$CH_2Cl_2^*$	$(6.8 \pm 1.2) \times 10^6$	-9.32
	3,5-DNB	DMSO	$(1.52 \pm 0.18) \times 10^2$	-2.98
		$CH_2Cl_2^*$	$(7.21 \pm 1.3) \times 10^5$	-7.99
Chlorin amidinium 96	Benzoate	DMSO	$(2.03 \pm 0.07) \times 10^3$	-4.51
	3,5-DNB	DMSO	$(1.61 \pm 0.08) \times 10^2$	-3.01

*Measured using UV-vis titration

When the corresponding 3,5-dinitroaromatics (3,5-DNB or 3,5-DNBA) were present, biexponential decays were observed. ET rates were determined by analysis of the fluorescence decay kinetic profiles as a function of the concentration of corresponding dinitroaromatics. In all system, it was found that one lifetime component was concentration-dependent and the other was concentration-independent. The concentration-dependent rate constant was assigned to the bimolecular ET processes and the concentration-independent rate constant was attributed to ET for the associated pairs. The unimolecular ET rates for these systems measured by this method, as well as the driving force of the ET reaction of each system, are summarized in Table 7. Before discussing the role played by proton coupling in the salt bridge, the impact of the permanent dipole moment associated with the salt bridge on the photoinduced ET rate must be addressed.

According to the classical and semiclassical ET theory, the ET rate constant k_{ET} can be expressed as

$$k_{ET} = (2\pi / h) V_R^2 (FC) \quad (4.1)$$

where V is the electronic coupling term that is distance dependent. FC is Franck-Condon factor and is expressed as:

$$FC = \frac{1}{4\pi\lambda k_B T} \exp\left(\frac{G^*}{k_B T}\right) \quad (4.2)$$

where k_B and T are, respectively, Boltzmann's constant and the temperature. G^* is the energy barrier for the ET reaction. According to the Marcus ET theory⁷⁸, it is expressed as:

$$G^* = -\frac{(\Delta G^0 + \lambda)^2}{4\lambda} \quad (4.3)$$

where λ is the reorganization energy containing contributions from solvent, as well as from molecular vibration of the donor-acceptor system; ΔG^0 is the standard free energy of reaction (negative of the driving force). Because of the permanent dipole moment of the salt bridge, we expect the free energy of the ET reaction in ZnPur(Am-COOH)DNB and ZnChl(Am-COOH)DNB will be affected differently compare to that in ZnPur(COOH-Am)DNB and ZnChl(COOH-Am)DNB. In ZnPur(Am-COOH)DNB and ZnChl(Am-COOH)DNB, the electron transfer opposes the dipole moment and therefore the ET will be energetically less favorable. Whereas, in ZnPur(COOH-Am)DNB and ZnChl(COOH-Am)DNB, the electron transfer is along the dipole moment and thus the ET reaction is more exothermic. Because the D-A separations for the four assemblies are the same, the free energy change associated with the permanent dipole from ZnPur(Am-COOH)DNB to ZnPur(COOH-Am)DNB and that from ZnChl(Am-COOH)DNB to ZnChl(COOH-Am)DNB should be the same in the same solvent. If dipole moment effects dominated the ET kinetics in these systems, the ET rate difference between ZnPur(Am-COOH)DNB and ZnPur(COOH-Am)DNB should be similar to that between ZnChl(Am-COOH)DNB and ZnChl(COOH-Am)DNB. However, this is not the case. A comparison of photoinduced ET rate data between ZnPur(Am-COOH)DNB and ZnPur(COOH-Am)DNB shows that switching the proton interface has a dramatic impact on ET rates for the purpurin system. For the chlorin system, switching the proton interface had only a minor effect when one compares the ET rates of ZnChl(Am-COOH)DNB to ZnChl(COOH-Am)DNB. The huge difference of ET rate constants between ZnPur(Am-COOH)DNB and ZnPur(COOH-Am)DNB compared to that between ZnChl(Am-COOH)DNB and ZnChl(COOH-Am)DNB implies factors other than

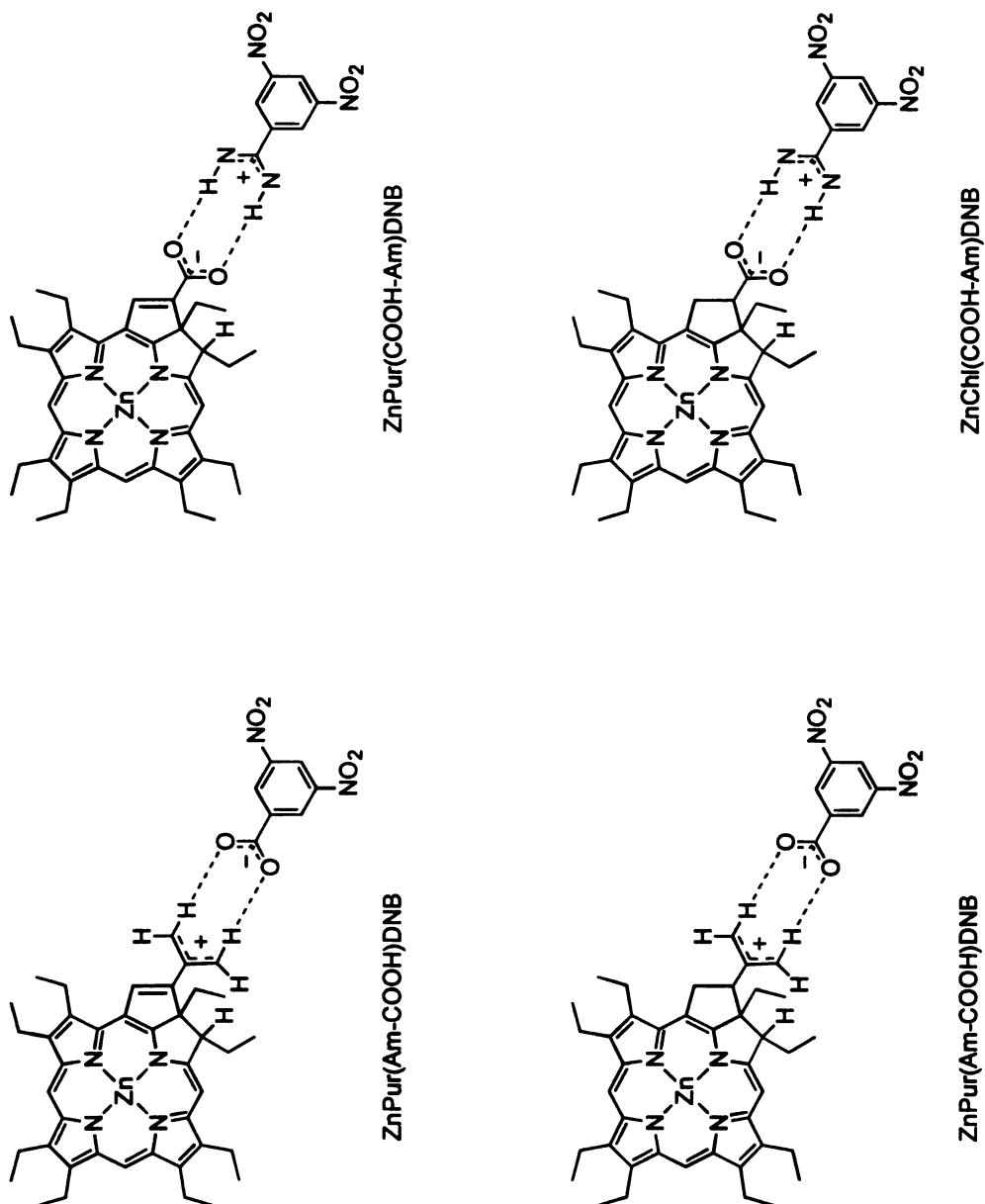


Figure 23. Summary of ET rates in purpurin and chlorin systems

Table 7. Distance, Driving Force and ET Rate Constants for Purpurin and Chlorin Systems

ET system	D-A Distance [*] (Å)	ΔG^0 (eV)	k_{ET} ($\times 10^8 \text{ s}^{-1}$)
ZnPur(Am-COOH)DNB	13.9	-0.54	0.85
ZnPur(COOH-Am)DNB	13.8	-0.53	15.0
ZnChl(Am-COOH)DNB	13.7	-0.67	1.2
ZnChl(COOH-Am)DNB	13.7	-0.64	3.0

^{*}Defined as the length of the vector connecting zinc directly to the center of 3,5-DNB and 3,5-DNBA. All distances were estimated with SPARTAN and the parameters for the salt bridge were fixed using those from the crystal structure of porphyrin amidinium **75**.

the dipole moment of salt bridge are involved in the ET reaction.

According to eq. 4.3, the Franck Condon factor is determined by both the driving force and the reorganization energy (λ) of the ET reaction. Reorganization energy occurs because the electron transfers at a much faster rate than the movement of solvent, and the solvent does not have enough time to adjust its dipole moment to optimize the solvation energy. Thus the ET product forms in a high-energy state; the energy required to relax to equilibrium is the reorganization energy. Therefore, the magnitude of λ is determined by the solvent and the size of electron donor and acceptor (the larger size of D-A molecule is, the less density of charge on its surface, and less reorganization energy). Marcus proposed that for a certain ET reaction, λ can be expressed as:

$$\lambda = e^2 [(2r_D)^{-1} + (2r_A)^{-1} - (R_{DA})^{-1}] (\epsilon_s^{-1} + \epsilon_{op}^{-1}) \quad (4.4)$$

where e is the charge of an electron, ϵ_s is the static and ϵ_{op} is the high frequency dielectric constant of the solvent, r_D and r_A is the radii of donor and acceptor, respectively and R_{DA} is their separation.

In ZnChl(Am-COOH)DNB and ZnChl(COOH-Am)DNB assemblies, the chlorin chromophores are decoupled from the salt bridge, and the ET event is independent from what happens at the salt bridge. Thus, ET reactions in these complexes behave normally. The ET rate differences between ZnChl(Am-COOH)DNB and ZnChl(COOH-Am)DNB reflect only the dipole moment effect of the salt bridge. However, the situation is more complicated for the purpurin systems. Wasielewski⁷⁹ has demonstrated that the reorganization energy for similar covalently linked Zn(II) porphyrin donor-acceptor systems is 0.9 eV. The ET driving force for ZnPur(Am-COOH)DNB and ZnPur(COOH-Am)DNB are 0.54 eV and 0.53 eV respectively. From eq. 4.3, the increase of the

reorganization energy should decrease the ET rate because $-\Delta G^0 < \lambda$ for these systems. This is exactly what we observed in our experiments. In ZnPur(Am-COOH)DNB, the photoinduced ET reaction produces a positive charge on purpurin **94**. Since the chromophore of **94** is coupled to the amidinium of the salt bridge, the presence of the positive charge will decrease the pKa of the amidinium group. On the donor side, the ET event results in a negative charge on 3,5-DNB and the pKa of the carboxylate group will increase. Such changes in pKa within the salt bridge will most likely drive the proton across the interface and the whole system will be stabilized by the proton transfer. This is not the case for ZnPur(COOH-Am)DNB. Here the proton is already residing on the acceptor, and hence it is likely to remain upon the arrival of the electron. Like the electron transfer, proton transfer can give rise to reorganization energy due to its positive charge. Hence, there is reorganization energy associated with ET *and* PT in ZnPur(Am-COOH)DNB, whereas for the case of ZnPur(COOH-Am)DNB, there is a reorganization energy that arises from ET only. This extra reorganization energy is believed to be responsible to the slow ET rate in ZnPur(Am-COOH)DNB.

In summary, comparisons of ET rates in the chlorin systems rule out the permanent dipole moment of the salt bridge as the major factor for the large ET rates difference between ZnPur(Am-COOH)DNB and ZnPur(COOH-Am)DNB of purpurin systems. Instead, that proton transfer within the salt bridge is believed to contribute to the slow electron transfer in ZnPur(Am-COOH)DNB. The relocation of proton causes extra reorganization energy for the ET reaction, thus giving rise to the slower ET rate.

V. Experimental

Nickel *meso*-formyloctaethylporphyrin 78

Freshly distilled phosphoryl chloride (2.74 ml) was added dropwise to dry DMF (2 ml) cooled in an ice-bath, and the solution was kept at room temperature for 30 min. Then the mixture was warmed up on water bath to 50 °C and a solution of Ni-OEP (500 mg, mol) in dry 1,2-dichloroethane (300 ml) was added dropwise with vigorous stirring, maintaining the temperature at 50 - 55 °C over a period of 15 min. The solution was then warmed for a further 1 h, a saturated solution of sodium acetate (200 ml) was added, and stirring and heating were continued for a further 2 h. The organic phase was separated and the water phase extracted with dichloromethane twice, which was added to the organic layer. The solvents were removed under reduced pressure and the residue was dissolved in dichloromethane and chromatographed on silica gel (CH₂Cl₂ eluent). The title compound was obtained in 85% yield. UV-vis: λ 402, 561, 643 nm; ¹H NMR (300 MHz, CDCl₃) δ 1.70 (24H, m, CH₃ of ethyl), 3.70 (16H, m, CH₂ of ethyl), 9.27 (2H, s, *meso* H), 9.30 (1H, s, *meso* H); MS found *m/e* 618; calcd 618.29 for C₃₇H₄₄N₄NiO

Nickel *meso*-(β -ethoxycarbonyl ethenyl)octaethylporphyrin 79

A solution of nickel *meso*-formyloctaethylporphyrin **78** (506 mg, 0.82 mmol) and (carbethoxymethylene)triphenylphosphorane (1.024 g, mmol) in xylene (50 mL) was heated under reflux for 18 hours. After the solution was cooled, the solvent was removed in vacuo and the resulting solid chromatographed on silica by using dichloromethane for elution. A minor fraction of nickel OEP was collected first, followed by a major red band.

Collection, removal of solvent, and crystallization of the resulting residue from dichloromethane-methanol gave the product (455 mg, 0.66 mmol) in 81% yield. m.p. 228-230 °C; UV-vis: λ_{max} 405, 530, 565 nm; ^1H NMR (300 MHz, CDCl_3) δ 1.30 (3H, t, CH_3 of ethyl ester), 1.75 (24H, m, CH_3 of peripheral ethyl), 3.78 (16H, m, CH_2 of peripheral ethyl), 4.28 (2H, q, CH_2 of ethyl ester), 5.25 (1H, d, α -H of acrylic ester), 9.41 (3H, s, *meso* H), 10.08 (1 H, d, β -H of acrylic ester); MS (CI 70 eV), m/e 688, calcd 688.32 for $\text{C}_{41}\text{H}_{50}\text{N}_4\text{O}_2\text{Ni}$

meso-(β -ethoxycarbonylethenyl)octaethylporphyrin 80

To a solution of the nickel complex **79** (455 mg, 0.66 mmol) in dichloromethane (80 mL), concentrated sulfuric acid (10 mL) was added and the mixture was kept stirred until all the porphyrin was extracted to the sulfuric acid layer. Ice (50 g) was added, followed by saturated aqueous sodium carbonate. After neutralization, the organic layer was collected, washed, and dried and the solvent was removed. Crystallization of the crude product from dichloromethane-methanol gave **80** (416 mg, 0.66 mmol) in 98% yield. m.p. 215-216 °C; UV-vis: λ_{max} 405; 530, 565; ^1H NMR (300 MHz, CDCl_3) δ -3.10 (2H, b, NH), 1.42 (3H, t, CH_3 of ethyl ester), 1.64 (6H, t, CH_3 of 3, 7-ethyl), 1.90 (18H, m, CH_3 of peripheral ethyl), 3.90 (4H, q, CH_2 of 3, 7-ethyl), 4.1 (12H, m, CH_2 of peripheral ethyl), 4.43 (2H, q, CH_2 of ethyl ester), 6.18 (1H, d, α -H of acrylic ester), 9.92 (1H, s, *meso* H), 10.06 (2H, s, *meso* H), 10.38 (1 H, d, β -H of acrylic ester); MS (CI 70eV), m/e 632, calcd 632.41 for $\text{C}_{41}\text{H}_{52}\text{N}_4\text{O}_2$

Cyclization of meso-(β -ethoxycarbonylethenyl)octaethylporphyrin to purpurin 81

A solution of **80** (416 mg, 0.66 mmol) in glacial acetic acid (80 ml) was heated under reflux in a nitrogen atmosphere for 24 hours. The solvent was removed in vacuo and the residue was dissolved in dichloromethane. Chromatography on silica with dichloromethane as eluant gave a major green fraction. Removal of the solvent and crystallization from dichloromethane-methanol gave purple microcrystals of **81** (300 mg, 72 % yield). UV-vis λ_{max} 433, 453, 503, 530, 568, 648, 695; ^1H NMR (300 MHz, CDCl_3) δ -1.05, -0.42 (each 1H, s, NH), -0.21 (3H, t, CH_3 of 3-ethyl), 1.75 (24 H, m, CH_3 of peripheral ethyl), 2.50, 2.9 (2H each, m, CH_2 of 1, 2-ethyl), 3.80 (m, 13H, CH_2 of peripheral ethyl, C-2 H), 4.00 (2H, q, CH_2 of ethyl ester), 9.20 (1H, s, H of isocyclic ring), 8.44, 9.48, 9.51 (each 1H, s, *meso* H); MS (CI 70eV), m/e 632, calcd 632.41 for $\text{C}_{41}\text{H}_{52}\text{N}_4\text{O}_2$

Hydrogenation of Purpurin ester to Chlorin ester **82**

Palladium on charcoal (10%) (20 mg) was added to a stirred solution of purpurin ester **81** (100 mg, 0.16 mmol) in THF (20 mL) containing triethylamine (2 drops). The resulting mixture was hydrogenated at room temperature, under a slightly positive pressure. After stirring overnight, the reaction mixture was filtered and the solution obtained vigorously stirred in air for 2.5 h. After complete oxidation of the intermediate porphyrinogen, followed by measuring the increasing intensity of an absorption at 660 nm in the visible spectrum, the solvent was removed in vacuo and the residue chromatographed on silica gel with 1% methanol in dichloromethane. The major blue band was collected, the solvent removed, and the crude product crystallized from dichloromethane-methanol to give the product (72 mg, 0.11 mmol) in 71% yield. UV-vis λ_{max} 403, 500, 535, 558, 610,

660 nm; ^1H NMR (300 MHz, CDCl_3) δ -2.00, -1.38 (each 1H, s, NH), -0.20 (3H, t, CH_3 of 3-ethyl), 1.55 (3H, t, CH_3 of ethyl ester), 1.75 (21H, m, CH_3 of peripheral ethyl), 2.80, 3.10 (2H each, m, CH_2 of 2, 3-ethyl), 3.85 (m, 12H, CH_2 of peripheral ethyl,), 4.45 (2H, m, CH_2 of ethyl ester), 4.46 (1H, m, C-2 H), 4.65, 4.82, 5.22 (1H each, m, H of isocyclic ring), 8.68, 9.58, 9.60 (each 1H, s, *meso* H); MS (CI 70eV), m/e 634, clcd 634.41 for $\text{C}_{41}\text{H}_{54}\text{N}_4\text{O}_2$

Purpurin carboxylic acid 83

A solution of purpurin ester **81** (100 mg, 0.16 mmol) in pyridine (15 ml) was heated to reflux under nitrogen and sodium hydroxide (1 g) in water (2 ml) was added. The mixture was then allowed to reflux overnight. After cooling to room temperature, water was added and the mixture was extracted with dichloromethane (15 ml) three times. The organic layer was combined and washed with water, dried over sodium sulfate. The solvent was removed under reduced pressure and residue chromatographed on silica with 3% methanol in dichloromethane. The crude product was crystallized from dichloromethane-methanol to give **83** (77 mg, 0.13 mmol) in 80% yield. m.p. $>275^\circ\text{C}$; UV-vis λ_{max} 428, 502, 526, 566, 639, 694; ^1H NMR ($\text{DMSO}-d_6$) δ -1.22, -0.58 (each 1H, s, NH), -0.35 (3H, t, CH_3 of 3-ethyl), 1.75 (24H, m, CH_3 of peripheral ethyl), 2.70, 3.15 (2H each, m, CH_2 of 2, 3-ethyl), 3.80 (m, 13H, CH_2 of peripheral ethyl, C-2 H), 4.02 (2H, q, CH_2 of ethyl ester), 9.24 (1H, s, H of isocyclic ring), 8.78, 9.52, 9.54 (each 1H, s, *meso* H), 12.62 (1H, s, carboxylic acid H); MS (FAB), m/e 605.2 (MH^+), clcd 605.37 for $\text{C}_{39}\text{H}_{49}\text{N}_4\text{O}_2$

General procedure for Zinc insertion:

Zinc acetate (100 mg) was added to a solution of purpurin or chlorin (0.1 mmol) in DMF (15 mL) and the mixture refluxed until chelation was complete (monitored by both UV-vis and TLC, ca. 5 min). The mixture was added to water and extracted with dichloromethane. The organic layer was washed with water several times. After removal of solvent, the solid residue chromatographed on silica gel (eluted with 3% methanol in dichloromethane) to give the product.

Zinc purpurine carboxylic acid 84

95% yield. m.p. 261-262 °C; UV-vis λ_{max} 436, 532, 579, 615, 662; MS (FAB) found m/e 666.2 (M^+), clcd 666.29 for $C_{39}H_{46}N_4O_2Zn$

Chlorin carboxylic acid 85

To a solution of chlorin ester **82** (72 mg, 0.11 mmol) in pyridine (10 mL), sodium hydroxide (0.5 g) in water (1 mL) was added. The mixture was heated to reflux for 2 h under nitrogen. After cooling, water was added and the mixture was extracted with dichloromethane (10 mL) three times. The organic layer was combined, washed with water and dried over sodium sulfate. The solvent was removed under vacuo and the residue chromatographed on silica gel with 7% methanol in dichloromethane. The crude product was crystallized from dichloromethane-methanol to give chlorin **85** (54 mg, 0.88 mmol) in 81% yield. m.p. >275 °C; UV-vis λ_{max} 401, 499.5, 558, 558, 608, 662; ^1H NMR (300 MHz, CDCl_3) δ -2.02, -1.44 (each 1H, s, NH), -0.18 (3H, t, CH_3 of 3-ethyl), 1.78 (24H, m, CH_3 of peripheral ethyl), 2.08 (2H, m, CH_2 of 2-ethyl), 2.80, 3.10 (2H each, m,

CH₂ of 2, 3-ethyl), 3.90 (m, 12H, CH₂ of peripheral ethyl,), 4.45 (2H, m, CH₂ of ethyl ester), 4.46 (1H, m, C-2 H), 4.65, 4.82, 5.22 (1H each, m, H of isocyclic ring), 8.68, 9.58, 9.60 (each 1H, s, *meso* H); MS (CI 70eV), m/e 606, clcd 606.37 for C₃₉H₅₀N₄O₂

Zinc chlorin carboxylic acid 86

95% yield. m.p. >275 °C; UV/vis: λ_{max} 410, 480, 513, 588, 634; MS (CI 70eV) found m/e 668, clcd 668.31 for C₃₉H₄₈N₄O₂Zn

Nickel *meso*-(β-cyanoethenyl)octaethylporphyrin 87

Diethyl cyanomethylphosphonate (1.0 g, 5.65 mmol) was added dropwise to a solution of sodium hydride (0.24 g, 60% dispersion in mineral oil) in dried THF (10 ml). The resulting solution was charged with *meso*-formyloctaethylporphyrin **78** (1.0 g, 1.62 mmol) in dried THF (20 ml). The mixture was heated under reflux in a nitrogen atmosphere for 1 hour and dichloromethane was added upon cooling to room temperature. The solution was washed with water three times and the organic layer was collected, dried with sodium sulfate and the solvent was removed in vacuo. The resulting solid was chromatographed on silica gel by using dichloromethane/hexane (1/1) for elution. Crystallization of the resulting residue from dichloromethane-methanol gave the porphyrin **87** (0.91 g, 1.48 mmol) in 87% yield. m.p. 228-230 °C; UV-vis: λ_{max} 405, 530, 565; ¹H NMR (300 MHz, CDCl₃) δ 1.75 (24H, m, CH₃ of peripheral ethyl), 3.78 (16H, m, CH₂ of peripheral ethyl), 4.58 (1H, d, α-H of acrylic nitrile), 9.41 (3H, s, *meso* H), 9.72 (1 H, d, β-H of acrylic nitrile); MS (CI 70eV), m/e 641, clcd 641.30 for C₃₉H₄₅N₅Ni

meso-(β -cyanoethenyl)octaethylporphyrin 88

To a solution of the nickel complex **87** (500 mg, 0.78 mmol) in dichloromethane (80 ml), concentrated sulfuric acid (15 ml) was added and the mixture was stirred until all the porphyrin was extracted to the sulfuric acid layer. Ice (50 g) was added, followed by saturated aqueous sodium carbonate. After neutralization, the organic layer was collected, washed, and dried and the solvent was removed. Crystallization of the crude product from dichloromethane-methanol gave the free base (450 mg, 0.78 mmol) in 98% yield. m.p. 215-216 °C; UV-vis: λ_{max} 406, 505, 539, 575, 626; ^1H NMR (300 MHz, CDCl_3) δ - 3.14 (2H, b, NH) 1.80 (24H, m, CH_3 of peripheral ethyl), 4.00 (16H, m, CH_2 of peripheral ethyl), 5.58 (1H, d, α -H of acrylic nitrile), 9.96 (1H, s, *meso* H), 10.04 (2H, s, *meso* H), 10.06 (1 H, d, β -H of acrylic nitrile); MS (CI 70eV), m/e 585, clcd 585.38 for $\text{C}_{39}\text{H}_{47}\text{N}_5$.

Cyclization of meso-(β - cyanoethenyl)octaethylporphyrin to purpurin 89

A solution of *meso*-[β -cyano vinyl]octaethylporphyrin **88** (450 mg, 0.78 mmol) in glacial acetic acid (80 ml) was heated under reflux in a nitrogen atmosphere for 24 hours. The solvent was removed in vacuo and the residue was dissolved in dichloromethane. Chromatography on silica gel with dichloromethane as eluant gave a major green fraction. Removal of the solvent and crystallization from dichloromethane-methanol gave purple microcrystals of **89** (368 mg, 81% yield). m.p. >275 °C; UV-vis λ_{max} 426, 523, 564, 635, 692; ^1H NMR (300 MHz, CDCl_3) δ -1.05, -0.45 (each 1H, s, NH), -0.22 (3H, t, CH_3 of 3-ethyl), 1.75 (21H, m, CH_3 of peripheral ethyl), 2.50, 2.95 (2H, m, CH_2 of 2, 3-ethyl), 3.80 (m, 13H, CH_2 of peripheral ethyl, C-2 H), 9.20 (1H, s, H of isocyclic ring), 9.51, 9.48, 8.49 (each 1H, s, *meso* H); MS (CI 70eV), m/e 585, clcd 585.38 for $\text{C}_{39}\text{H}_{47}\text{N}_5$.

Chlorin nitrile 90

89 (120 mg, 0.20 mmole) was hydrogenated under the condition described previously to give 88 mg of title compound (75% yield). m.p. >275 °C; UV-vis: λ_{max} 402, 498, 558, 610, 660 nm; ^1H NMR (300 MHz, CDCl_3) δ -2.35, -1.70 (each 1H, s, NH), -0.30 (3H, t, CH_3 of 3-ethyl), 1.75 (21H, m, CH_3 of peripheral ethyl), 2.10, 2.80 (2H each, m, CH_2 of 2, 3-ethyl), 3.85 (m, 12H, CH_2 of peripheral ethyl), 4.15 (1H, m, C-2 H), 4.30, 5.02, 5.04 (1H each, m, H of isocyclic ring), 8.45 (1H, s, *meso* H), 9.60 (2H, s, *meso* H); MS (CI 70eV), m/e 587, clcd 587.38 for $\text{C}_{39}\text{H}_{47}\text{N}_5$

Nickel purpurin nitrile 91

Nickel insertion was accomplished following the procedure described previously. m.p. >275 °C; UV-vis: λ_{max} 424, 511, 555, 605, 648; ^1H NMR (300 MHz, CDCl_3) δ -0.10 (3H, t, CH_3 of 3-ethyl), 1.65 (21H, m, CH_3 of peripheral ethyl), 2.00, 2.65 (2H, m, CH_2 of 2, 3-ethyl), 3.55 (m, 13H, CH_2 of peripheral ethyl), 3.78 (1H, m, C-2 H), 8.80 (1H, s, H of isocyclic ring), 7.80 (1 H, s, *meso* H), 9.00 (2H, s, *meso* H); MS (CI 70 eV), m/e 641, clcd 641.30 for $\text{C}_{39}\text{H}_{45}\text{N}_5\text{Ni}$

Nickel purpurin amidium chloride 92

The nickel purpurin nitrile **91** obtained from last step and dried toluene (20 ml) was added to a Schlenck tube. After the system was purged with argon three times, chloromethylaluminum(III) amide (2 mL, 2 mmol) was introduced by a syringe. The reaction mixture was stirred at 80 °C for 3 days under an argon atmosphere. The reaction

mixture was cooled and the aluminum complex was decomposed by carefully pouring the solution into a slurry of silica gel (5 g) in chloroform. The mixture was stirred for 5 min and the silica gel was filtered. The filtercake was further washed with methanol. Evaporation of the filtrate and purification of the residue by chromatography on silica gel (25% methanol in dichloromethane) afforded the title compound in 81% yield. m.p. 220 °C (dec.); UV-vis: λ_{max} 436, 532, 579, 615, 662 nm; ^1H NMR (300 MHz, CDCl_3) δ -0.20 (3H, t, CH_3 of 3-ethyl), 1.55 (21H, m, CH_3 of peripheral ethyl), 2.65, 2.80 (2H each, m, CH_2 of 2, 3-ethyl), 3.60 (m, 13H, CH_2 of peripheral ethyl), 4.00 (1H, m, C-2 H), 8.20 (1 H, s, *meso* H), 8.80, 8.96 (2H each, b, NH of amidinium), 9.10 (1H, s, H of isocyclic ring), 9.12, 9.20 (1H each, s, *meso* H); MS (FAB) found m/e 659.5 (MH^+), clcd 659.33 for $\text{C}_{39}\text{H}_{49}\text{N}_6\text{Ni}$

Zinc purpurin amidium chloride 94

65% yield. m.p. 248 °C (dec.); UV-vis λ_{max} 406, 442, 540, 626, 674; MS (FAB) found m/e 665.4 (MH^+), clcd 665.33 for $\text{C}_{39}\text{H}_{49}\text{N}_6\text{Zn}$

Nickel Chlorin nitrile 95

Nickel insertion was accomplished by following the procedure described previously to give **95** in 86% yield. m.p. >275 °C; UV-vis: λ_{max} 401, 492, 582, 626 nm; ^1H NMR (300 MHz, CDCl_3) δ 0.15 (3H, t, CH_3 of 3-ethyl), 1.60 (21H, m, CH_3 of peripheral ethyl), 1.85, 2.30 (2H each, m, CH_2 of 2, 3-ethyl), 3.55 (m, 12H, CH_2 of peripheral ethyl), 3.80 (1H, m, C-2 H), 3.92, 4.42, 4.80 (1H each, m, H of isocyclic ring), 7.65 (1 H, s, *meso*), 9.10 (2H each, s, *meso* H); MS (CI 70eV), m/e 643.31, clcd 643.30 for $\text{C}_{39}\text{H}_{47}\text{N}_5\text{Ni}$

Nickel chlorin amidinium chloride 96

The chlorin nitrile **95** (110 mg, 0.17 mmol) was treated with chloromethylaluminium amide using the procedure described previously to afford 116 mg of the title compound in 93% yield. m.p. 255 °C (dec.); UV-vis: λ_{max} 401, 496, 584, 626 nm; ^1H NMR (300 MHz, CDCl_3) δ -0.50 (3H, t, CH_3 of ethyl), 1.60 (21H, m, CH_3 of peripheral ethyl), 1.70 1.80 (2H each, m, CH_2 of 2, 3-ethyl), 3.50 (m, 12H, CH_2 of peripheral ethyl), 3.65 (1H, m, C-2 H), 3.70, 3.82, 4.15 (1H each, m, H of isocyclic ring), 6.95 (2H, br, NH of amidinium), 7.55, 9.00, 9.05 (1H each, s, *meso* H), 9.10 (2H, br, NH of amidinium) ; MS (FAB), m/e 661.1 (MH^+), clcd 661.34 for $\text{C}_{39}\text{H}_{51}\text{N}_6\text{Ni}$

Zinc chlorin amidium chloride 98

70% yield. m.p. >275 °C; UV-vis λ_{max} 410, 480, 513, 588, 634; MS (FAB), m/e 667.3 (MH^+), clcd 667.35 for $\text{C}_{39}\text{H}_{51}\text{N}_6\text{Zn}$

Chapter V

Synthesis of Water Soluble Porphyrin-Quinone

I. Introduction

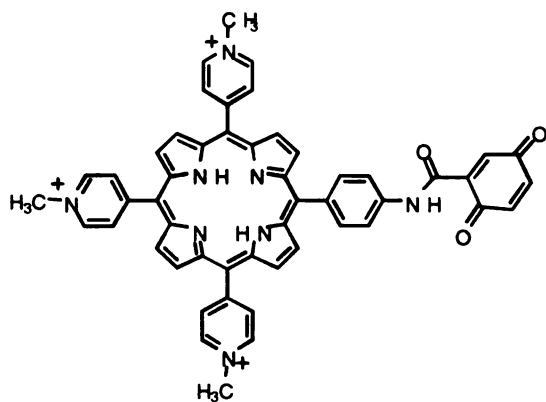
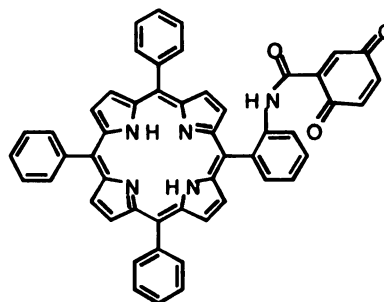
The primary photochemical step in photosynthesis consists of the transfer of an electron from the excited state of a porphyrin chromophore to an acceptor molecule to generate a transient radical-ion pair. The fundamental factors governing the efficiency of the light-induced electron transfer process and those that prevent the rapid back electron transfer in the charge separated species, are not well understood. In order to gain insights into these factors, there has been much effort expended on the development of potentially photoactive donor-acceptor model compounds. Most of these consist of a porphyrin acting as the light absorbing electron donor, and a chemically attached quinone as the electron acceptor. Since Kong and Loach⁸⁰ reported the synthesis of first covalently linked porphyrin-quinone system, a number of groups synthesized covalently linked porphyrin-quinone complexes in a variety of structures. Strategies used for linking the donor and acceptor include amide,⁸¹ diester and diamide-linked polymethylene chains,⁸² rigid triptycenyl⁸⁴ and bicyclo[2.2.2]octyl⁸⁵ spacer, “capped”⁸⁶ structures. Both fluorescence quenching and transient absorption techniques have been employed to study

the photo-induced electron transfer process in these systems.

The majority of electron transfer studies involving porphyrin-quinone complexes have been carried out in aprotic solvents, in which proton transfer effect is not important to the ET process. However, if the ET reaction is carried in a protic solvent such as water, the situation is different. In the photo-induced electron transfer reaction, the quinone is reduced to a semi-quinone, resulting a marked pKa increase at the quinone (pKa of quinone⁸⁷ is -1 and that for semi-quinone is 4.1⁸⁸), which then can be protonated by the solvent. In this case, proton transfer is involved in the ET reaction and may have significant effect on ET events. Unfortunately, for most porphyrin quinone complexes, the poor solubility of porphyrin molecules in aqueous solution prevents the ET study from being carried out in the aqueous solvent. To conduct the ET studies in aqueous solution, we need to design and synthesize a new porphyrin quinone complex that is water-soluble

Tetramethylpyridinium porphyrin is well known to be water soluble, therefore we decided to take advantage of this structure to synthesize our water soluble porphyrin quinone complex. Molecular dyad **108** illustrates the strategy for such an approach. The overall structure of **108** is analogous to the triphenylporphyrin amide quinone (TPPAQ) which has been synthesized by Tabushi's group.⁸⁹ The porphyrin moiety of **108** is covalently linked to a quinone via an amide linkage. The whole molecule is relatively rigid due to the partial double bond character of the carbon-heteroatom bond in the amide group. Compared to TPPAQ, apart from that the quinone was connected to the para-position instead of the ortho-position, porphyrin moiety of **108** was modified with three methylpyridinium groups. This hydrophilic property of methyl pyridinium should ensure

that the molecule is soluble in water, which serves as the proton source for the protonation reaction.

**108****TPPAQ**

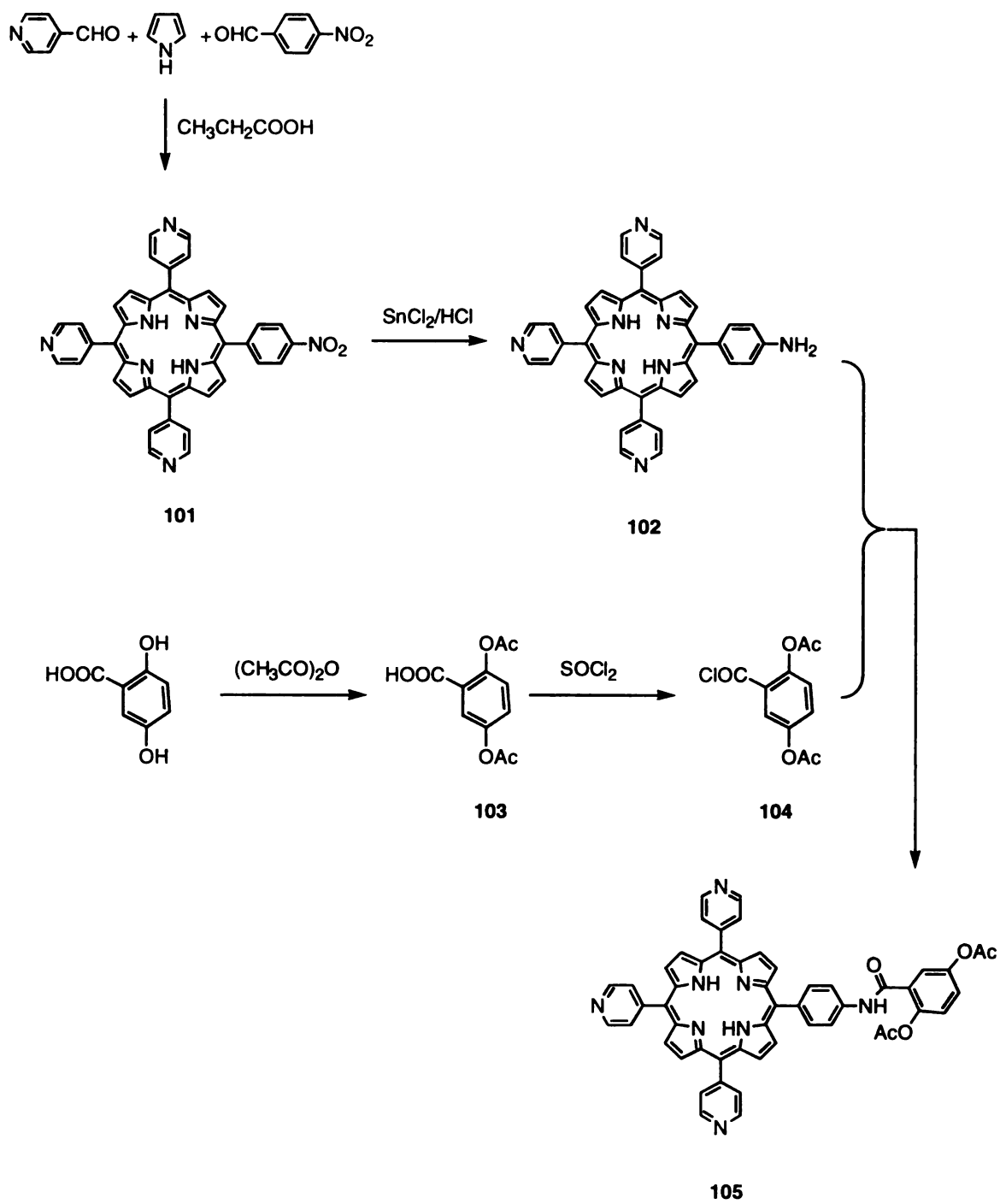
II. Results and Discussion

A. Synthesis

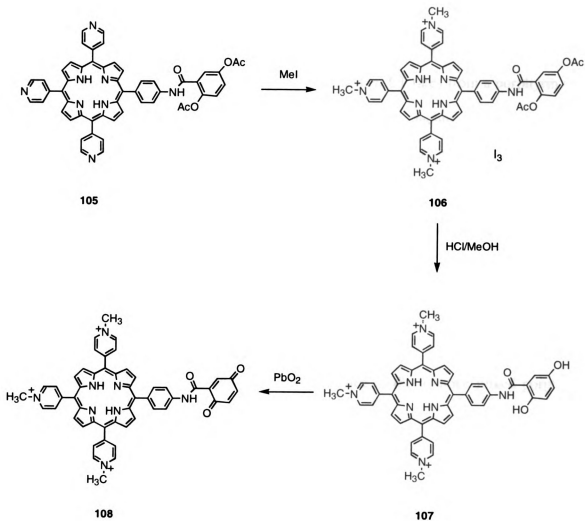
The strategy for the synthesis of dyad **108** is analogous to that used in Tabushi's group for making TPPAQ. The synthesis of unsymmetrical porphyrins having three pyridine and one nitro-phenyl groups at the *meso* position of the macrocycle was carried out in acid medium according to the classical Adler-Longo method.⁹⁰ A propionic acid solution of 1.75 equivalents of 4-nitrobenzaldehyde, 3 equivalents of 4-pyridinecarboxaldehyde and 4 equivalents of pyrrole was refluxed for 1.5 h in the presence of acetic anhydride. This mole ratio was chosen because it afforded the best yield of the desired [5-(4'-nitrophenyl)-10,15,20-tris(4'-pyridyl)]porphyrin **101**. Thus, **101** was obtained in 5% yield after several purification cycles on silica gel to separate the other porphyrins (tetrapyridylporphyrin, bis-nitrophenyl-bis-pyridylporphyrin, tris-

nitrophenylpyridyl-porphyrin, tetranitrophenylporphyrin). The amino functional group was obtained by reducing the nitro group by means of stannous chloride in an acidic media (6 M HCl). After purification, the 5-(4'-aminophenyl)-10,15,20-tris(4'-pyridyl)-porphyrin **102** was obtained as purple crystals in 80% yield. For the quinone half of the complex, a commercially available quinone precursor, 2,5-dihydroxybenzoic acid was employed. The hydroxy groups of 2,5-dihydroxybenzoic acid were protected by treating with acetic anhydride under acidic conditions to give acetoxyster **103**. This synthetic step was carried out to overcome the instability of the hydroquinone functional group during the linking reaction. Attaching this moiety to the porphyrin via an amide linkage was effected by activating **103** with thionyl chloride to give 1-chlorocarbonyl-2,5-diacetoxystere **104**, which was then reacted with porphyrin **102** to yield porphyrin dyad **105** in 85% yield (Scheme 17).

The further transformation of **105** is described in Scheme 18. The methylation of **105** was carried out following a literature procedure.⁹¹ Porphyrin **105** was refluxed with a large excess of methyl iodide in chloroform/methanol (90:10) under nitrogen to give **106** in 84% yield. Proton NMR (in DMSO-d₆) indicated that all pyridine groups were methylated to methyl pyridinium groups. The acetoxystere groups of **106** were selectively hydrolyzed in methanolic HCl (apparent pH was 1) following the procedure described by Tabushi⁸⁹ to give porphyrin hydroquinone **107**. Compound **107** was then oxidized by PbO₂⁹² in methanol at room temperature to give **108** in 71% yield. The formation of quinone was indicated by the upfield shift of quinone protons compared to hydroquinone. Porphyrin quinone dyad **108** is photolabile and tends to decompose when exposed to light. Therefore, the oxidation was carried out in the dark. In actuality, all synthetic



Scheme 17



Scheme 18

operations utilizing porphyrin were done with minimum amount of light. Porphyrin **108** is soluble in water. Since the ET studies will be performed in a buffered solution, it is not necessary to perform an ion exchange to ensure the presence of a single anion in the molecule.

B. Preliminary ET studies

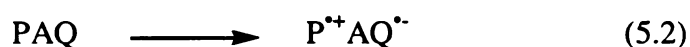
Porphyrin **108** shows a good solubility in water, allowing ET experiments to be carried out in aqueous buffer solution. The photoinduced ET rates from a porphyrin to a quinone were measured using a fluorescence quenching technique. Fluorescence lifetimes of **108** and **106** were measured in water at different pH by a single photon counting technique using a picosecond dye laser. Fluorescence intensity of the quinone-linked porphyrin **108** was decreased as compared to that of the corresponding reference compound **106**. Based on the fluorescence lifetimes, electron-transfer rates, were estimated by using equation (5.1):

$$k_{ET} = \tau^{-1} - \tau_{ref}^{-1} \quad (5.1)$$

where k_{ET} is the electron transfer rate, τ is the lifetime of the quinone-linked porphyrin and τ_{ref} is the lifetime of the reference substance.

The charge recombination process was studied by using a nanosecond transient absorption technique. Spectral changes after the laser flash for **108** were very similar to those obtained on oxidation of *meso*-tetraphenylporphyrins (TPP) to their cationic radicals.⁹³ Thus, the difference spectrum obtained after laser excitation of **108** was consistent with the formation of $P^{*+}AQ^{\cdot-}$. Rate constants were obtained by analyzing the decay of this absorption. Figure 24 shows the rate constants for both the forward (CS) and back (CR) ET measured at different pH.

The rate for ET from porphyrin to quinone displays strong pH dependence and the ET rate increases with the pH of the solvent. These results can be explained by using PCET theory. Accordingly, the electron transfer from a porphyrin to a quinone is accompanied by the proton uptake from the solvent (eq. 5.1). This process is competing with the process that contains no proton uptake (eq. 5.2).



The thermodynamic stability of the quinone product is determined by the pH of the solvent. At low pH, $\text{P}^{++}\text{AQ}^{\bullet}\text{H}$ is more stable than $\text{P}^{++}\text{AQ}^{\bullet-}$, and eq. 5.1 represents the main pathway for the ET from the porphyrin to the quinone. As we discussed previously, proton uptake can give rise to extra reorganization energy; thus, the observed ET rate is slow. At higher pH, $\text{P}^{++}\text{AQ}^{\bullet-}$ is thermodynamically preferred and thus eq. 5.2 represents the major pathway for the ET, in which the observed ET is faster because no proton is involved.

The involvement of proton in the ET reaction is supported by the charge recombination kinetics. Compared to other porphyrin-quinone systems,⁹⁴ the back ET is extraordinary slow and thus results in a long-lived charge separation state. This can be rationalized as a protonation of the semiquinone radical, which traps the electron at the acceptor and thus forms a stable state.

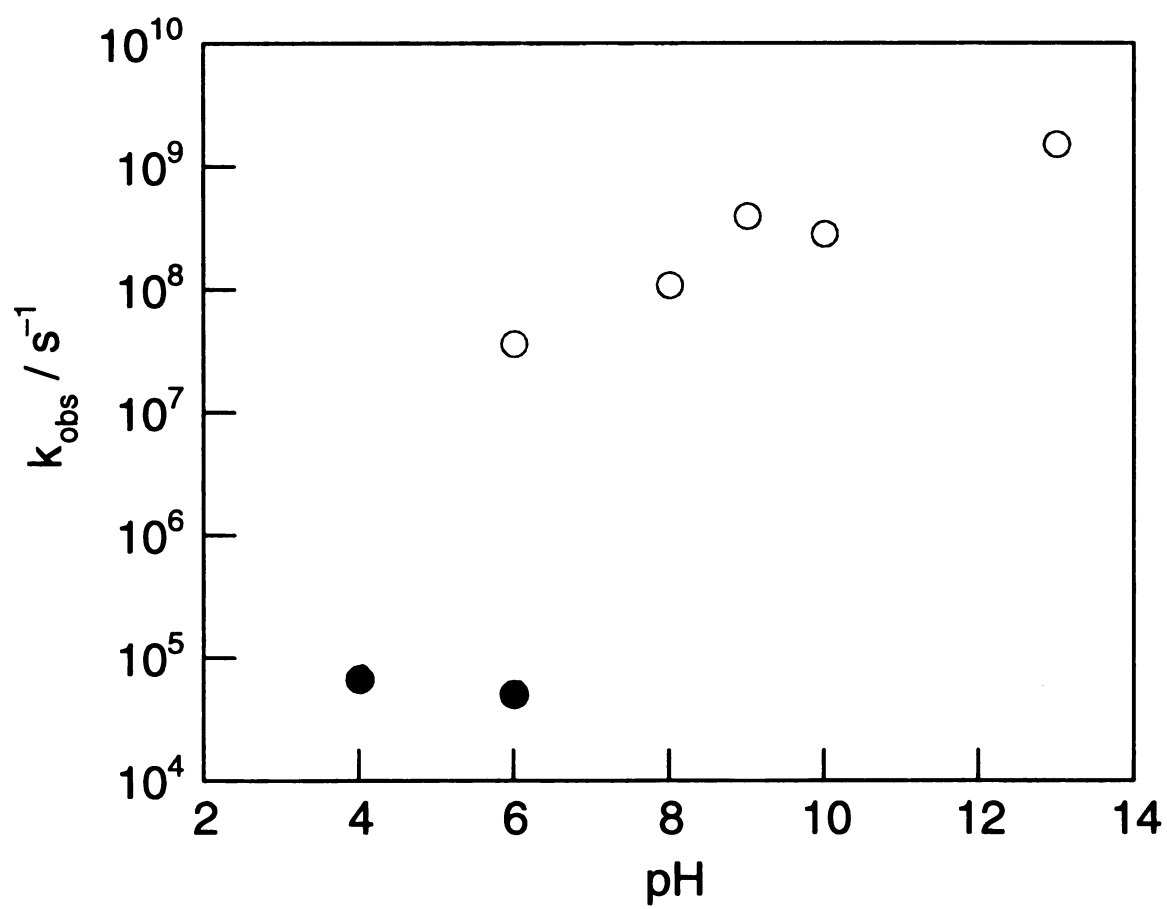


Figure 24. pH-dependence of forward ET (O) and back ET rates (●)

III. Experimental

5-(4-nitrophenyl)-10, 15, 20-tris(4'-pyridyl)porphyrin **101**

A mixture of 4-nitrobenzaldehyde (3 g, 0.020 mol, 1.75 eq) and acetic anhydride (15 ml) was heated to 110°C in propionic acid (135 ml). To this solution pyridinecarboxaldehyde (3.2 mL, 0.034 mol, 3 eq) was slowly added followed by pyrrole (3.1 mL, 0.045 mol, 4 eq) and the mixture was refluxed for 1.5 h. Most of solvent was removed by distillation under reduced pressure. The residue was neutralized with 2 M ammonia solution and collected by filtration. After drying in air, the solid was dissolved in dichloromethane and the insoluble residue was filtered off. The solvent was removed from the solution under vacuum and the resulting residue was purified by column chromatography on silica gel (dichloromethane/methanol 96:4). This process was repeated three times to give the desired compound (0.4 g, 0.6 mmol) in 5.3% yield. UV-visible (CH_2Cl_2): λ 418; 512; 546; 586; 640 nm. ^1H NMR (300 MHz, CDCl_3): δ -2.989 (2H, s, NH); 8.15 (6H, d, 3, 5-pyridine); 8.38 (2H, d, 3, 5-(4-nitrophenyl)), 8.81 (2H, d, 2, 6-(4-nitrophenyl)); 8.87 (6H, m, β -pyrrole); 9.06 (6H, d, 2, 6-pyridine); MS (CI 70eV), m/e = 662, calcd 662.21 for $\text{C}_{41}\text{H}_{26}\text{N}_8\text{O}_2$

5-(4-Aminophenyl)-10,15,20-tris(4-pyridyl)porphyrin **102**

Stannous chloride dihydrate (0.23 g, 1.0 mmol, 8 eq.) was added to porphyrin **101** (70 mg, 0.11 mol) in 6 M hydrochloric acid (6 ml) and the mixture was stirred at room temperature for 15 h. The mixture was neutralized with 2 M ammonium hydroxide, then extracted with dichloromethane. The solution was washed with water and the organic

layer was dried over sodium sulfate. The solvent was evaporated to dryness and the residue crystallized from dichloromethane/methanol to give **102** (56 mg, 0.089 mmol) in 80.5% yield. UV-visible (CH_2Cl_2): λ_{max} 420; 516; 552; 592; 646 nm. ^1H NMR (300 MHz, CDCl_3): δ -2.87 (2H, s, NH), 7.06 (2H, d, 3, 5-(4-aminophenyl)); 7.97 (2H, d, 2, 6-(4-aminophenyl)); 8.15 (6H, d, 3, 5-pyridine); 8.79 (2H, d, β -pyrrole); 8.83(s, 4H, β -pyrrole); 9.01(2H, d, β -pyrrole); 9.05 (6H, d, 2, 6-pyridine); MS (CI 70 eV), m/e = 632, clcd 632.24 for $\text{C}_{41}\text{H}_{28}\text{N}_8$

2, 5- Diacetoxybenzoic acid **103**

2, 5-Dihydroxybenzoic acid (3.85 g, 25 mmole), acetic anhydride (14.5 mL) and sulfuric acid (0.1 mL) were warmed for 25 minutes on a steam bath and then poured onto 25 g of ice. The mixture was allowed to stand overnight and the precipitate that formed was collected by filtration. The product was recrystallized from a mixture of benzene/hexane to give 4.4 g (74%) of the title compound. mp 117-118 °C; ^1H NMR (300 MHz, CDCl_3): δ 2.27(3H, s, CH_3), 2.30 (3H, s, CH_3), 7.10 (1H, d, aromatic), 7.35 (1H, dd, aromatic), 7.8 (1H, d, aromatic); MS (CI 70 eV) m/e = 238, clcd 238.05 for $\text{C}_{11}\text{H}_{10}\text{O}_6$

2, 5- Diacetoxybenzoyl Chloride **104**

A mixture of 2, 5 diacetoxybenzoic acid **103** (200 mg, 0.84 mmol) and freshly distilled thionyl chloride (3 ml) was refluxed for 5 h under nitrogen. The solution was allowed to stand at room temperature for 15 hours and then evaporated to dryness under vacuum to give 180 mg of **104** (83% yield). mp 93-95 °C; ^1H NMR (300 MHz, CDCl_3): 2.35 (6H, s, CH_3), 7.18 (1H, d, aromatic), 7.43 (1H, dd, aromatic), 7.98(1H, d, aromatic); MS (CI 70

eV), $m/e = 256$, clcd 256.01 for $C_{11}H_9O_5Cl$

5-[4'-(2'',5''-diacetoxybenzoyl)aminophenyl]-10,15,20-tris(4'-pyridyl)porphyrin **105**

Porphyrin **102** (100 mg, 0.16 mmol) in dry dichloromethane (50 ml) and pyridine (0.5 mL) was added to the acid chloride **104** obtained from the previous step. The reaction mixture was stirred for 1 h under nitrogen. The solution was washed with water three times and then concentrated by rotary evaporation. The resulting porphyrin was purified on silica gel (eluting with dichloromethane containing 3% methanol) to give the title compound (113 mg, 0.13 mmol) in 83% yield. UV-vis: λ_{\max} 418, 513, 546, 589, 645 nm; 1H NMR (300 MHz, $CDCl_3$): 2.40, 2.52 (3H each, s, CH_3 of acetoxy), 7.30 (1H, d, aromatic), 7.36 (1H, dd, aromatic) 7.78 (1H, d, aromatic), 8.06 (2H, d, amide phenyl), 8.18 (6H, m, 3, 5-pyridyl), 8.22 (2H, d, amide phenyl), 8.64 (1H, s, amide H), 8.88 (6H, m, β -pyrrole), 8.98 (2H, m, β - pyrrole), 9.06 (6H, m, 2, 6-pyridyl); MS (FAB), $m/e = 852.2$, clcd 852.28 for $C_{52}H_{36}N_8O_5$

5-[4'-(2'',5''-diacetoxybenzoyl)aminophenyl]-10,15,20-tris(4'-methylpyridinium) porphyrin iodide **106**

A solution containing porphyrin **105** (113 mg, 0.13 mmol), 1:9 ethanol-chloroform (10 ml) and methyl iodide (3 ml) was refluxed under nitrogen overnight. The precipitate was collected by filtration, washed with chloroform and air dried to give the title compound (150 mg, 0.12 mmol) in 90% yield. UV-vis: λ_{\max} 423, 521, 556, 584, 648 nm; 1H NMR (300 MHz, $DMSO-d_6$): 2.38, 2.40 (3H each, s, CH_3 of acetoxy), 4.75 (9H, m, CH_3 of pyridinium), 7.42 (1H, d, aromatic), 7.48 (1H, dd, aromatic), 7.66 (1H, d, aromatic), 8.14

(2H, m amide phenyl), 8.22 (6H, m, 3, 5-pyridyl), 8.28 (2H, m amide phenyl), 9.00-9.18 (9, m, pyridyl, β -pyrrole, amide H), 9.50 (6H, m, 2, 6-pyridyl).

5-[4'-(2'',5'')-diacetoxybenzoyl]aminophenyl]-10,15,20-tris(4'-methylpyridinium)-
porphyrin iodide **107**

Dry HCl gas was bubbled through a solution of porphyrin **106** (50 mg, 0.039 mmol) in methanol (10 mL) for 1 min, and the resulting mixture was stirred under nitrogen for 30 min. The solvent was then removed under vacuum to give 30 mg of porphyrin **107**. UV-vis: λ_{\max} 422, 519, 554, 582, 648 nm; ^1H NMR (300 MHz, DMSO- d_6): 4.70 (9H, m, CH_3 of pyridinium), 6.95 (2H, m, aromatic), 7.48 (1H, m, aromatic), 8.20 (8H, m, aromatic), 8.28 (2H, m amide phenyl), 9.00-9.18 (9, m, pyridyl, β -pyrrole, amide H), 9.50 (6H, m, 2, 6-pyridyl)

5-[4'-(2'',5'')-diacetoxybenzoyl]aminophenyl]-10,15,20-tris(4'-methylpyridinium)-
porphyrin **108**

Lead dioxide (200 mg) was added to a solution of porphyrin hydroquinone **107** in methanol (10 mL). The mixture was stirred for 10 min and then filtered through a cintered filter funnel. The filtrate was collected and the solvent was removed under vacuum to give 15 mg of **108**. UV-vis: λ_{\max} 424, 520, 554, 582, 647 nm; ^1H NMR (300 MHz, DMSO- d_6): 4.70 (9H, m, CH_3 of pyridinium), 6.78 (1H, d, aromatic), 6.90 (1H, m, quinone), 7.42 (1H, d, quinone), 8.04 (2H, d, amide phenyl), 8.14 (2H, d, amide phenyl), 8.35 (1H, br, amide H), 8.90 (6H, d, pyridinium), 9.20 (8H, m, β -pyrrole), 9.35 (6H, d, pyridinium)

REFERENCES

1. P. Mithchell, *Nature* **1961**, 191, 144
2. a) M. S. Graige, M. L. Paddock, J. M. Bruce, G. Feher, M. Y. Okamura, *J. Am. Chem. Soc.* **1996**, 118, 9005. b) B. G. Malmström, *Acc. Chem. Res.* **1993**, 26, 332. c) G. T. Babcock, C. Varotsis, *SPIE-Int. Soc. Opt. Eng. Biomol. Spectrosc. III* **1993**, 1890, 104.
3. H. Koike, M. Ikeuchi, T. Hiyama, Y. Inoue, in *Current Research in Photosynthesis*, Vol. 1 (Eds.: M. Baltscheffsky), Kluwer, Dordrecht, 1989, p 2351
4. (a) G. Renger, *Angew. Chem., Int. Ed. Engl.* **1987**, 26, 643. (b) J. Barbar, *Trends Biochem. Sci.* **1987**, 12, 321. (c) G. Feher, J. P. Allen, M. Y. Okamara, D. C. Rees, *Nature*, **1989**, 339, 111
5. (a) M. Gunner, *Curr. Top. Bioenerg.* **1991**, 16, 319. (b) G. T. Babcock, B. A. Barry, R. J. Debus, C. W. Hoganson, M. Atamian, L. McIntosh, I. Sithol, C. F. Yocum, *Biochemistry* **1989**, 28, 9557
6. J. R. Winkler, B. G. Malmström, H. B. Gray, *Biophys. Chem.* **1995**, 54, 199
7. (a) M. I. Verkhovsky, J. E. Morgan, M. Wikström, *Biochemistry* **1995**, 34, 7483. (b) P. Sarti G. Antonini, F. Malatesta, B. Vallone, M. Brunori, *Ann. N. Y. Acad. Sci.* **1990**, 550, 161. (c) T. M. Antalis, G. Palmer, *J. Biol. Chem.* **1982**, 257, 6194
8. S. Iwata, C. Ostermeier, B. Ludwig, H. Michel, *Nature* **1995**, 375, 660

9. T. Tsukihara, H. Aoyama, E. Yamashita, T. Tomizaki, H. Yamaguchi, K. Shinzawa-Itoh, R. Nakashima, R. Yaono, S. Yoshikawa, *Science* **1995**, 269, 1069
10. (a) P. Ädelroth, P. Brzezinski, B. G. Malmström, *Biochemistry* **1995**, 34, 2844.
(b) S. Hallén, P. Brzezinski, B. G. Malmström, *Biochemistry* **1994**, 33, 1467
11. P. Ädelroth, H. sigurdson, S. Hallén, P. Brzezinski, *Proc. Natl. Acad. Sci. U.S.A.* **1995**, 93, 12292
12. P. Brzezinski, *Biochemistry* **1996**, 35, 5611
13. A. Labahn, M. L. Paddock, P. H. McPherson, M. Y. Okamura, G. Feher, *J. Phys. Chem.* **1994**, 98, 3417
14. (a) P. H. Mcpherson, M. Y. Okamura, G. Feher, *Biochim. Biophys. Acta* **1988**, 934, 348. (b) P. Maróti, C. A. Wraight, *Biochim. Biophys. Acta* **1988**, 934, 329
15. (a) V. Y. Shafirovich, S. H. Courtney, N. Ya, N. E. Geacintov. *J. Am. Chem. Soc.* **1995**, 117, 4920. (b) R. A. Binstead, M. E. McGuire, A. Dorletogbu, W. K. Seok, L. E. Roecker, T. J. Meyer, *J. Am. Chem. Soc.* **1992**, 114, 173. (c) H. Miyasaka, A. Tabata, K. Kamada, N. Mataga, *J. Am. Chem. Soc.* **1993**, 115, 7335
16. J. -H. Fuhrhop, *Angwe. Chem., Int. edt. Engl.* **1974**, 13, 321
17. (a) M. R. Wasielewski, *Chem. Rev.* **1992**, 92, 435. (b) H. Kurreck, M. Huber, *Angew. Chem., Int. Ed. Engl.* **1995**, 34, 849. (c) D. Gust, T. A. Moore, A. Moore, *Acc. Chem. Res.* **1993**, 126, 198
18. A. Osuka, T. Nagat, K. Maruyama, *Chem. Lett.* **1991**, 481
19. A. Osuka, K. Maruyama, N. Mataga, T. Asahi, I. Yamazaki, N. Tamai, Y. Nishimura, *Chem. Phys. Lett.* **1991**, 181, 413

20. A. Osuka, s. Nakajima, K. Maruyama, N. Mataga, T. Asahi, *Chem. Lett.* **1991**, 1003
21. J. L. Sessler, B. Wang, A. Harriman, *J. Am. Chem. Soc.* **1993**, 115, 10418
22. C. Turro, C. K. Chang, G. E. Leroi, R. I. Cukier, D. G. Nocera, *J. Am. Chem. Soc.* **1992**, 114, 4013
23. M. R. Wasielewski, M. P. Niemczyk, W. A. Svec, E. B. Pewitt, *J. Am. Chem. Soc.* **1985**, 107, 1080
24. T. A. Moore, D. Gust, P. Mathis, J. -C. Mialocq, C. Chachaty, R. V. Bensasson, E. J. Land, D. Doizi, P. A. Liddell, W. R. Lehman, G. A. Nemeth, A. L. Moore, *Nature* **1984**, 307, 630
25. (a) D. Gust, T. A. Moore, A. L. Moore, D. Barrett, L. O. Harding, L. R. Makings, P. A. Liddell, F. C. De Schryver, M. Van der Auweraer, R. Bensasson, M. J. Rougee, *J. Am. Chem. Soc.* **1988**, 110, 321. (b) D. Gust, T. A. Moore, A. L. Moore, L. R. Makings, G. R. Seely, X. Ma, T. T. Trier, F. Gao, *J. Am. Chem. Soc.* **1988**, 110, 7567. (c) D. Gust, T. A. Moore, A. L. Moore, G. R. Seely, P. A. Liddell, L. R. Makings, X. Ma, S. J. Lee, F. Gao, *Tetrahedron* **1989**, 45, 4867. (d) D. Gust, T. A. Moore, A. L. Moore, F. Gao, D. K. Luttrull, J. M. DeGraziano, X. Ma, L. R. Making, S. J. Lee, T. T. Trier, E. Bittersmann, G. R. Seely, S. Woodward, R. V. Bensasson, M. Rougee, F. C. De Schryver, Van der Auweraer, *J. Am. Chem. Soc.* **1991**, 113, 3638. (e) D. Gust, T. A. Moore, A. L. Moore, , S. J. Lee, E. Bittersmann, D. K. Luttrull, A. A. Rehms, J. M. DeGraziano, X. Ma, F. Gao, R. E. Belford, T, T. Trier, *Science* **1990**, 248, 199

26. S -C Hung, A. N. Macpherson, S. Lin, P. A. Liddell, G. R. Seely, A. L. Moor, T. A. Moore, D. Gust, *J. Am. Chem. Soc.* **1995**, 117, 1657
27. (a) J. A. Robert, J. P. Kirby, D. G. Nocera, *J. Am. Chem. Soc.* **1995**, 117, 8051.
(b) J. P. Kirby, J. A. Roberts, D. G. Nocera, submitted for publication
28. J. D. Puglisi, L. Chen, A. D. Frankel, J. R. Williamson, *Proc. Natl. Acad. Sci. U.S.A.* **1993**, 90, 3680
29. N. P. Pavletich, C. O. Pabo, *Science* **1991**, 252, 809
30. E. H. Howell, J. E. Villafranca, M. S. Warren, S. J. Oatley, J. Kraut, *Science* **1986**, 231, 1125
31. W. L. Jorgensen, J. Pranata, *J. Am. Chem. Soc.* **1990**, 112, 2008
32. G. Müller, J. Riede, P. Schmidtchen, *Angew. Chem., Int. Ed. Engl.* **1988**, 27, 1516
33. (a) A. Lewis, *Proc. Natl. Acad. sci. U. S. A.* **1978**, 75, 549. (b) B. Honig, T. Ebrey, R. H. Callender, U. Dinur, M. Ottolenghi, *Proc. Natl. Acad. Sci. U.S.A.* **1979**, 76, 2503
34. (a) O. Kalisky, M. Ottolenghi, B. Honig, r. Korenstein. *Biochemistry* **1981**, 20, 649. (b) D. Ort, W. W. Parson, *J. Biol. chem.* **1978**, 253, 6158. (c) J. Ternier, C. - L. Hsieh, A. R. Burns, M. A. El-Sayed, *Proc. Natl. Acad. Sci. U.S.A.* **1979**, 76, 3046. d) M. Braiman, R. Mathies, *Biochemistry* **1980**, 19, 5421
35. (a) M. Wikström, K. Krab, *Biochim. Biophys. Acta* **1979**, 549, 177. (b) M. Wikström, K. Krab, M. Saraste, *Cytochrome Oxidase, A Synthesis*; Academic Press: New York, 1981
36. (a) B. Ward, P. M. Callahan, R. Young, G. T. Babcock, C. K. Chang, *J. Am.*

- Chem. Soc.* **1983**, 105, 634. (b) B. Ward, C. K. Chang, R. Young, *J. Am. Chem. Soc.* **1984**, 106, 3943
37. Cukier, R. I. *J. Phys. Chem.* **1994**, 98, 2377
38. G. Schwarzenbach and K. Lutz, *Helv. Chim. Acta.* **1940**, 23, 1162
39. (a) H. A. Staab, J. Weiser, M. Futscher, G. Voit, A. Rückemann, C. Anders, *Chem. Ber.* **1992**, 125, 2285. (b) H. A. Staab, G. Voit, J. Weiser, M. Futscher, *ibid.* **1992**, 125, 1203. (c) C. Krieger, M. Dernbach, G. Voit, T. Carell, H. A. Staab, *Chem. Ber.* **1993**, 126, 811
40. (a) A. Pinner, Fr. Klein, *Ber.*, **1877**, 10, 1889. (b) A. Pinner, *Die imidoäther und ihre Derivate*, Oppenheim, Berlin, 1892
41. R. A. Garigipati, *Tetrahedron Lett.* **1990**, 31, 1969
42. J. I. Levin, Turos, S. M. Weinreb, *Syn. Commun.* **1982**, 12, 989
43. J. P. Kirby, N. A. Van Dantzig, C. K. Chang, D. G. Nocera, *Tetrahedron Lett.* **1995**, 36, 3471
44. G. A. Olah, T. Keumi, *Synthesis*, **1979**, 112
45. J. L. Sessler, V. L. Capuano, A. Harriman, *J. Am. Chem. Soc.* **1993**, 115, 4618
46. D. H. R. Barton, S. Z. Zard, *J. Chem. Soc., Chem. Commun.* **1985**, 1098
47. (a) I. Abdalmuhdi, C. K. Chang, *J. Org. Chem.* **1985**, 50, 411 (b) S. S. Eaton, G. R. Eaton, C. K. Chang, *J. Am. Chem. Soc.* **1985**, 107, 3177
48. K. M. Smith, *Porphyrin and Metalloporphyrins*, Amsterdam - New York - Oxford, 1975
49. C. K. Chang, M. H. Hatada, A. Tulinsky, *J. Chem. Soc., Perkin Trans. II*, **1983**,

- 371,
50. W. I. White in *The Porphyrins*; (Eds.: D. Dolphin), Vol. 1, Academic Press: New York, **1978**, pp. 303 – 335
 51. P. J. F. de Rege, S. A. Williams, M. J. Therien, *Science* **1995**, 269, 1409
 52. J. S. Lindsey, I. C. Schreiman, H. C. Hsu, P. C. Kearney, A. M. Marguerettaz, *J. Org. Chem.* **1987**, 52, 827
 53. (a) G. T. E. Graham, F. H. Westheimer, *J. Am. Chem. Soc.* **1958**, 80, 3030. (b) K. B. Wiberg, T. Mill, *J. Am. Chem. Soc.* **1958**, 80, 3022.
 54. M. Davie, A. E. Parsons, *Z. Phys. Chem. NF* **1959**, 20, 34
 55. G. Häfelinger in *The Chemistry of Amidines and Imidates*; (Eds.: S. Patai); John Wiley & Sons: London – New York – Sydney – Toronto, 1975, pp. 1 - 84
 56. J. J. López-Garriga, G. T. Babcock, J. F. Harrison, *J. Am. Chem. Soc.* **1986**, 108, 7251.
 57. J. J. López-Garriga, S. Hanton, G. T. Babcock, J. F. Harrison, *J. Am. Chem. Soc.* **1986**, 108, 7251
 58. D. M. Collins, J. L. Hoard, *J. Am. Chem. Soc.* **1970**, 92, 3761
 59. L. Sacconi, *Transition Metal Chem.* **1968**, 4, 199
 60. J. L. Hoard, *Ann. N. Y. Acad. Sci.* **1973**, 206, 18
 61. T. A. Hamor, W. S. Caughey, J. L. Hoard, *J. Am. Chem. Soc.* **1965**, 87, 2305
 62. E. F. Meyer, *Acta Cryst.* **1992**, B28, 2162
 63. (a) R. J. Abraham, F. Eivazi, H. Pearson, K. M. Smith *J. Chem. Soc., Chem. Commun.* **1976**, 698. (b) C. K. Chang, *J. Heterocycl. Chem.* **1977**, 14, 1285

64. C. S. Wilcox, E. Kim, D. Romano, L. H. Kuo, A. L. Burt, D. P. Curran, *Tetrahedron* **1995**, 51, 621
65. K. A. Connors, *Binding Constants, The Measurement of Molecular Complex stability*; Wiley-Interscience: New York, 1978; pp. 24-28
66. M. T. Blanda, J. H. Horner, M. Newcomb, *J. Org. Chem.* **1989**, 54, 4626
67. L. J. Schaad, M. D. Joesten, *Hydrogen bond*, Marcel Dekker, INC.: New York, **1974**, p 53
68. C. S. Wilcox, *Frontiers in Supramolecular Organic Chemistry and Photochemistry*; (Eds.: H.-J. Schneider, H. Durr) VCH: Weinheim, **1991**; p. 123 .
69. R. B. Woodward, W. A. Ayer, J. M. Beaton, F. Bickelhaupt, R. Bonnett, P. Buchschacher, G. L. Closs, H. Dutier, J. Hannah, F. P. Hauch, S. Ito, A. Langemann, E. LeGoff, W. leimgruber, W. Lwowski, J. Sauer, Z. Valenta, H. Volz, *J. Am. Chem. Soc.* **1960**, 82, 3800
70. J. -H. Fuhrhop, *Angwe. Chem., Int. edt. Engl.* **1974**, 13, 321
71. R. Schlözer, J. -H. Fuhrhop, *Angwe. Chem., Int. edt. Engl.* **1975**, 14, 363
72. A. R. Morgan, N. C. Tertel, *J. Org. Chem.* **1986**, 51, 1347
73. R. B. Woodward in *Selected Organic Syntheses*; (Eds.: I. Fleming), John Wiley & Sons: London – New York – Sydney – Toronto, **1973**, pp. 112 - 114
74. R. Bonnett, G. f. Stephenson, *J. Chem. Soc., Chem. Commun.* **1966**, 1600
75. C. K. Chang, *Biochemistry* **1980**, 19, 1971
76. H. Scheer, H. H. Inhoffen in *The porphyrins*; (Eds.: D. Dolphin); Vol. 11 Academic Press: New York, **1978**; p 45

77. H. Scheer, H. H. Inhoffen, In "The porphyrins"; D. Dolphin, Ed.; Academic Press: New York, 1978; Vol 11, pp 45
78. (a) R. A. Marcus, N. Sutin, *Biochim. Biophys. Acta* **1985**, 811, 265. (b) N. S. Hush, *Coord. Chem. Rev.* **1985**, 54, 135
79. M. R. Wasielewski, M. P. Niemczyk, W. A. Svec, E. B. Pewitt, *J. Am. Chem. Soc.* **1985**, 107, 1080
80. J. L. Y. Kong, P. A. Loach in *Frontiers of Biological Energetics—Electrons to Tissues*, (Eds: P. L. Dutton, J. S. Leigh, A. Scarpa), Academic Press: New York, **1978**, pp. 73-82
81. I. Tabushi, N. Koga, M. Yanagita, *Tetrahedron Lett.* **1979**, 3, 257
82. (a) J. L. Y. Kong, P. A. Loach, *Heterocycl. Chem.* **1980**, 17, 737. (b) J. L. Y. Kong, K. G. Spears, P. A. Loach, *Photochem. Photobiol.* **1982**, 35, 545. (c) T.-F. Ho, A. R. McIntosh, J. R. Bolton, *Nature (London)* **1980**, 286, 254.
83. (a) A. R. McIntosh, A. Siemiarzuck, J. R. Bolton, M. J. Stillman, T. -F. Ho, A. C. Weedon, *J. Am. Chem. Soc.* **1983**, 105, 7215. (b) A. Siemiarzuck, A. R. McIntosh, T. -F. Ho, M. J. Stillman, K. J. Roach, A. C. Weedon, J. R. Bolton, J. S. Connolly, *J. Am. Chem. Soc.* **1983**, 105, 7224. (c) T. -F. Ho, A. R. McIntosh, A. C. Weedon, *Can. J. Chem.* **1984**, 62, 967
84. (a) M. R. Wasielewski, M. P. Niemczyk, W. A. Svec, E. B. Pewitt, *J. Am. Chem. Soc.* **1985**, 107, 1080. (b) M. R. Wasielewski, M. P. Niemczyk, *J. Am. Chem. Soc.* **1984**, 106, 5043.
85. (a) A. D. Joran, B. A. Leland, G. G. Geller, J. J. Hopfield, P. B. Dervan, *J. Am.*

- Chem. Soc.* **1984**, 106, 6090. (b) B. A. Leland, A. D. Joran, P. M. Felker, J. J. Hopfield, A. H. Zewail, P. B. Dervan, *J. Phys. Chem.* **1985**, 89, 5571. (c) J. R. Bolton, T. -F. Ho, S. Liauw, A. Siemiarzuk, C. S. K. Wan, A. C. Weedon, *J. Chem. Soc., Chem. Commun.* **1985**, 559
86. (a) J. S. Lindsey, D. C. Mauzerall, H. Linschitz, *J. Am. Chem. Soc.* **1983**, 105, 6528. (b) K. N. Ganesh, J. K. M. Sander, *J. Chem.Soc., Perkin Trans. I* **1982**, 1611. (c) M. P. Irvine, R. J. Harrison, G. S. Beddard, P. Leighton, J. K. M. Sander, *Chem. Phys.* **1986**, 104, 315
87. K. T. Finlay in *The Chemistry of the Quinonoid Compounds* (Eds.: S. Patai), part 2, Wiley, New York, **1974**, p942
88. Y. A. Ilan, G. Czapski, K. Meisel, *Biochim. Biophys. Acta* **1976**, 430, 209
89. I. Tabushi, N. Koga, M. Yanagita, *Tetrahedron Lett.* **1979**, 3, 257
90. A. D. Adler, F. R. Longo, J. D. Finarelli, J. Goldmacher, J. Asour, L. Korsakoff, *J. Org. Chem.* **1976**, 32, 476
91. P. Hambright, E. B. Fleischer, *Inorganic Chemistry*, **1970**, 7, 1757
92. R. Kuhn, I. Hammer, *Chem. Ber.* **1950**, 83, 413
93. Z. Gasyna, W. R. Browett, M. J. Stillman, *Inorg. Chem.* **1985**, 24, 2440
94. J. A. Schmidt, A. R. McIntosh, A. C. Weedon, J. R. Bolton, J. S. Connolly, J. K. Hurley, M. R. Wasielewski, *J. Am. Chem. Soc.* **1988**, 110, 1733

APPENDIX

Selected ^1H NMR spectra

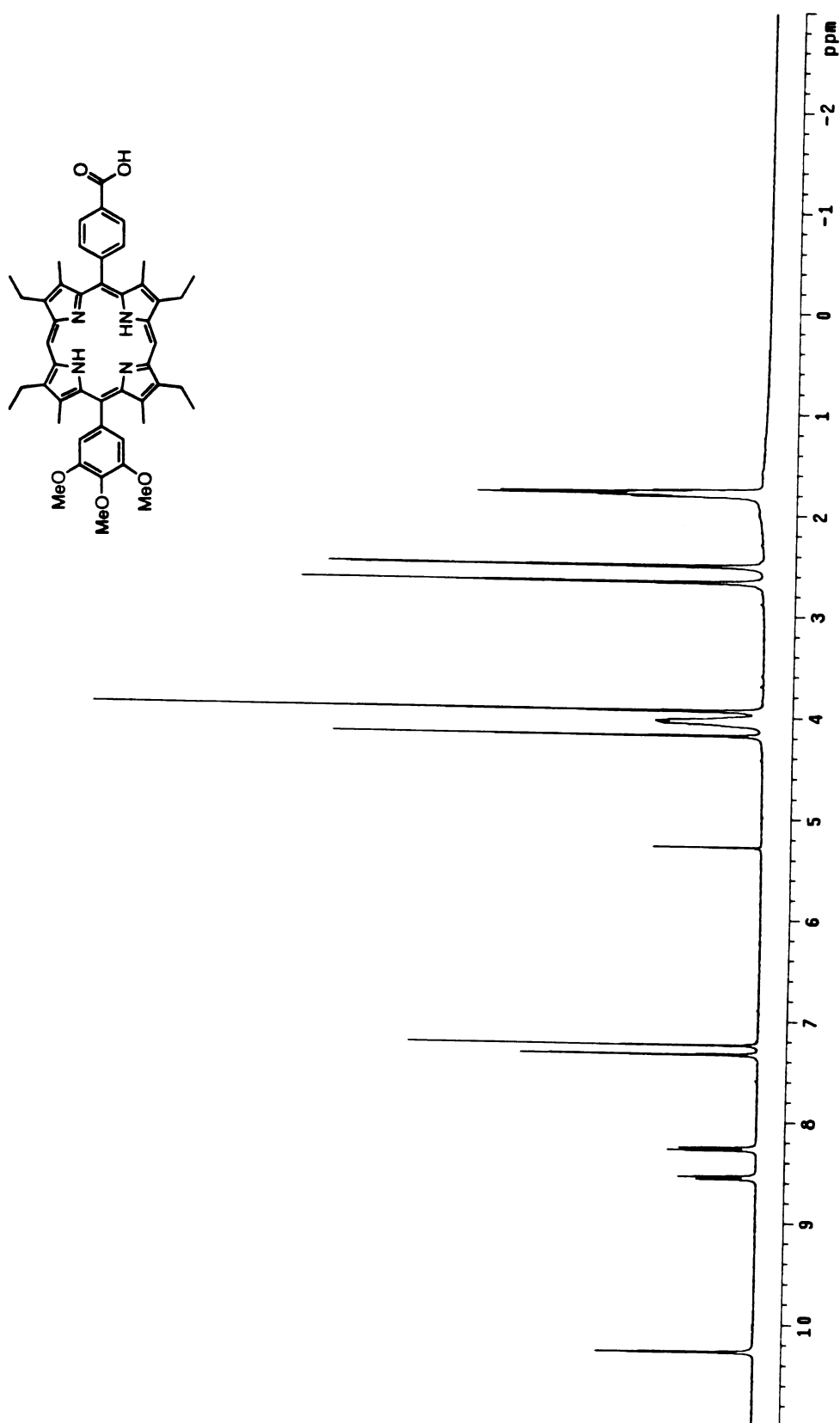


Figure A-1. 300 MHz ^1H -NMR spectrum of **48** in CDCl_3

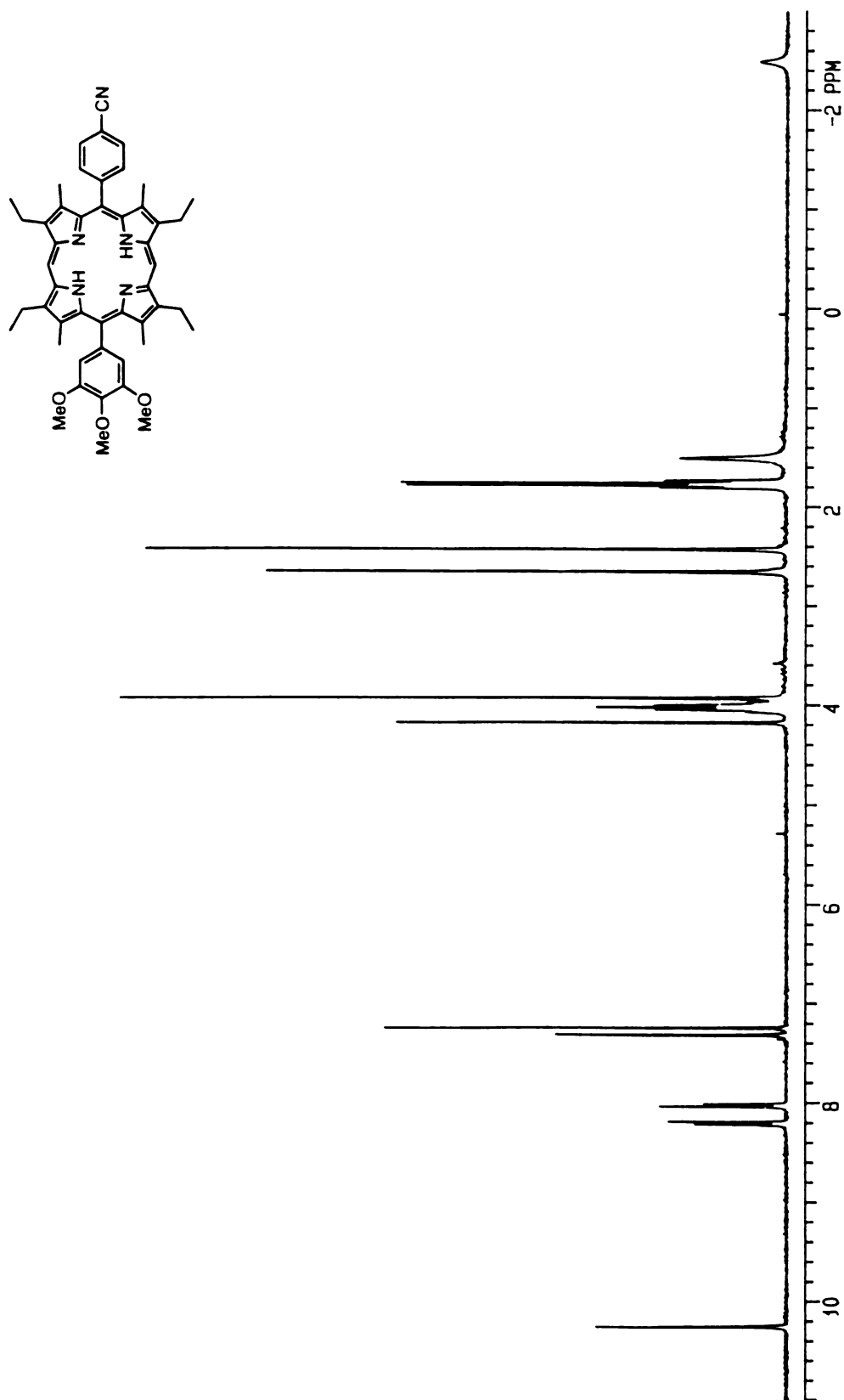


Figure A-2. 300 MHz ^1H -NMR spectrum of **51** in CDCl_3

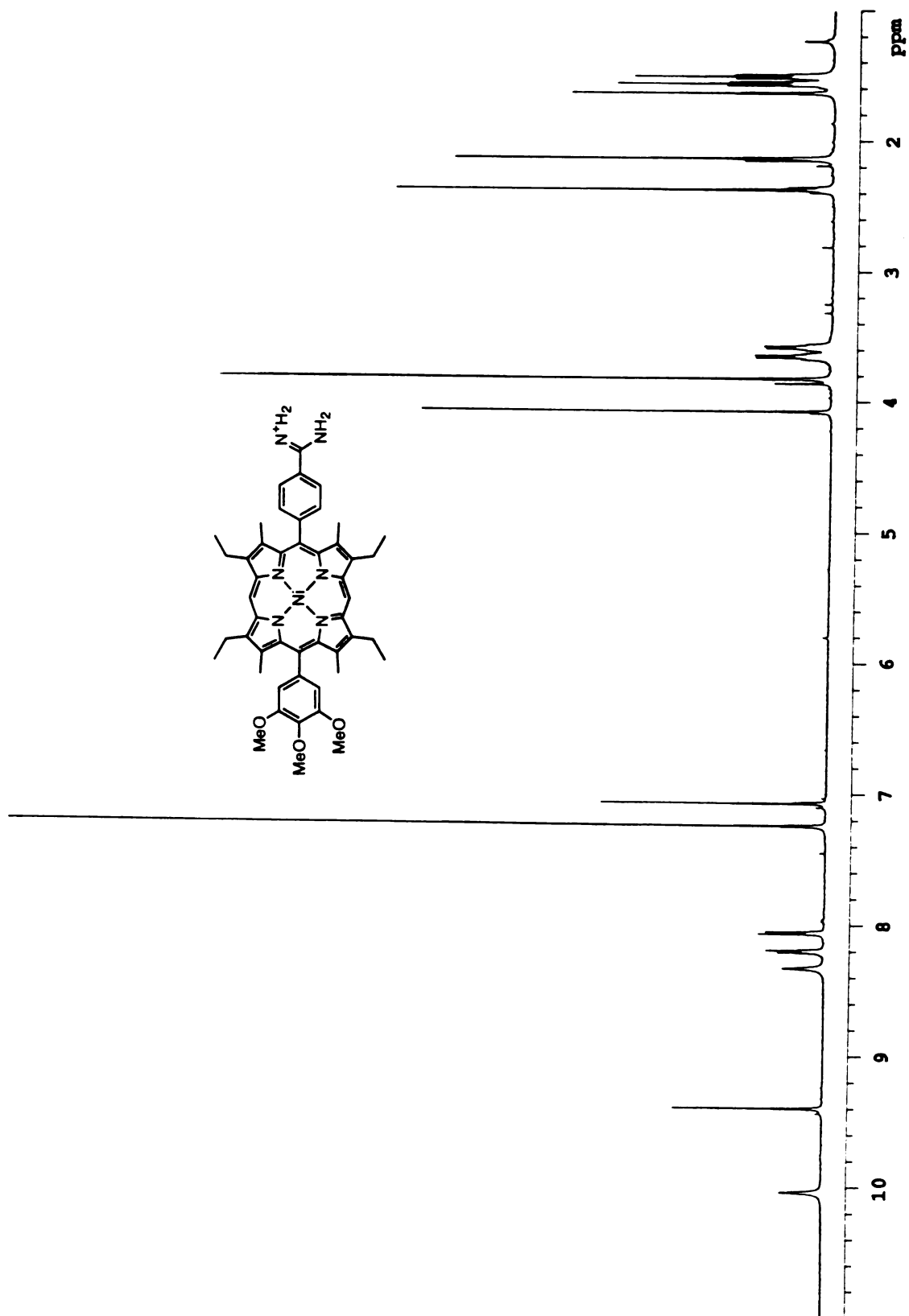


Figure A-3. 300 MHz ^1H -NMR spectrum of **53** in CDCl_3

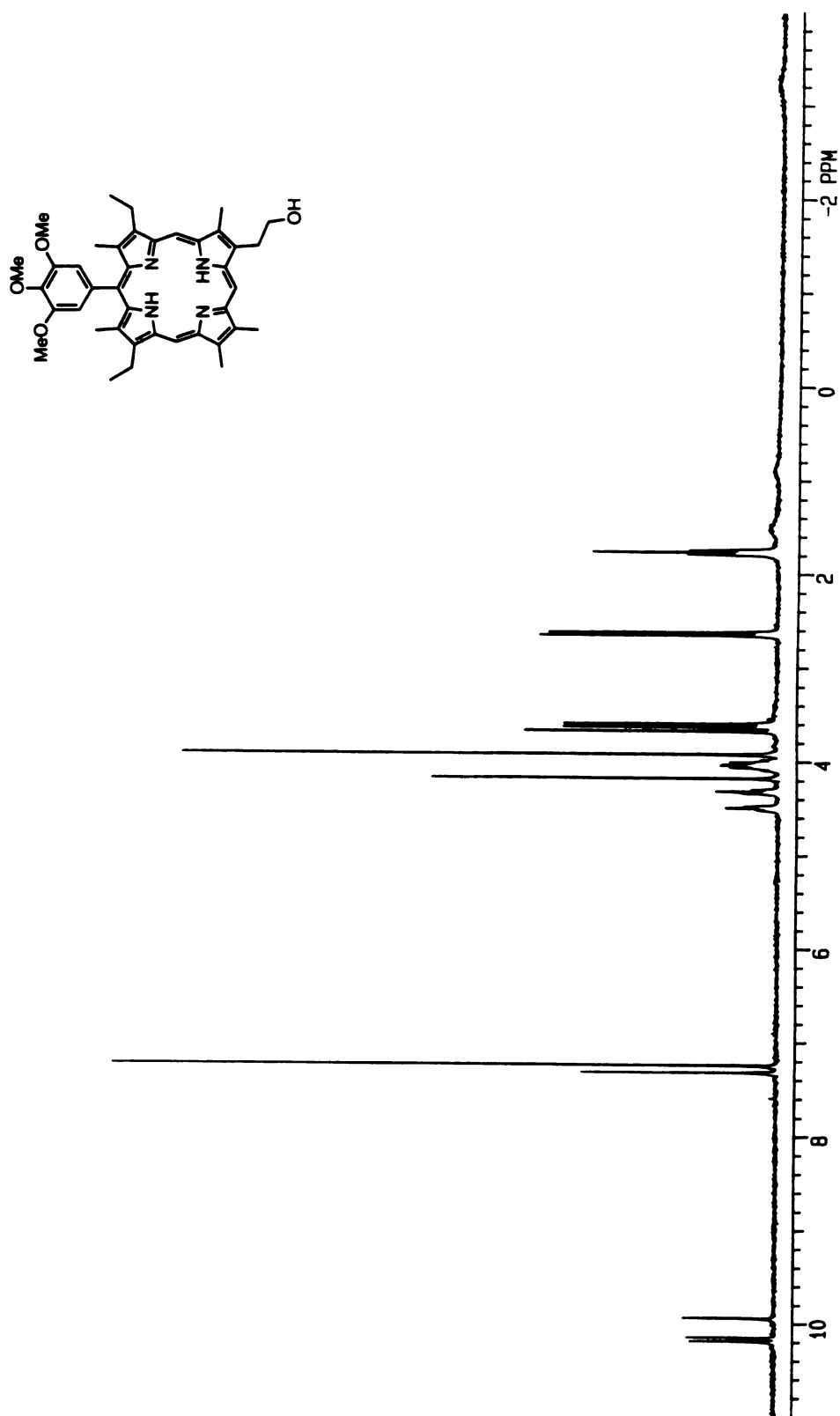


Figure A-4. 300 MHz ^1H -NMR spectrum of **66** in CDCl_3

Figure A-5. 300 MHz ^1H -NMR spectrum of 67 in CDCl_3

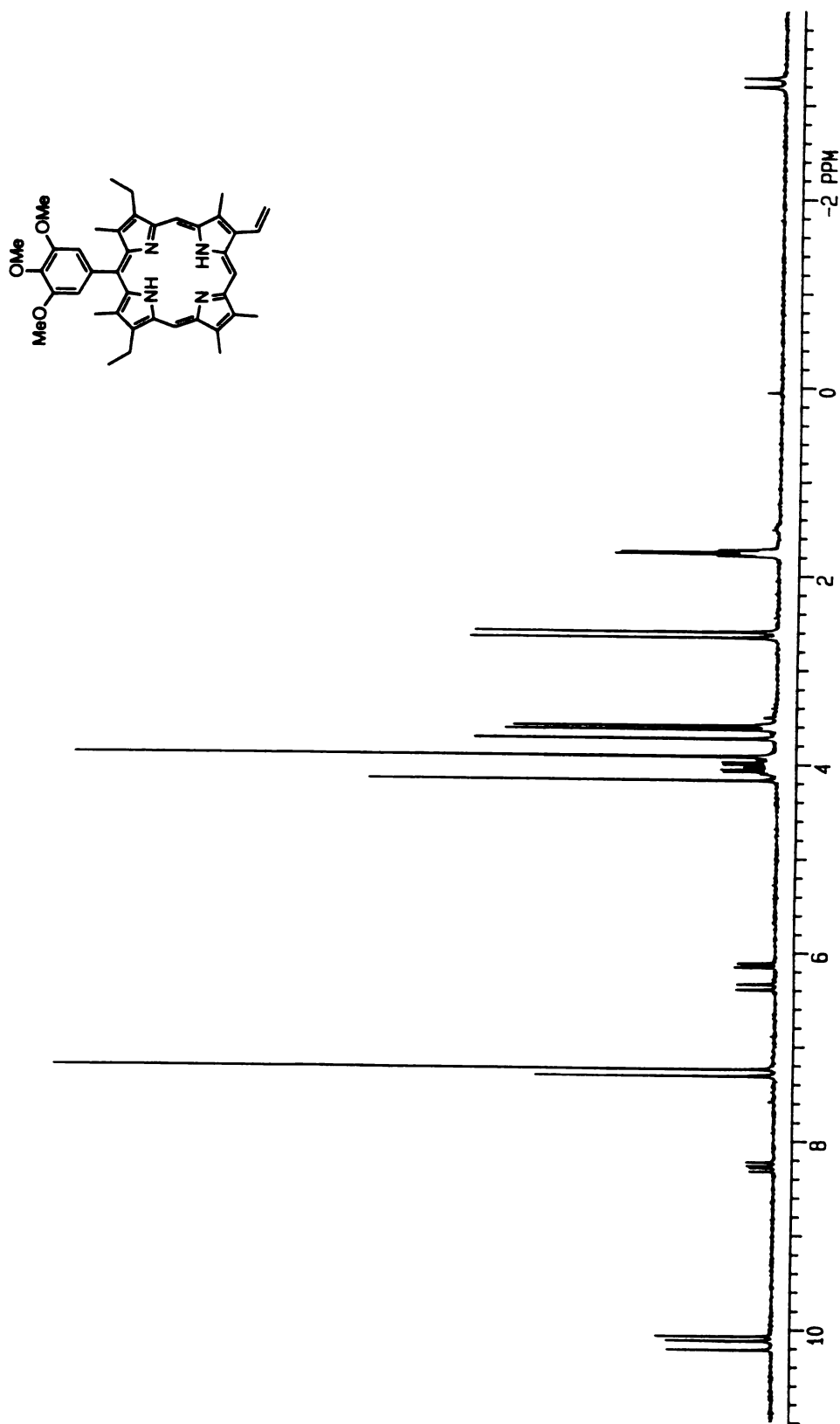


Figure A-6. 300 MHz ^1H -NMR spectrum of **68** in CDCl_3

Figure A-7. 300 MHz ^1H -NMR spectrum of 69 in CDCl_3

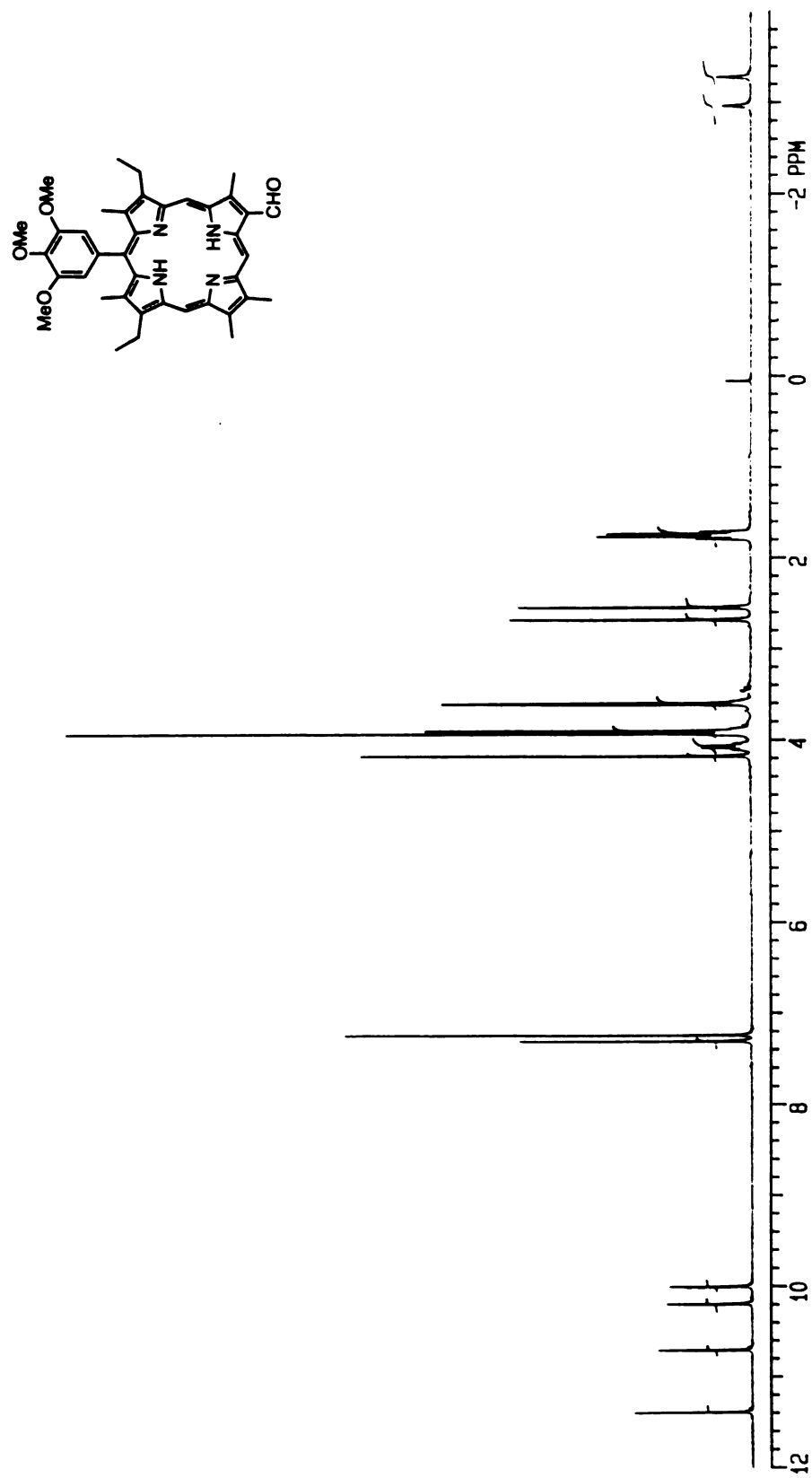


Figure A-8. 300 MHz ¹H-NMR spectrum of 70 in CDCl₃

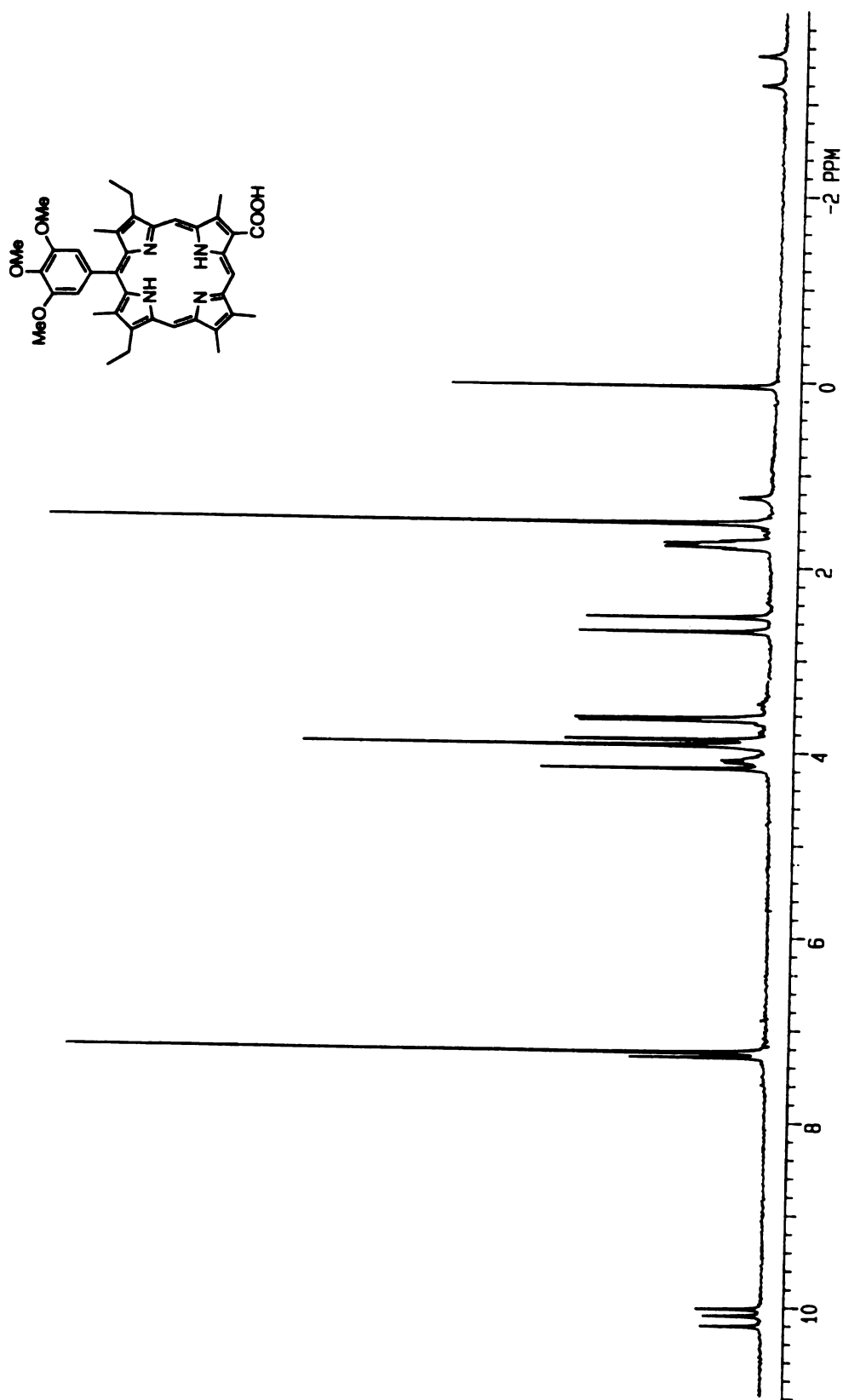


Figure A-9. 300 MHz ^1H -NMR spectrum of **71** in CDCl_3

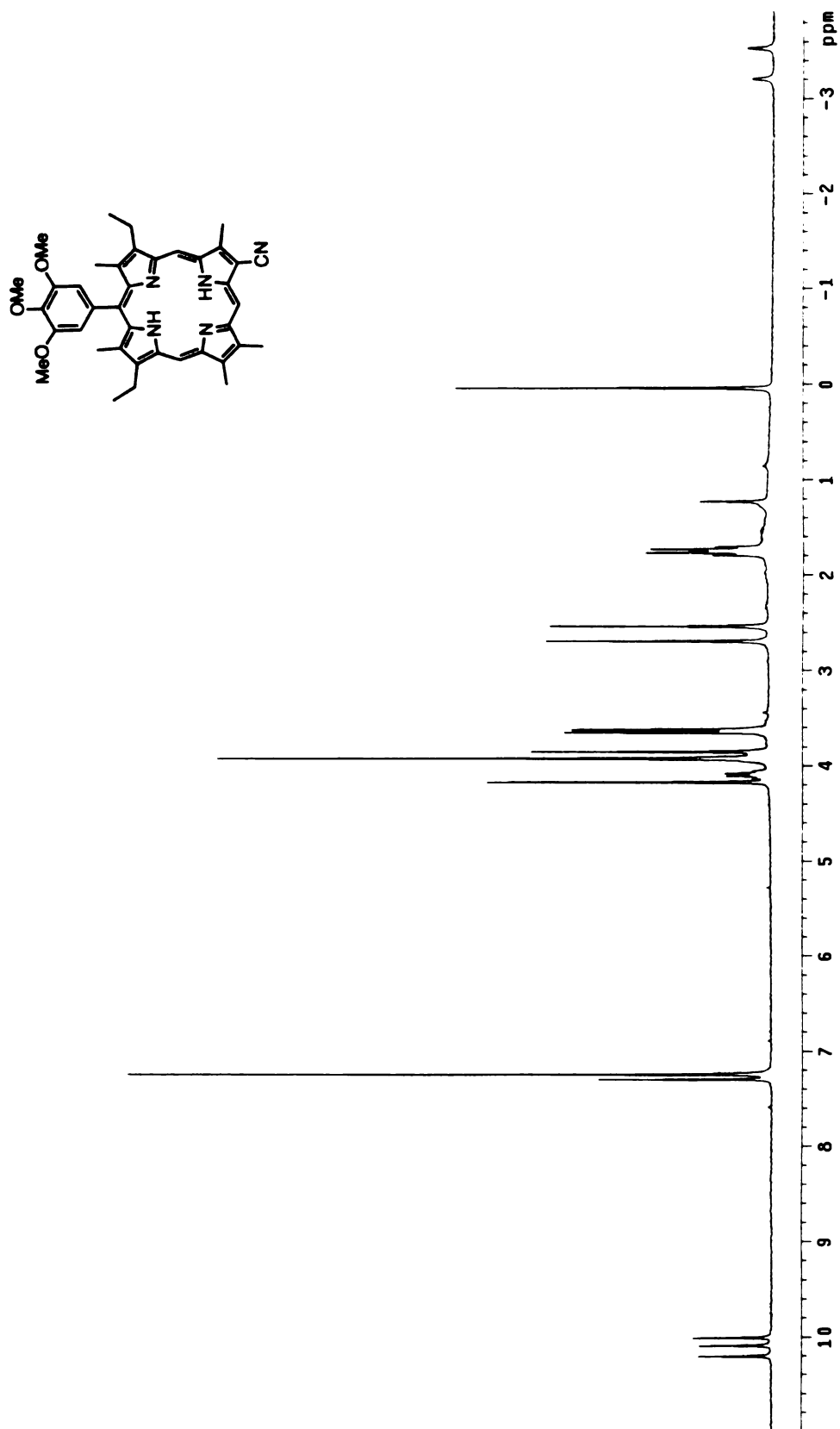


Figure A-10. 300 MHz ^1H -NMR spectrum of 73 in CDCl_3

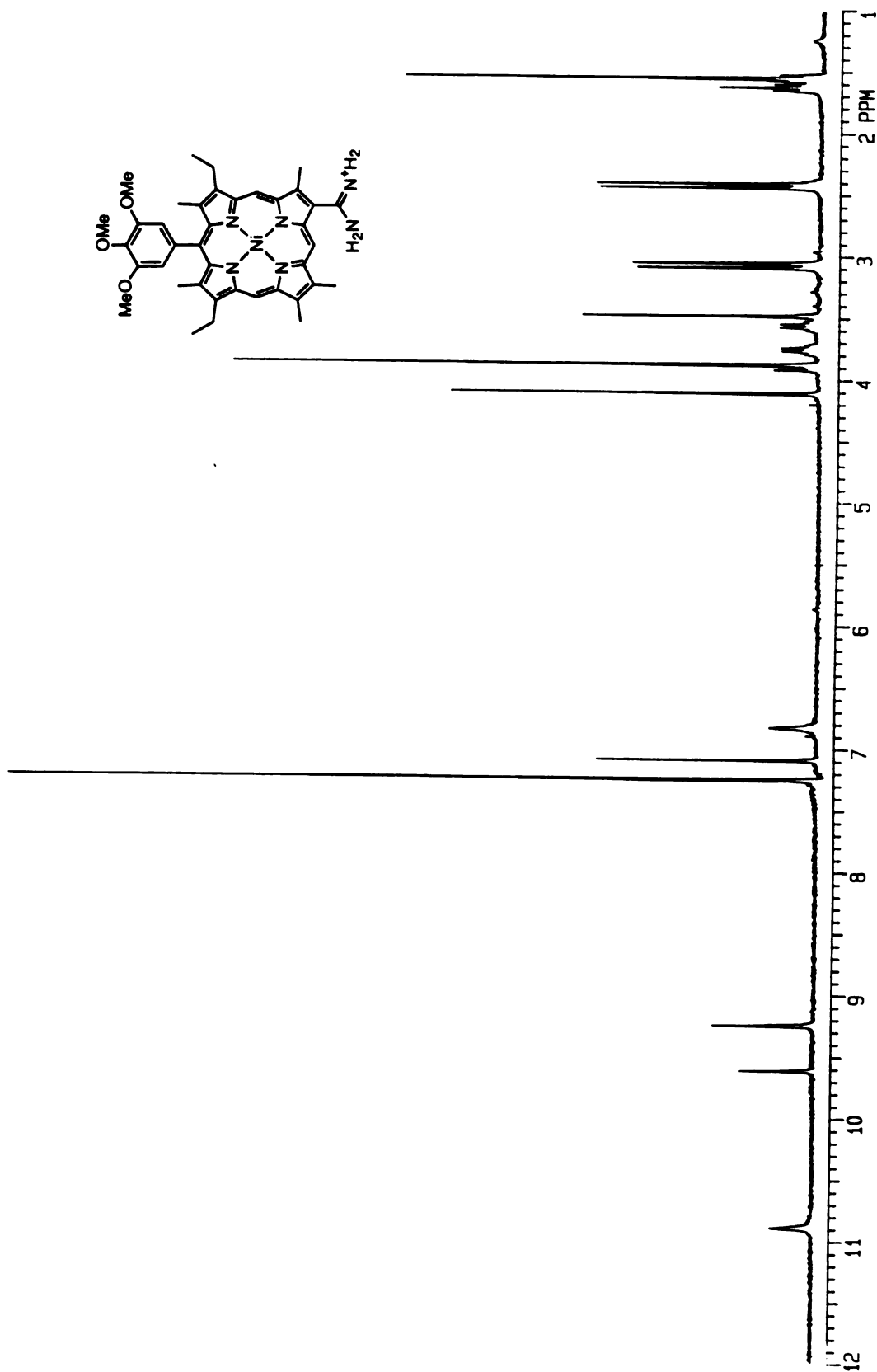


Figure A-11. 300 MHz ^1H -NMR spectrum of **75** in CDCl_3

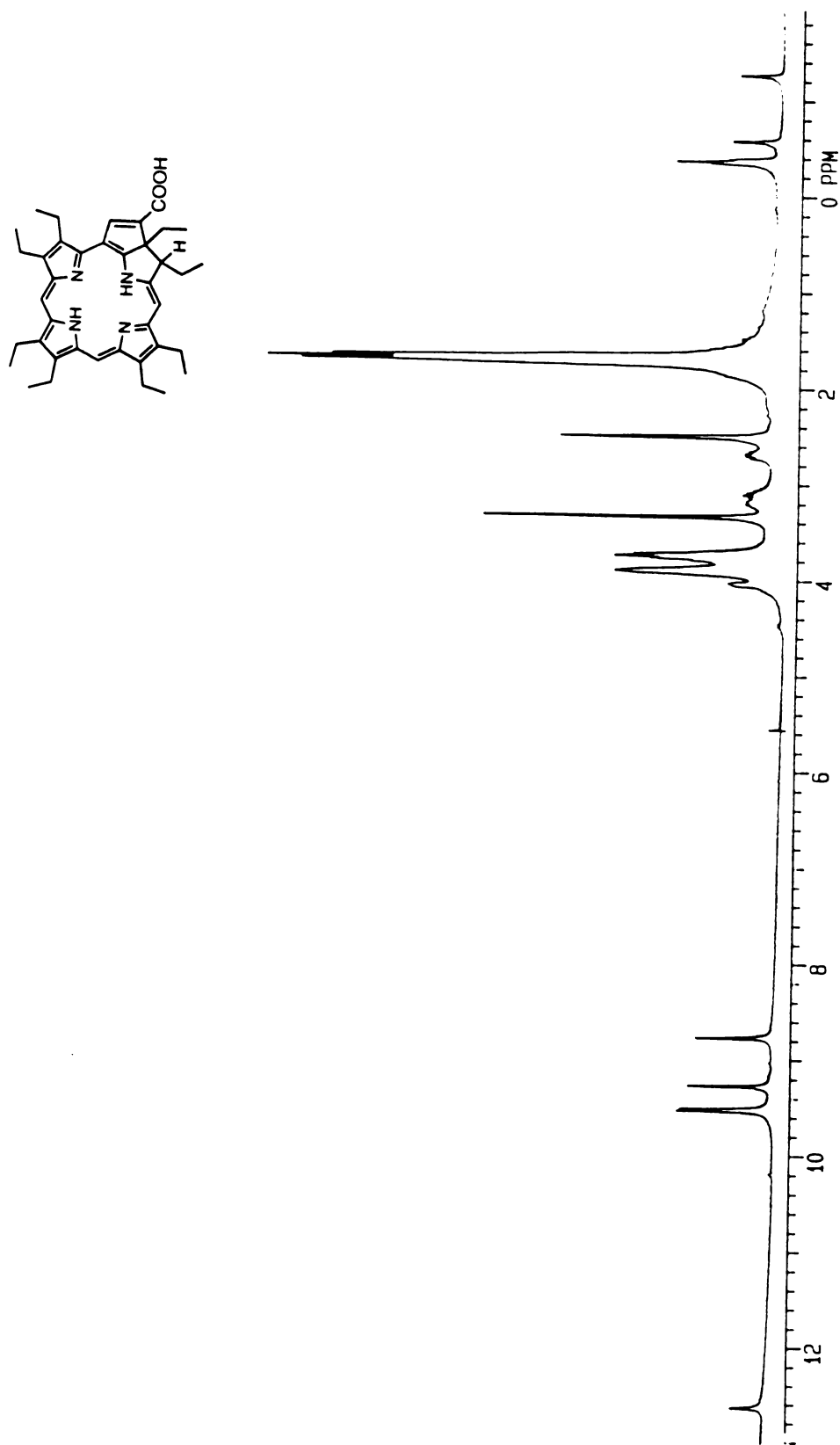


Figure A-12. 300 MHz ^1H -NMR spectrum of **83** in DMSO-d_6

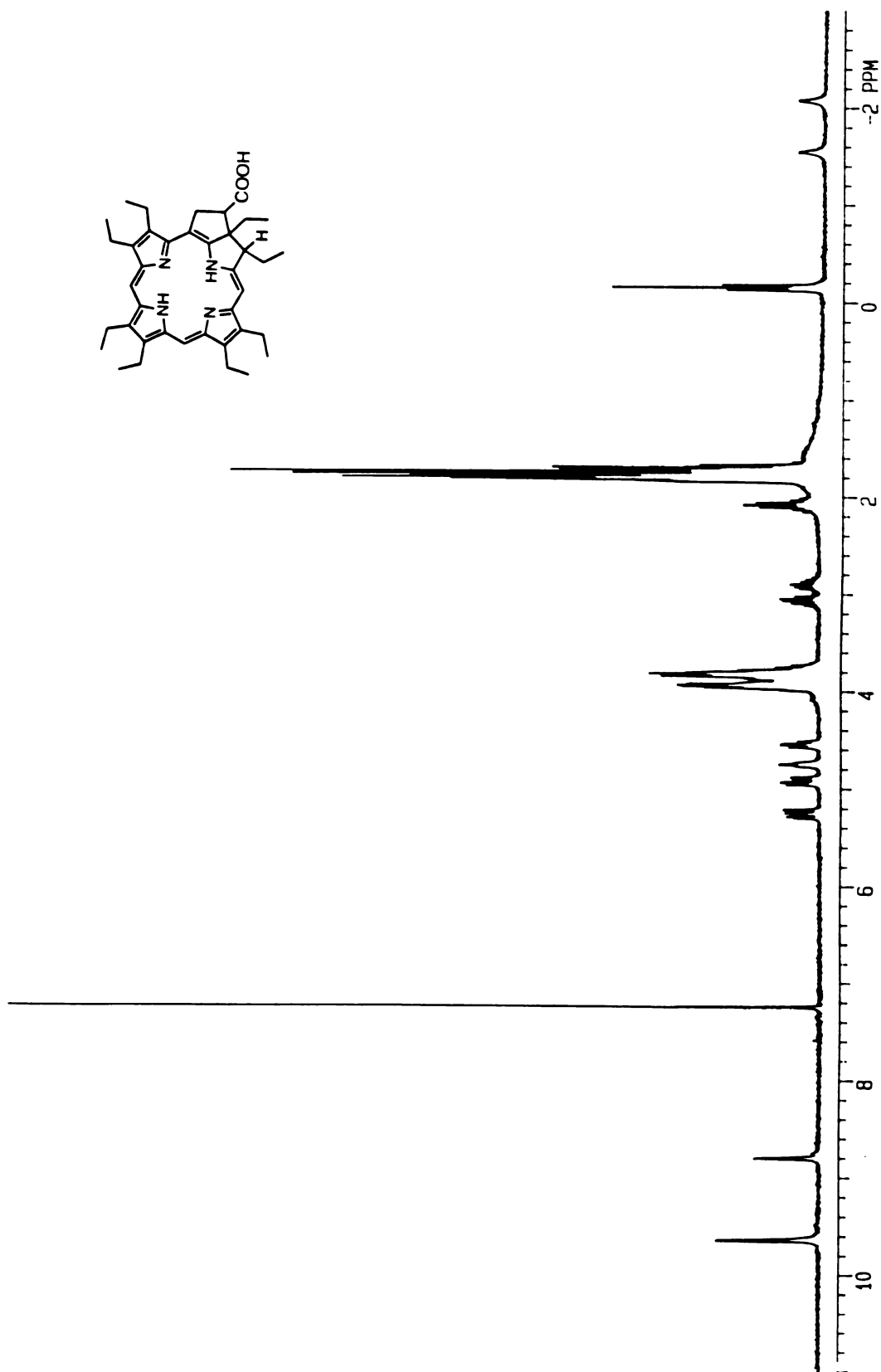


Figure A-13. 300 MHz ^1H -NMR spectrum of **85** in CDCl_3

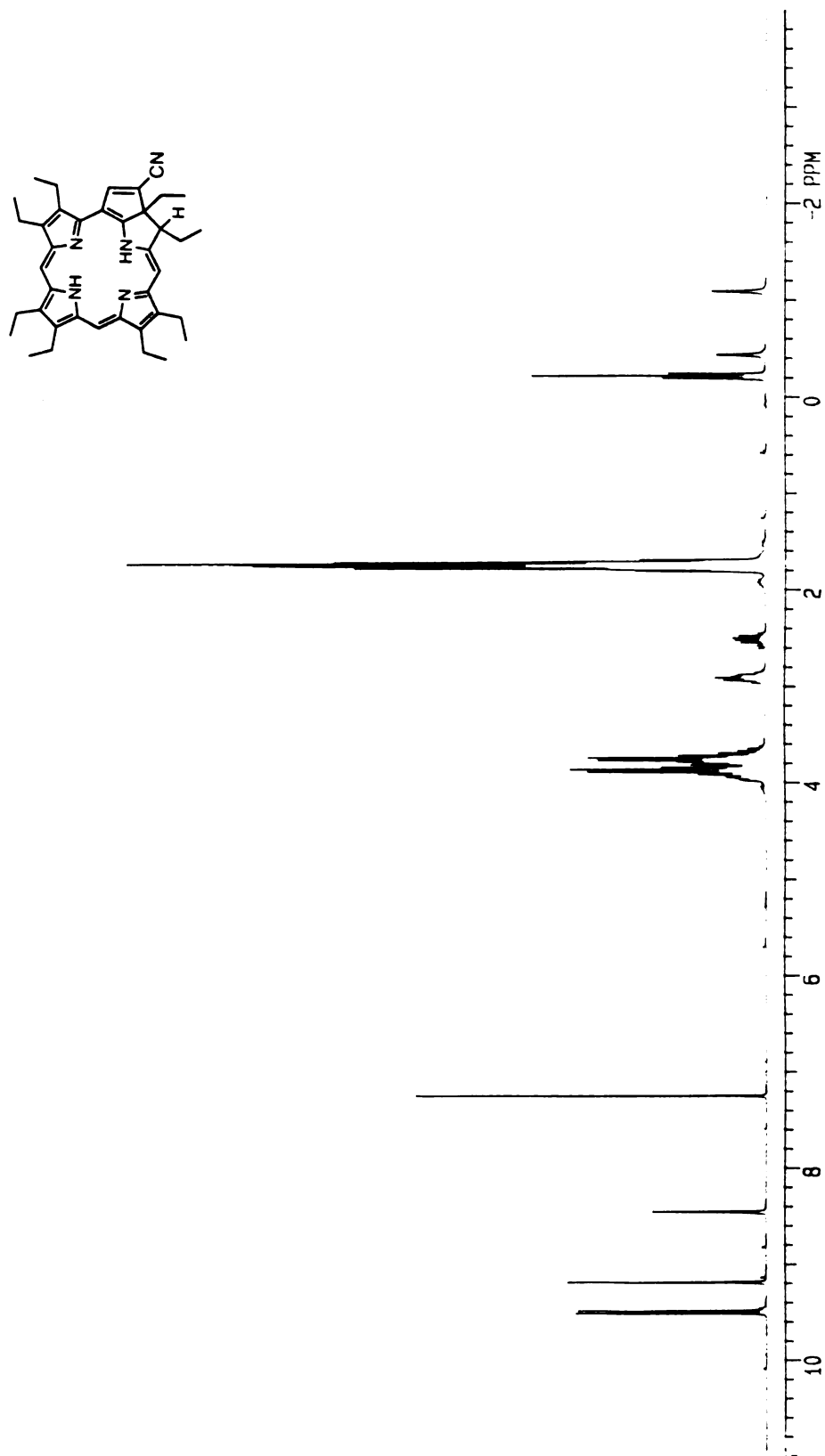


Figure A-14. 300 MHz ^1H -NMR spectrum of **89** in CDCl_3

Figure A-15. 300 MHz ^1H -NMR spectrum of **90** in CDCl_3

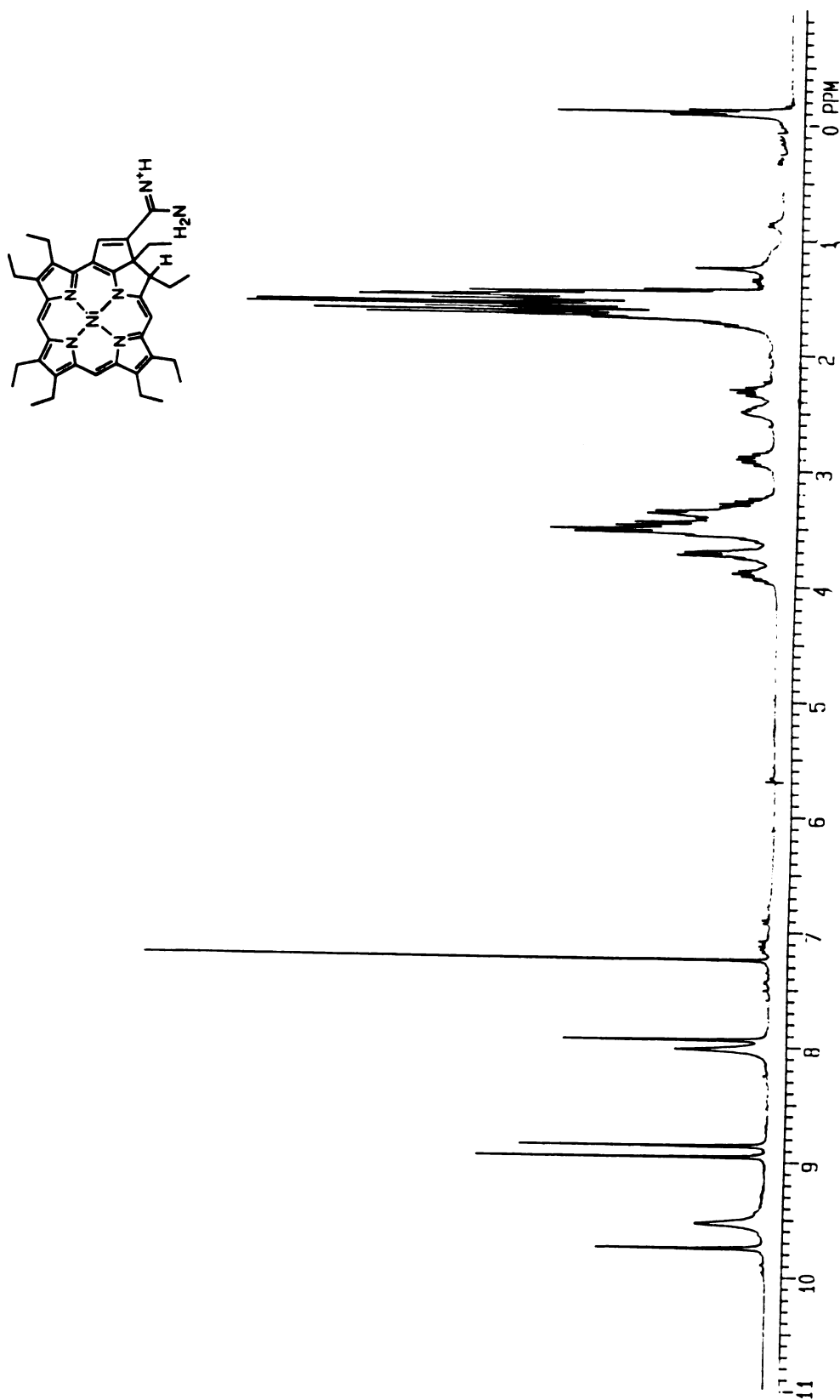


Figure A-16. 300 MHz ^1H -NMR spectrum of 92 in CDCl_3

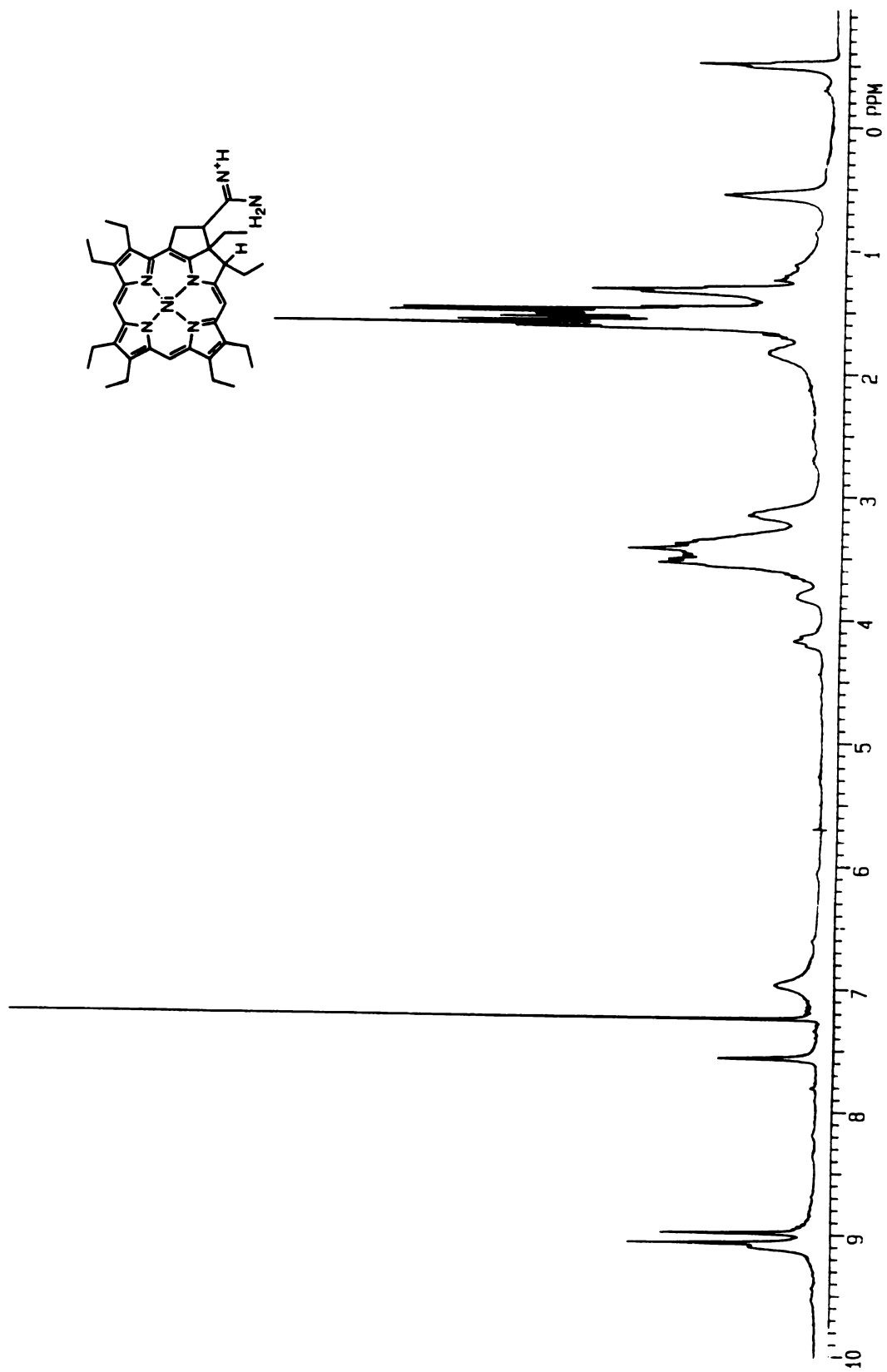


Figure A-17. 300 MHz ^1H -NMR spectrum of 96 in CDCl_3

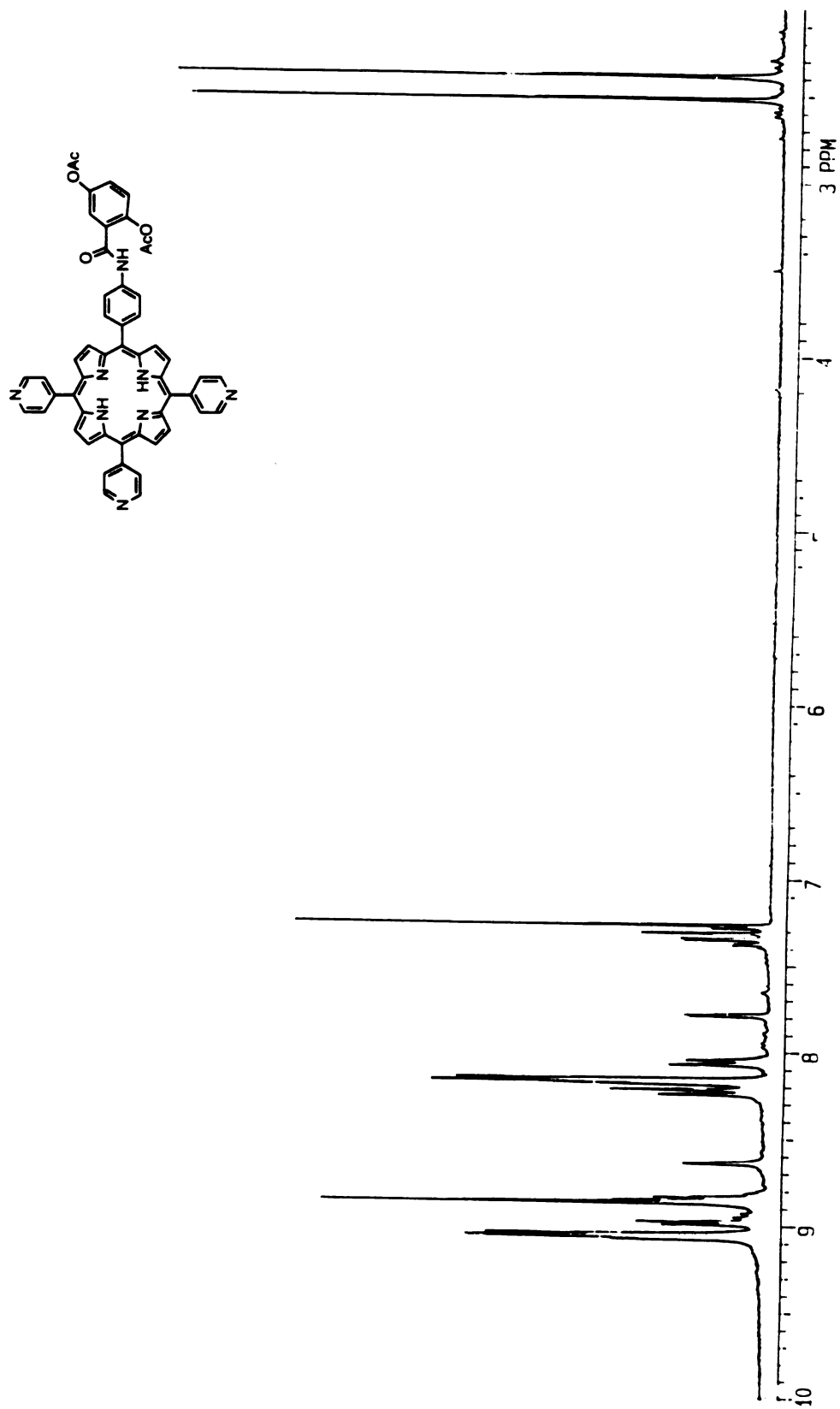


Figure A-18. 300 MHz ¹H-NMR spectrum of **105** in CDCl₃

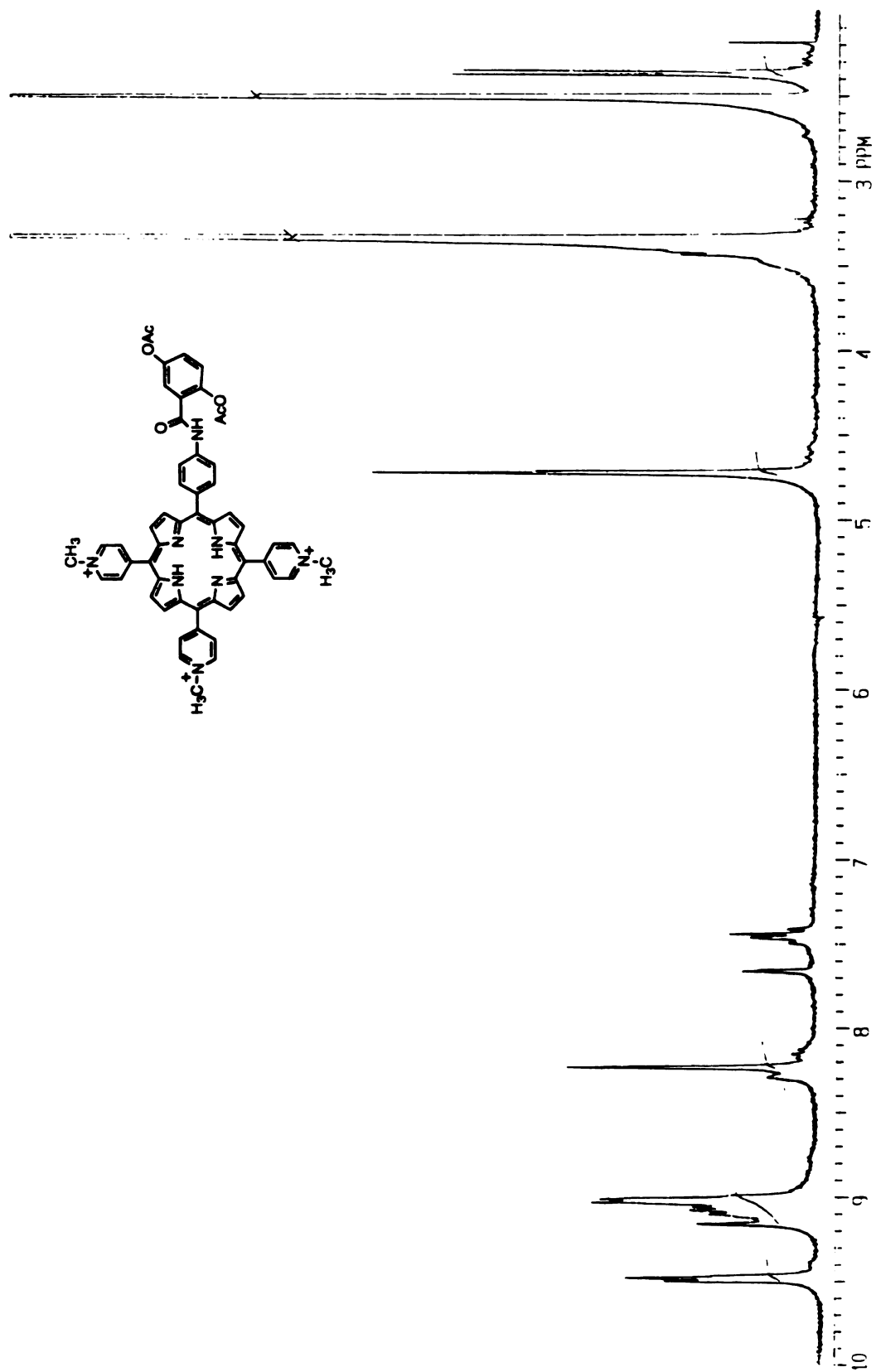


Figure A-19. 300 MHz ¹H-NMR spectrum of 106 in DMSO-d₆

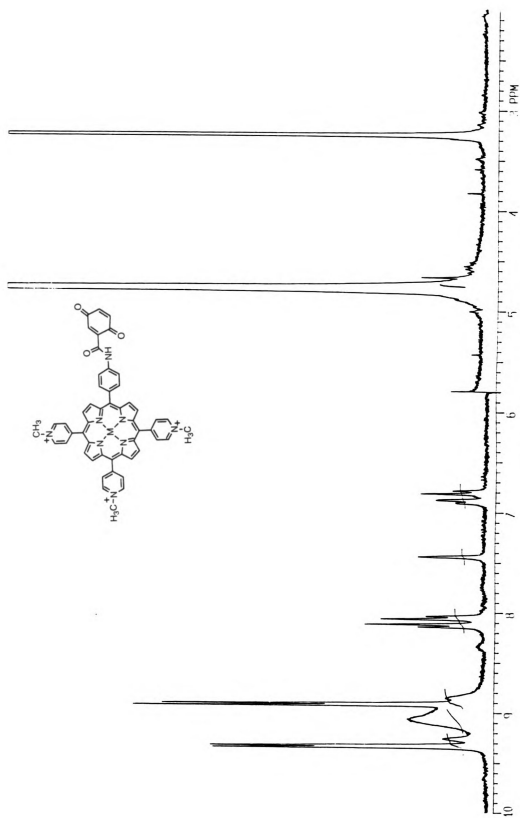


Figure A-20. 300 MHz ^1H -NMR spectrum of 108 in D_2O